Integration of Nuclear Spectrometry Methods as a New Approach to Material Research

IAEA
International Atomic Energy Agency

Integration of
Nuclear Spectrometry Methods
as a New Approach to
Material Research

The following States are Members of the International Atomic Energy Agency:

AFGHANISTAN	GHANA	NORWAY
ALBANIA	GREECE	OMAN
ALGERIA	GUATEMALA	PAKISTAN
ANGOLA	HAITI	PALAU
ARGENTINA	HOLY SEE	PANAMA
ARMENIA	HONDURAS	PARAGUAY
AUSTRALIA	HUNGARY	PERU
AUSTRIA	ICELAND	PHILIPPINES
AZERBAIJAN	INDIA	POLAND
BAHRAIN	INDONESIA	PORTUGAL
BANGLADESH	IRAN, ISLAMIC REPUBLIC OF	QATAR
BELARUS	IRAQ	REPUBLIC OF MOLDOVA
BELGIUM	IRELAND	ROMANIA
BELIZE	ISRAEL	RUSSIAN FEDERATION
BENIN	ITALY	SAUDI ARABIA
BOLIVIA	JAMAICA	SENEGAL
BOSNIA AND HERZEGOVINA	JAPAN	SERBIA
BOTSWANA	JORDAN	SEYCHELLES
BRAZIL	KAZAKHSTAN	SIERRA LEONE
BULGARIA	KENYA	SINGAPORE
BURKINA FASO	KOREA, REPUBLIC OF	SLOVAKIA
BURUNDI	KUWAIT	SLOVENIA
CAMBODIA	KYRGYZSTAN	SOUTH AFRICA
CAMEROON	LATVIA	SPAIN
CANADA	LEBANON	SRI LANKA
CENTRAL AFRICAN	LESOTHO	SUDAN
REPUBLIC	LIBERIA	SWEDEN
CHAD	LIBYA	SWITZERLAND
CHILE	LIECHTENSTEIN	SYRIAN ARAB REPUBLIC
CHINA	LITHUANIA	TAJIKISTAN
COLOMBIA	LUXEMBOURG	THAILAND
CONGO	MADAGASCAR	THE FORMER YUGOSLAV
COSTA RICA	MALAWI	REPUBLIC OF MACEDONIA
CÔTE D'IVOIRE	MALAYSIA	TUNISIA
CROATIA	MALI	TURKEY
CUBA	MALTA	UGANDA
CYPRUS	MARSHALL ISLANDS	UKRAINE
CZECH REPUBLIC	MAURITANIA	UNITED ARAB EMIRATES
DEMOCRATIC REPUBLIC	MAURITIUS	UNITED KINGDOM OF
OF THE CONGO	MEXICO	GREAT BRITAIN AND
DENMARK	MONACO	NORTHERN IRELAND
DOMINICAN REPUBLIC	MONGOLIA	UNITED REPUBLIC
ECUADOR	MONTENEGRO	OF TANZANIA
EGYPT	MOROCCO	UNITED STATES OF AMERICA
EL SALVADOR	MOZAMBIQUE	URUGUAY
ERITREA	MYANMAR	UZBEKISTAN
ESTONIA	NAMIBIA	VENEZUELA
ETHIOPIA	NEPAL	VIETNAM
FINLAND	NETHERLANDS	YEMEN
FRANCE	NEW ZEALAND	ZAMBIA
GABON	NICARAGUA	ZIMBABWE
GEORGIA	NIGER	
GERMANY	NIGERIA	

The Agency's Statute was approved on 23 October 1956 by the Conference on the Statute of the IAEA held at United Nations Headquarters, New York; it entered into force on 29 July 1957. The Headquarters of the Agency are situated in Vienna. Its principal objective is "to accelerate and enlarge the contribution of atomic energy to peace, health and prosperity throughout the world''.

INTEGRATION OF NUCLEAR SPECTROMETRY METHODS AS A NEW APPROACH TO MATERIAL RESEARCH

Final report of a coordinated research project
2006–2009

For further information on this publication, please contact:

FOREWORD

In 2006, the IAEA initiated a coordinated research project (CRP) on 'Unification of Nuclear Spectrometries: Integrated Techniques as a New Tool for Material Research' as one of the elements of a project on 'Improvements in Nuclear Spectrometry Applications'. The major objective was to assist laboratories in Member States in enhancing proper utilization of nuclear analytical methods and to help them develop nuclear instruments for special applications.

An overall objective of the CRP was to help Member States to improve characterization of materials by the effective utilization of nuclear spectrometry instruments and techniques as well as by developing integrated/unified instruments and analytical methodologies in support of environmental pollution monitoring, industry, study of cultural heritage, human health, agriculture, etc. These techniques can be used in small laboratories as well as in state of the art synchrotron sources.

The specific research objectives of the CRP included development (or upgrading) of integrated multifunctional instruments based on nuclear spectrometries and related techniques as well as development of software for the handling and operation of integrated multifunctional instruments, including data acquisition. The CRP also covered: development (or upgrading) of integrated analytical approaches/methodologies and software for processing and presentation of data collected by multifunctional instruments; extension of the applications of integrated/unified instruments; and synergistic and complementary use of nuclear spectrometries, with the aim of assisting end users of nuclear spectrometries in various fields.

The CRP covered a period of four years (2006–2009). Twelve laboratories from both developed and developing Member States and the IAEA's Laboratories participated.

The first research coordination meeting (RCM) was held in Vienna, from 16 to 20 April 2007. The participants presented progress reports, reviewed the status of the instrumentation and methodologies available, and agreed on a detailed work plan for the CRP.

The second (final) RCM was held in Athens, Greece, from 11 to 15 May 2009. The participants reviewed and summarized the overall research results of the CRP, assessed the impact of the CRP and identified outstanding research related to integration of nuclear spectrometry techniques and analytical methodologies. This publication presents the results of the CRP.

The IAEA officers responsible for this publication were A. Markowicz and K. Will of the IAEA Laboratories, Seibersdorf.

EDITORIAL NOTE

CONTENTS

SUMMARY

1. INTRODUCTION

During the last years the IAEA supported a substantial number of laboratories in Member States in establishing nuclear spectrometry facilities for various applications. These laboratories are being used in support of applied research, teaching and education in nuclear science and technology as well as for providing analytical services for industry, environmental studies, study of cultural heritage, food and agriculture and human health. In most cases the nuclear analytical techniques such as energy dispersive X ray fluorescence (EDXRF), particle induced X ray emission (PIXE), particle induced gamma emission (PIGE), Rutherford backscattering (RBS), etc. are used independently and provide information on a specific characteristic of the analyzed materials. In order to characterize the materials in a comprehensive way or to improve the quality of the analytical services provided by the laboratories, a combined use of a few techniques is often required. In recent years advanced laboratories, such as synchrotron sources, started to perform measurements by use of the integrated instruments and simultaneous processing of data where outputs of the analytical techniques are used as inputs to a common data processing procedure. In this way the quality of characterization of various materials by using multiple analytical techniques improved considerably. In order to coordinate the research efforts of the laboratories towards better integration and unification of nuclear spectrometries this CRP was proposed under the Project D.3.03 'Improvements in nuclear spectroscopy applications'. The CRP has contributed to the objectives of this Project by enhancing proper utilization of nuclear analytical methods in Member States and helping them to develop nuclear instruments for special applications.

One of the major areas of integration was the application of synchrotron radiation sources for X ray micro-fluorescence, micro-diffraction, X ray microscopy, micro-tomography, and absorption techniques used for elemental analysis, 2D and 3D imaging and chemical speciation. Portable XRF spectrometers were used with other techniques for integrated applications and better utilization of the equipment. Software simulation programs were also implemented to design integrated nuclear spectroscopy systems to optimize the measurement geometries, detection limits, and spatial resolution. A combination of XRF-PIXE and PIXE-PIGE setups and integration of data processing procedures were used to extend the applicability range of the X ray emission techniques for a better characterization of the materials.

Integration and unification of nuclear spectrometries were achieved including hardware and software components, measurements and data collection, data processing and data interpretation.

Six research contracts and six research agreements were awarded under the CRP. The results of the studies carried out in the framework of the CRP have been published in a number of research articles. The reference list including published and submitted research articles is presented at the end of the document.

The CRP has assisted Member States to improve characterization of materials by the utilization of nuclear spectrometry instruments and techniques as well as by developing integrated/unified instruments and analytical methodologies. These techniques have been applied as laboratory-based measurements as well as in synchrotron facilities. As a consequence of this CRP, nuclear spectrometries have been more widely utilized and new

special applications implemented in support of environmental studies, industry, study of cultural heritage, human health, agriculture and biology among others.

2. COUNTRY REPORTS

During the 2nd RCM, individual country reports were presented by the Chief Scientific Investigators. In the presented reports a summary of the work carried out and achievements at their laboratories related to integration and unification of nuclear spectrometry techniques was given. The individual country reports are included in this publication. The specific outputs of the CRP are presented in Table 1.

TABLE 1. SUMMARY OF THE CRP OUTPUTS

Output	Achievements for individual countries
Integrated and multifunctional instruments with technical documentation	AUL: PIXE-PIGE-RBS techniques have been integrated and automated controlled unattended 24 hr operation.
	BEL–KJ/PVE: Micro-XRF + micro-Raman integrated in the PRAXIS transportable instrument.
	BEL–RVG: Optimization of EPXMA integrated with micro-Raman spectroscopy, and EPXMA with micro-Auger and micro-XRF spectroscopy.
	CRO: PIXE and XRF integrated in one set-up.
	CUB: XRD was refurbished and EDXRF automation was carried out. Integration is conceptualized but needs to be completed.
	GRE: An integrated PIXE and XRF set-up was completed (installed and operated) with technical documentation.
	ITA: XRF and Raman portable equipment optimized for analysis of works of art.
	SLO: EDXRF and TXRF integrated in one set-up.
Software packages for handling and operation of multi-functional instruments	AUL: PIXE-PIGE-RBS individual software analysis modules were completed.
	BEL–KJ/PVE: XRF and XRD 2D-scanning in IDL implemented.
	CUB: XRD and XRF modules were developed for control and operation of the instruments.
	ITA: Bench-top XRF and portable XRF software for gold and painted layer analysis were completed.

Integrated software packages for data processing and presentation	AUL: PIXE-PIGE modules only were successfully combined for full matrix corrections.
	BEL–RVG: EPXMA software upgraded to quantify low Z element analysis.
	CRO: Software package for combined PIXE and XRF excitation was completed.
	CUB: Software development is still in progress.
	GRE: Software was completed for simulation of the PIXE induced XRF measurements and optimization of experimental conditions.
	SLO: Integrated software for EDXRF and TXRF analysis was implemented.
	USA: Initial integration of confocal micro-XRF and micro computed X ray tomography for visualization.
Improved analytical methodologies based on combined use of various nuclear spectrometries	ARG: TXRF, IR and GC-MS techniques, micro-Raman spectrometry and SEM-EDX in archaeometry.
	AUS: SR-TXRF + XANES, micro-XRF + -XANES were completed. GE-XRF+XANES were successfully integrated.
	AUL: Automatic matrix corrections for oxides and light elements up to calcium have been successfully tested on real samples.
	BEL–KJ/PVE: Integrated XRF, micro-XRF, Confocal – micro-XRF, XANES, micro-XRD in combination with non-nuclear techniques (Micro-Raman, UV and IR) were applied to cultural heritage and geological - environmental problems.
	BEL–RVG: Characterization of different environmental samples by combined use of EPXMA, micro-Raman and XRF.
	CRO: PIXE and XRF were integrated, successfully, operated and tested on reference materials.
	GRE: Measurement and analysis conditions for the integrated PIXE-XRF technique were optimized.
	ITA: Pre-Colombian and contemporary gold alloy analyses were carried out.
	SLO: EXAFS in combination with TXRF + XRF + micro-PIXE analyses were accomplished.

	UAE: Materials processing and analysis methodology for XRD, optical absorption, XANES and XMCD for diluted magnetic semi-conductors were achieved.
	USA: Initial integration of confocal micro-XRF and micro-tomography accomplished.
New applications of nuclear spectrometries for better characterization of materials	AUL: New pseudo-Bragg law developed for Bremsstrahlung background stripping in PIXE spectra of multi-elemental matrices.
	ARG: Synchrotron radiation, micro-XRF + SAXS for polymers and SR – micro-XRF + XRD in human bones.
	AUS: SR-TXRF + XANES of aerosols and silicon wafer surfaces and confocal micro-XRF + XRF-XANES on human bones samples.
	BEL–RVG: EPMA - XRF, micro-Raman for preventive conservation in museums, indoor aerosols versus health and river sediment fingerprinting.
	BEL–KJ/PVE: Milli-XRF applied to hidden paint–layers, combined confocal micro-XRF, micro-XRD and micro-XAS for geological applications; combined micro-XRF, micro-XAS and micro-Raman for pigments identification and investigation of ancient illustrated manuscripts.
	GRE: Terrestrial analogue rock samples characterized using multiple exciting X ray beams through PIXE induced XRF.
	ITA: Temporal and spatial monitoring of pollution changes using outdoor marble statues with field portable XRF.
	SLO: Applications of EXAFS in plant physiology studies and analysis of mineral composition of bee honey by TXRF to determine botanical and geographical origin.
	UAE: Optical absorption applied to band gap studies. XRD, XANES and XMCD to study electronic properties of diluted magnetic semiconductors.
	USA: Developed standardized parameters for confocal micro-XRF data acquisition. New material studies include inertial confinement fusion targets, uranium oxide particles, paint samples.

Research papers, reports, conference contributions	Detailed list of publications is in Attachment 4.
	ARG: 1 organized meeting, 3 contributions to conferences, 2 papers submitted, 1 paper published, 2 reports.
	AUL: 2 conferences, 2 journals, 1 external report.
	AUS: 2 papers published, 3 reports, 6 conference contributions.
	BEL–KJ/PVE: 6 papers published, 10 conference contributions.
	BEL–RVG: 27 papers published, 30 conference contributions.
	CUB: 2 papers.
	GRE: 10 papers published, 11 conferences, 1 organized conference, 2 workshops, 4 reports.
	ITA: 1 paper published, 1 book chapter published, 4 papers submitted, 2 conference contributions.
	SLO: 7 published papers.
	GER: 15 papers published (information submitted after the RCM).
Providing fundamental knowledge of physical phenomena	AUL: Non-empirical PIXE background spectra for elements up to silicon automatically generated from theory.
	AUS: Absorption phenomenon in TXRF-XANES was studied and GE-XRF/XANES developed.
	BEL–KJ/PVE: Immobilization of U^{+4} by reduction of U^{+6} by arseno-pyrite layers on iron-oxide particles in geological deposits.
	GRE: Obtained data on resonant Raman scattering (Al) and cascade effect on Fe-L fluorescence lines.
	ITA: Evaluation of XRF characteristic emission intensity ratios.
	SLO: Prediction of artificial standards from basic principles.
	UAE: Fundamental understanding of coupling mechanisms, from electronic and magnetic properties in diluted magnetic semiconductors.

The next Table presents overall assessment towards achieving the specific objectives of the CRP.

TABLE 2. OVERALL ASSESSMENT TOWARDS ACHIEVING THE SPECIFIC OBJECTIVES OF THE CRP

Specific objective	Countries
Development (or upgrading) of integrated multifunctional instruments based on nuclear spectrometries and related techniques	AUL, AUS, CRO, CUB, BE-KJ/PVE, GRE, ITA, SLO
Development of software for handling and operation of integrated multifunctional instruments including data acquisition	AUL, CRO, CUB, ITA, BEL-KJ/PVE
Development (or upgrading) of integrated analytical approaches/methodologies and software for processing and presentation of data collected by multifunctional instruments	ARG, AUL, BEL-KJ/PVE, BEL-RVG, CRO, CUB, GRE, ITA, SLO, UAE, USA
Development of new applications of integrated/unified instruments to assist end-users of nuclear spectrometries in various fields	ARG, AUS, BEL-RVG, BEL-KJ/PVE, GRE, SLO, UAE, USA
Development of synergistic and complementary use of nuclear spectrometries	ARG, AUL, AUS, BEL-KJ/PVE, BEL-RVG, GRE, ITA, SLO, UAE, USA

In summary, most of the initial objectives set at the beginning of the CRP have been achieved and in some cases surpassed. All the participants agreed that the CRP effort was rewarding on multiple levels including the following:

(1) The scientific achievements have advanced nuclear spectrometric knowledge and methodologies for materials characterization.
(2) The development of new fundamental information.
(3) The development of new collaborative efforts.

3. FACTORS AFFECTING CRP

The members of the CRP identified the following factors affecting the overall performance of the CRP during the three years of operation:

- Lack of reference materials for 2D and 3D micro-analytical techniques.

- Lack of accurate fundamental parameters related to the specific area of the generation and interaction of X ray s with matter.
- The problems of representative sampling associated with the identification, handling and manipulation of micro-samples.
- Compatibility and integration/interpretation of the results for analytical techniques with different information masses.
- Insufficient time effectiveness and insufficient reliability when using integrated analytical techniques.
- A requirement for broad ranging expertise to effectively operate and maintain multiple technique systems.
- Lack of high-speed detection systems such as energy-dispersive pixelated detector systems.

4. IMPACT OF THE CRP

The CRP has had the following specific impacts:

- Dissemination of applied research into the public domain.
- Increased collaboration and international networking.
- Enhanced cooperation between natural and social scientists through collaborative research and joint meetings.
- CRP has enhanced and stimulated training for early-career scientists.
- Improved scientific background for professionals in various applied fields.
- Stimulated interest in new topics for member states (cultural heritage, environmental applications, confocal spectrometries for micro-XRF and micro-PIXE analysis).
- Integrated techniques in fundamental understanding of the properties of diluted magnetic semiconductors were utilized.
- Triggered new projects related to the subject of CRP, such as country framework program to establish a XRF lab for cultural heritage and environmental applications, as well as ARASIA projects for the UAE.
- Bridged the gap and confirmed the need for small and large scale laboratories.
- Identified gaps in fundamental knowledge which need to be re-assessed.
- Improved characterization of materials by combining many techniques on one sample.
- Improved laboratory infrastructure with additional instrumentation.
- Improved matrix corrections for broad range of samples.
- Increased ability for automatic batch processing of hundreds of samples, improving sample throughput.
- Developed user friendly GUI for sample Ion Beam analysis utilized by non-specialist external users (biologists, archaeologists, geologists, material and environmental scientists) from 37 universities across Australia.
- Enhanced use of the integration of nuclear and non-nuclear techniques, but also increased standalone instrumental applications.
- Identified XRS as the technique of choice in cultural heritage characterization.
- Offered new analytical possibilities for the characterization of cultural heritage artifacts/materials within country of origin.
- Resulted in better understanding of the applicability range of integrated techniques (micro-XRF and micro-Raman, micro-XRF and micro-XRD).

- Demonstrated the necessity to combine macro- and milli-beam techniques for screening prior to localized micro-scale investigations.
- Advanced research into plant physiology by introducing quantitative analysis approaches.
- Integrated SR-TXRF and XANES as very successful method for the speciation at trace levels, applied to aerosol and silicon wafer analyses.
- Combined SR-TXRF-XANES is now available for potential users at HASYLAB.
- Increased the understanding of absorption as a limiting factor in SR-TXRF-XANES resulting in the development of GE-XRF-XANES.
- Identified the need for reference materials on the micro-scale and enhanced the development towards this need based on new collaborations among CRP members.
- PIXE induced XRF proved promising for the determination of X ray fundamental parameters.

5. FURTHER RESEARCH RELATED TO THE SCOPE OF THE CRP

The participants of the CRP have identified the following research topics as being worthwhile to pursue:

- The further development of 3D-reference materials.
- The complete integration of XRF-XRD.
- Further investigation of alterations of the sample integrity during preparation, manipulation and measurement procedures (for instance oxidation).
- EXAFS investigations of As implants in ultra-shallow junctions together with NAA.
- The integration of RBS into PIXE-PIGE modules.
- A better understanding of atomic Bremsstrahlung background component in 5-16 keV energy range of PIXE spectra.
- A better understanding of the failure of additive Bragg rule for matrices above $Z=13$.
- The digitization of the XRF controls and its implementation with the PIXE control software.
- The development of characterization protocols for handling and operating instruments with different analytical range, resolution and broad range of samples.
- The improvement and evaluation of the cost-effectiveness of characterization techniques.
- Introduction and testing of new quantitative approaches in WDXRF analysis compared with EDXRF.
- The enhancement of our understanding and knowledge about fundamental phenomena related to the interaction of X ray s with matter.
- The expansion of the applications of X ray based techniques to the development and characterization of new materials, food products, bio-fuels, pharmaceutical products.
- The use of XRS for monitoring and screening of inorganic contaminants in olive-oil, sunflower oil, fruit-juices together with other consumer products in compliance with Restriction of Hazardous Substances (ROHS).
- The improvement of instrumentation for imaging (large area detectors, better resolution of optical focusing devices).
- Characterization and elemental 3D imaging of biological samples.
- Improved field portable instrumentation and suitable in situ methodologies for cultural heritage investigations.

6. CONCLUSIONS AND RECOMMENDATIONS

The CRP has assisted Member States to improve characterization of materials by the utilization of nuclear spectrometry instruments and techniques. This has been achieved through the development of integrated/unified instruments and analytical methods which have been implemented by laboratory-scale and synchrotron facilities, thereby increasing the application of nuclear spectrometries across a wide range of disciplines, including environmental issues, industry, cultural heritage, human health, geology, biology, agriculture and food products.

Specifically, the CRP has developed/constructed/evaluated integrated multifunctional instruments based on these nuclear spectrometries, as well as new software for handling and operation of instruments including data acquisition, processing and presentation of data. This has greatly assisted new end-users across a broad range of disciplines to take advantage of these techniques.

Major accomplishments have been detailed in Table 1. Examples of multifunctional instruments that were successfully integrated include TXRF-EDXRF, SR-TXRF-XANES, PIXE-PIGE, PIXE-XRF, Micro-XRF and Micro-XRD, Portable XRF and Micro-Raman. These techniques have been successfully applied for instance to the analysis of Pre-Colombian and contemporary gold artifacts, discovery of hidden underlying Van Gogh in "Patch of Grass", identification of airborne-pollutants in New York Metropolitan Museum of Art and Krakow Royal castle and pigments in Manos and Susques caves in Argentina.

Furthermore, several areas have been identified which need to be addressed by future research including:

- Substantial inaccuracies of certain key fundamental atomic parameters, such as fluorescence yields, Coster-Kronig transition probabilities, ionization cross sections
- Strong need for well-characterized 2D and 3D micro-reference materials.
- Development of protocols for handling and operating instruments with different analytical range, resolution and sample characteristics for a broad range of materials.
- Handling and maintaining sample integrity during preparation and analysis.
- The improvement and evaluation of the cost-effectiveness of analytical techniques to optimize competitiveness of XRS.
- Development of new applications

Future research in these areas is therefore important and could be pursued in future CRP efforts.

The following recommendations resulted from the CRP:

(1) The outputs of this CRP should be made widely available to the analytical laboratories and potential users.
(2) Taking into account the advantages and uniqueness of XRS techniques, a support should be given to the efforts of States to establish, implement and effectively use these newly developed techniques, instruments and methodologies.
(3) Mechanisms are needed to support the efforts of XRS community in the determination of fundamental parameters, for example the international initiative on X ray fundamental parameters.
(4) The participants have identified significant new research areas (see details in Section 5) for possible support in the future.

COUNTRY REPORTS

COMPOSITIONAL CORRELATION BETWEEN PIGMENTS FOUND IN EXCAVATIONS AND ON HUMAN BONES INVESTIGATED WITH MICRO-RAMAN SPECTROMETRY AND SCANNING ELECTRON MICROSCOPY

C.VÁZQUEZ
Comisión Nacional de Energía Atómica (CNEA),
Buenos Aires,
Argentina

L. DARCHUK, E.A. STEFANIAK, R. VAN GRIEKEN
University of Antwerp,
Antwerp,
Belgium

O.R. PALACIOS
Facultad de Ingeniería,
Buenos Aires,
Argentina

Abstract

The results for prehistoric pigments from excavations and pigments on coloured child bones from North Patagonia, Argentina, are reported. To analyze their composition we used two micro-analytical techniques – micro-Raman spectrometry and scanning electron microscopy coupled with X ray detector.

1. Introduction

Analyses of ancient paint pigments components could cast a light on ancient ritualistic ceremonies and pigment preparation technologies, applied by early social groups for their art [1–4]. The hypothesis of their peculiar life style demands evidence lines in order to draw out their variety and differences among them. One of the ways to reconstruct the life style of this ancient society is investigation of prehistoric pigments.

The objects of investigation presented here are excavated prehistoric pigments and coloured child bones found in North Patagonia, This region is located to the South of the Colorado River, including Río Negro and El Neuquén provinces.

The pigment powders were collected in the Carriqueo rock shelter archaeological site and the colored bones of newborn come from Traful I cave. The buried remains of a baby (Fig. 1) have been found in the archaeological layer corresponding to the period of about 8000–9000 years ago. The skeleton was laid on its back. All bones, including the ribs, were completely articulated [5]. Significantly, the head and the first cervical vertebra were missing.

FIG. 1. Skeleton (black-white photo) and pictures of coloured child bones.

Additionally, on both scapulas some vertebrae and ribs and one humerus (upper arm bone), reddish-brown spots, dark blue and black areas were observed. These facts can suggest a secondary funeral or some type of a ritual ceremony.

The task of our investigation was to determine and to compare the composition of prehistoric pigments from excavated layers and pigments covering child bones to assess origin and production techniques, as well as to investigate the recurrence of the pigments used in the region [6–12].

We used two micro-analytical techniques, micro-Raman spectrometry (MRS) to look for molecular composition and scanning electron microscopy coupled with energy-dispersive X ray detector (SEM/EDX) to detect the average elemental composition of the investigated samples. For the study of cultural heritage objects, MRS is one of the most informative methods [13, 14].

2. Experimental

Prehistoric pigments samples were collected from different layers of an excavation. First of all the pigment samples were divided into several colour groups according to different shades of yellow, orange, red and brown; one pigment was green. When looking at the red pigment samples, different shades could be distinguished, ranging from orange to dark red. Colour indices were assigned according to Munsell Soil Charts [15].

MRS measurements were carried out by a Renishaw InVia unit with laser excitation at 785 nm, in the range between 100 and 3200 cm^{-1} with a spectral resolution of 2 cm^{-1}. Spectrum accumulation was used to improve the signal-to-noise ratio.

Elemental analysis of the prehistoric pigments was performed on a JEOL JSM 6300 SEM (JEOL, Tokyo, Japan) equipped with a backscattered electron detector (BSE), a secondary electron detector (SE) and an energy dispersive X ray detection system was used. A Si (Li) X ray detector PGT (Princeton Gamma Tech, Princeton, NJ, USA) was employed for acquiring the X ray spectra. Accelerating voltage: 20 kV, current: 1 nA.

3. Results and discussion

The Raman spectra collected from reddish spots show a weak haematite (iron (III) oxide, α-Fe_2O_3) band at 296 cm^{-1} and a typical band of magnetite (Fe_3O_4) at 680 cm^{-1}. Usually red ochre has been found in adult burials as a sign of special funeral ceremony. This natural mineral consists of hematite (Fe_2O_3) as a red pigment.

Strong sharp bands in the spectral region appear at 500–600 cm^{-1} and 1300–1600 cm^{-1}; bands at 520 cm^{-1} and 550 cm^{-1} correspond to calcium oxalate (whewellite $CaC_2O_4 \times H_2O$ and weddellite $CaC_2O_4 \times 2H_2O$) . The intense band at 1460–1490 cm^{-1} is the result of overlapping of three bands: 1464, 1477 and 1490 cm^{-1} and can be assigned to the C=O symmetric stretching mode of whewellite and weddellite. These detected calcium oxalates could be explained by the reaction of calcium carbonate with oxalic acid produced by lichens present in this site with a humid atmosphere on the surface of the child bones [16–21].

The Raman shift at 964 cm^{-1} is ascribed to the phosphate stretching mode of hydroxyapatite. Bone tissue is represented by apatite material that contains also carbonate components — carbonate hydroxyapatite, with an approximate formula $Ca_{10}(PO_4)_6(OH)(CO_3)$.

The elementary composition of coloured child bone surface revealed by SEM/EDX shows a high content of Ca and P corresponding to bone hydroxyapatite, whewellite and weddellite. SEM analysis also demonstrates the presence of such elements as Fe, Al, Si, K, Na, Mg, Mn, which are main components of the visible reddish spots on the bone.

Elemental analysis of the prehistoric pigments was fulfilled by SEM/EDX. For yellowish, reddish, brown, beige pigments we detected Ca, C, O, Mg, Fe, Si, K, Na. Several pigments contain S and Mg. This set of elements can form the following minerals: haematite, jarosite, magnetite, and, additionally, phosphate compounds.

As a result of SEM/EDX analysis we can conclude that their basic component is yellow (colouring mineral is goethite) or red ochre (colouring mineral is haematite) [22]. They also contain inclusions of some minerals, such as jarosite, magnetite, oxalates, phosphates (see Table 1). These minerals have suitable hardness to be powdered and used for paint pigments.

TABLE 1. MINERALS WITH SUITABLE COMPOSITION AND HARDNESS FOR PREHISTORIC PIGMENTS CONSISTENT

Mineral	Colour	Hardness
Red ochre Fe_2O_3 +clay+silicate	red	1,5–2 as talc-gypsum
Goethite FeO(OH)	red-brown	1,5–2 as talc-gypsum
Erdit $NaFe^{2+}S_2 \times 2H_2O$	copper-red, red, black	2 as gypsum
Haapalaite $2(Fe, Ni)S \times 1,6(Mg, Fe^{2+})(OH)_2$	bronze red	1 as talc
Sideronatrite $Na_2Fe^{3+}(SO_4)_2(OH) \times 3H_2O$	yellow, yellow-brown, paleorange	1,5–2 as talc-gypsum
Metahohmannitr $Fe^{3+}_2[O(SO_4)_2] \times 4H_2O$	orange-yellow	1,5–2 as talc-gypsum
Palygorskite $(Mg, Al)_2Si_4O_{10}(OH) \times 4H_2O$	red-yellow	2–3 as gypsum -calcite

Vashegytite $Al_{11}(PO_4)_9(OH)_6 \times 38H_2O$	red-brown	2–3 as gypsum -calcite
Jarosite $KFe_3(SO_4)_2(OH)_6$	amber yellow or brown	2,5–3,5 as calcite
Whewellite $CaC_2O_4 \times H_2O$	white	3 as calcite
Weddellite $CaC_2O_4 \times 2H_2O$	white	3 as calcite

Elementary composition analysed by SEM/EDX demonstrated strong similarity among pigments with the same colour shade, e.g. vinous – brown **2** and **26** or yellow – gold **8** and **9**. For two groups of pigments (pigments **13** and **20** and pigments **10**, **11** and **24**) the different elemental composition was detected, although these pigments have the same colour shade. They were probably prepared and used by different ancient social groups in different time periods.

The results of elementary investigation allow us to suppose that green-grey pigment may be formed by glauconite (terre-verte) $(K, Na)(Fe, Al, Mg)(Al, Si)Si_3O_{10} \times (OH)_2$ — (coloured components – iron hydrates, magnesium oxide hydrate) and aluminosilicates

The chemical composition of the pigment **24** was compared to the element content of the pigment visible on the child bone as reddish spots. It revealed a similar Al/Fe/Mg ratio: 17.1/13.2/1.6 for pigment **24** and 19/14/2 for the reddish bone spots. It is very likely that the same pigment was used for funeral ceremony of the child. In case of the other investigated pigments, the concentration of iron is higher than that of aluminium.

4. Conclusion

The basic component of the investigated prehistorically pigments is yellow or red ochre containing iron oxides, which can give yellow, red or brown colours. The elements determined as major components (Fe, Al, Si, K, Na, Mg, P) can form hematite, goethite, jarosite, magnetite, and phosphates compounds.

Several groups of prehistorically pigments have the same colour shade but different elemental and molecular composition which can be explicated that they were prepared and used by different groups in different time period.

Based on the chemical composition of the investigated pigments we selected one red-brown pigment which was characterised by a similar elemental content ratio obtained for the pigment covering the prehistoric child bones. This information suggests us to conclude that this pigment was employed for some ritual burial ceremony by ancient social groups living in this region. In addition, considering that the Carriqueo rock shelter and Traful 1 cave are more than 50 km away and separated by the Limay river, these results demonstrate that this geographical situation was not a barrier for inhabitants of the North Patagonian region. On the other hand, evidences of the use of similar pigments for rock paintings and drawings in this area have been mentioned by several authors [17].

REFERENCES

[1]   CHALMIN, E., MENU, M., VIGNAUD, C., Analysis of rock art painting and technology of Palaeolithic painters, Meas. Sci. Technol. **141** (2003) 590–1597.

[2]   LEWIS-WILLIAMS, J.D., DOWSON, T.A., The signs of all times: entropic phenomena in Upper Palaeolithic art, Current Anthropology **29** (1988) 201–245.

[3]   EDWARDS, H.G.M., DRUMMOND, L., RUSS, J., Fourier-transform Raman spectroscopic study of pigments in native American Indian rock art: Seminole Canyon, Spectrochimica Acta A: Molecular and Biomolecular Spectroscopy **54** (1988) 1849–1856.

[4]   CHALMIN, E., MENU, M., VIGNAUD, C., Analysis of rock art painting and technology of Palaeolithic painters, Meas. Sci. Technol. **14** (2003) 1590–1597.

[5]   CRIVELLI MONTERO, E.A., CURZIO, D., SILVEIRA, M.J., La estratigrafía de la Cueva Traful I (provincia del Neuquén), Præhistoria **1** (1993) 9–160.

[6]   LANATA, J.L., Zonas de explotación de recursos en Cueva Traful I. Comunicaciones Primeras Jornadas de Arqueología de la Patagonia; Rawson, Trelew (1987) 145–152.

[7]   LANATA, J.L., Paleoenvironments and hunting zones at Cueva Traful I, MS in the possession of the author.

[8]   PEARSON, P., Mice and the postglacial history of the Traful Valley of Argentina, J. Mamm. **68** (1987) 469–478.

[9]   PALACIOS, O., RAMOS, M., Alero Carriqueo: análisis de una muestra de instrumentos líticos. Resumen en Actas del VIº Congreso Argentino de Americanistas, Buenos Aires, Argentina (2008) 80.

[10]   CRIVELLI MONTERO, E.A., CORDERO, A., PALACIOS, O., RAMOS, M., Especialización funcional de sitios durante el período ceramolítico de la cuenca del río Limay: el caso del alero Carriqueo, Actas del XVI Congreso Nacional de Arqueología Argentina, Argentina **3** (2007) 339–345.

[11]   EINWOGERER, T., et al., Upper Palaeolithic infant burials, Nature **444** (2006) 285–286.

[12]   MARSHACK, A., Paleolithic Ochre and the Early Uses of Color and Symbol, Current Anthropology **32** (1981) 188–191.

[13]   COUPRY, Cl., Application of Raman microspectrometry to art objects, Analysis **28** (2000) 39–46.

[14]   BELL, I.M., CLARK, R.J.H., GIBBS, P.J., Raman spectroscopic library of natural and synthetic pigments (pre- ~ 1850 AD), Spectrochimica Acta Part A **53** (1997) 2159–2179.

[15]   Munsell Soil Color Charts. Munsell Color. New Windsor, Macbeth, United States. 1994.

[16]   DEL MONTE, M., SABBIONI, C., ZAPPIA, G., The origin of calcium oxalates on historical buildings, monuments and natural out-crops, Science of the Total Environment **67** (1987) 17–39.

[17]   VÁZQUEZ, C., et al., Pigment characterization by scanning electron microscopy and X ray diffraction techniques: archaeological site El Trebol, Nahuel Huapi, Rio Negro, Argentina, Report IAEA/AL/ **181** (2007) 29–34.

[18] WATCHMAN, A.L., A summary of occurrences of oxalate-rich crusts in Australia, Rock Art Res. **7** (1990) 44–50.

[19] WATCHMAN, A.L, Age and composition of oxalate-rich crusts in the Northern Territory. Australia, Stud. Conserv. **36** (1991) 24–32.

[20] SCOTT, D.A., HYDER, W.D., A study of some Californian Indian rock art pigments, Stud. Conserv. **38** (1993) 155–173.

[21] RUSS, J., KALUARACHCHI, W.D., DRUMMOND, L., EDWARDS, H.G.M., The natural of a whewellite-rich rock crust associated with pictographs in Southwestern Texas. Stud. Conserv. **44** (1999) 91–103.

[22] DARCHUK, L., et al., Composition of pigments on human bones found in excavations in Argentina studied with micro-Raman spectrometry and scanning electron microscopy. e-PRESERVATION Science **6** (2009) 112–117.

BLACK PIGMENTS OF ROCK ART: IDENTIFICATION OF INORGANIC AND ORGANIC COMPONENTS BY COMBINING ANALYTICAL TECHNIQUES

C. VÁZQUEZ
Comisión Nacional de Energía Atómica (CNEA), Buenos Aires, Argentina

M.S. MAIER, S.D. PARERA
UMYMFOR and Departamento de Química Orgínica, Universidad de Buenos Aires,
Buenos Aires, Argentina

H.D. YACOBACCIO, P. SOLA
Instituto de Arqueología, Universidad de Buenos Aires, Buenos Aires, Argentina

Abstract

Archaeological samples are complex in composition since they generally comprise a mixture of materials submitted to deterioration factors largely dependent on the environmental conditions. Therefore, the integration of analytical tools such as TXRF, FT-IR and GC-MS can maximize the amount of information provided by the sample. Recently, two black rock art samples of camelid figures at Alero Hornillos 2, an archaeological site located near the town of Susques (Jujuy Province, Argentina), were investigated. TXRF technique, selected for inorganic information, as well as FT-IR and GC-MS were employed in order to discover inorganic and organic composition of the black pigments.

1. Introduction

Studies on rock art have an outstanding role in the development of Argentine archaeology, but only a few attempts have been made to analyze the chemical composition of the paints used.

Following up with these studies about the components of prehistoric rock paintings, the inorganic and organic components of two black rock art samples from the archaeological site Alero Hornillos 2 (23º 13' 47'' S, 66º 27' 22'' W) were investigated. It is located in the Quebrada Agua Dulce about 20 km northern of the town of Susques (Jujuy Province, Argentina), at 4020 m above sea level.

The complete rock art represented on these cave walls is painted in black and in red colours (from reddish yellow to dark red). These plain paintings constitute a simple panel with 17 almost complete figurative camelid figures and five schematized human figures. There are, at least, three types of camelids: two legs black, four legs black and four legs red. All representations are stylized, non-schematized small figures (Fig. 1). The paintings show superposition of black and red figures, suggesting two manufacturing events: the first would be the four-legged red camelids associated with the red anthropomorphic figures and the second the four-legged black camelids. The two-legged camelids are not superimposed to any red figure, but their execution could be associated with the other black motives. TXRF was then selected as a micro-analytical technique for the inorganic characterization of the pigment [1]. This technique is specially recommended, considering the small amount of sample (a few micrograms) required for the analysis and the low detection limit achieved (in the part per billion range).

FT-IR helps in a preliminary identification of the main molecular constituents present in organic residues and in the selection of conditions of sample preparation for further analysis by a more informative technique, such as GC-MS [2]. In order to search for the presence of

organic compounds as binders, a combination of these spectroscopic and chromatographic techniques were employed in both black painting samples.

The purpose of this work was to determine the nature of the black pigment, painting preparation and application in order to enlarge the understanding of the artistic practices and technological knowledge of the early inhabitants of this area in the northern region of Argentina.
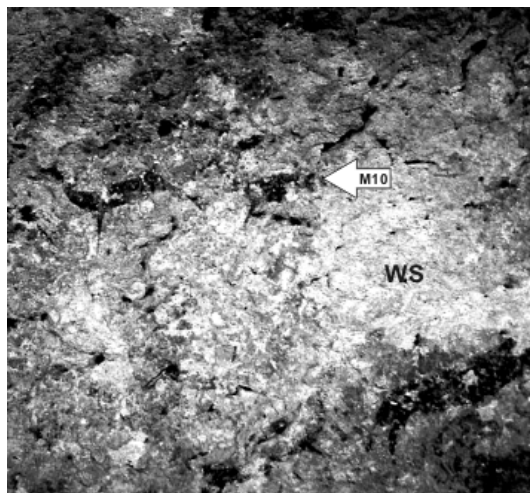
FIG. 1. Black camelid figures. The arrow points out the extraction site of the M10 black painting sample from one of the two legs camelids. WS indicates rock weathered sector.

2. Experimental

2.1. Instruments

For TXRF measurements, an X ray Fluorescence spectrometer, composed of a Philips generator, equipped with a fine focus Mo X ray tube was employed. Total reflection was achieved by a TXRF module designed by the Atominstitut der Österreichischen Universitäten.

Infrared spectra were obtained on a Nicolet Magna 550 Fourier transform spectrometer. For each sample 32 scans were recorded in the 4000 to 400 cm^{-1} spectral range in the transmittance mode with a resolution of 4 cm^{-1}. GC was performed on a Hewlett-Packard 5890A chromatograph equipped with a flame ionization detector and an ULTRA 2 column (30 m $\times$ 0.25 mm i.d.).

3. Conclusions

TXRF spectrum of sample M10 shows the presence of manganese (120 µg/kg for M10 and 180 µg/kg for M15) and iron (300 µg/g and 250 µg/g for M10 and M15, respectively) among other major elements (sulfur and calcium). Further elements (potassium, vanadium, titanium, rubidium, strontium and zinc) detected, coming from the rock support, are unfailingly present in the taken samples. The high calcium and sulfur contents confirm the presence of gypsum, also identified by FT-IR analyses, commonly used in rock paintings as an inorganic extender of the pigment. The manganese content in both samples could be ascribed to manganese dioxide used as a black pigment in rock art or to the presence of an umber, that is a dark

earthy pigment containing manganese oxides in addition to iron oxides [3, 4]. The association of iron and manganese in mineral phases is very common in nature and, in the region of Susques where the archaeological site Hornillos 2 is located, there are numerous sources of this kind [5–7]. This information together with the detected presence of manganese and iron in both samples suggest that the black pigment is an iron and manganese oxide.

Looking for any lipidic residual organic compounds, fragments of both black samples were extracted with a chloroform/methanol (2:1) mixture. Both samples contained appreciable quantities of organic compounds: 962 μg/g (M10) and 36780 μg/g (M15). The extracts were analysed by FT-IR showing the presence of organic components, most likely lipids. The most important features were the presence of a broad carbonyl absorption band at 1729 cm^{-1} together with bands attributable to C-H stretchings of CH_3 and CH_2 groups at 2934–2861 and 1466–1387 cm^{-1}. The carbonyl band at 1729 cm^{-1} could arise from fatty acids or from acylglycerol groups. FT-IR spectra of vegetable oils and animal fats contain a strong, sharp carbonyl band at 1750–1740 cm^{-1} due to the ester group while fatty acids of these sources show the carbonyl band around 1715 cm^{-1}. Therefore, broadening of the carbonyl band at 1729 cm^{-1} in the spectra of the organic extracts of samples M10 and M15 indicate the presence of acylglycerides of plant and/or animal provenance together with the formation of free fatty acids by hydrolysis.

Analysis by GC-MS of the carboxylic acid methyl esters prepared from the lipids extracted from the black painting samples (M10 and M15) showed that the main organic constituents were palmitic ($C_{16:0}$) and stearic ($C_{18:0}$) acids together with minor saturated ($C_{14:0}$, $C_{15:0}$, iso-$C_{16:0}$, $C_{17:0}$) and unsaturated ($C_{16:1}$ and $C_{18:1}$) fatty acids. The fatty acid distribution in both samples, with a greater abundance of palmitic acid ($C_{16:0}$) than stearic acid ($C_{18:0}$), is typical of degraded animal fats. The small amounts of odd carbon numbered, straight-chain compounds, specifically $C_{15:0}$ and $C_{17:0}$, as well as the presence of branched-chain iso-$C_{16:0}$ point to a ruminant animal source due to microbial activity in their digestive system. The presence of bone remains of South American camelids, such as vicuna (*Vicugna vicugna*) and guanaco (*Lama guanicoe*), in the archaeological record of the site reinforces this assumption. These bone remains show evidences of having been processed in order to extract the marrow content and the fat of the trabecular tissue.

The GC-MS total ion chromatogram of the fatty acid methyl esters of the lipids extracted from sample M10 also showed the presence of minor saturated hydrocarbons of 22, 23, 24 and 25 carbons and a mixture of coeluting 24-methylcholestane (M^+=386) and 24-methylcholestene (M^+=384). Sample M15 contained, in addition to fatty acid methyl esters, minor hydrocarbons and cholestane (M^+=372), characterized by its molecular ion and an intense peak at m/z 217 in its mass spectrum. The presence of n-alkanes together with steranes and sterenes, presumably derived from sterols in higher plants [8], is not easy to explain. These compounds are characteristic components of bitumens, mixtures of complex natural hydrocarbons and oxidized products that have been used as adhesives [9], embalming materials [10] and as black pigments [11, 12].

This paper has demonstrated that the combination of these three analytical techniques (TXRF, FT-IR, GC-MS) allowed a complete characterization of the inorganic and organic components of both black rock paintings. In nature, the geochemical affinity relating iron and manganese elements enhances a variety of earthy pigments or rich clay materials, where the dark colour is due to manganese oxides. These oxides associations were frequently used in rock art as black pigments. Their naturally occurrence in mineral ores and different kinds of Earth's crust deposits is common in this region. The large gypsum content in the two painting samples is

consistent with the ancient mode of making these wall representations. However, one of the most significant results of this investigation is the fact that the inorganic phase of these paintings contains measurable amounts of organics components. The presence of lipids in the organic residues associated to the rock paintings and the fatty acids distribution suggest an animal source as a potential binder in the preparation of the paints. The presence of unsaturated fatty acids ($C_{16:1}$ and $C_{18:1}$) in the archaeological samples from Hornillos 2 indicates that the lipids were preserved under the favourable dry environmental conditions of the Puna region. The results obtained in this investigation induce us to suggest that the early inhabitants of this region employed at least three principal components to prepare their black painting mixtures: (1) iron and manganese oxide (the pigment), (2) gypsum (the extender), and (3) an animal fat (the binder). Apparently, the paint recipes of these cave-wall figures were the same for both black camelid types, suggesting that both types were painted in a short period of time [13]. Besides, the identification of gypsum in both samples allowed us to infer that the painting pigment preparation consisted in grinding and mixing the iron and manganese oxides and gypsum with a fluid animal fat as binder to perform the paintings. The results of this research are the first report on the inorganic and organic components of rock paintings in Northwestern Argentina and they contribute to enlarge the archaeological knowledge of this region.

Acknowledgements

REFERENCES

[1] VON BOHLEN, A., Total Reflection Flurescence Spectrometry: A Versatile Tool for Ultra-Micro Analysis of Objects of Cultural Heritage, (2004) e-Preservationscience 1: 23–34.

[2] REGERT, M., GARNIER, N., DECAVALLAS, O., CREN-OLIVÉ, C., ROLANDO, C., Structural characterization of lipid constituents from natural substances preserved in archaeological environments, Meas Sci Technol. **14** (2003) 1620–1630.

[3] HRADIL, H., GRYGAR, T., HRADILOVÁ, J., BEZDICKA, P., Clay and iron oxide pigments in the history of painting, Appl Clay Sci. **22** (2003) 223–36.

[4] HELWIG, K., (2007). Iron oxide pigments. Natural and synthetic. In Berrie BH (ed) Artists´pigments. A handbook of their history and characteristics. Volume 4 Archetype Publications, London.

[5] NULLO, F.E., (1988) Descripción geológica de la Hoja 4 a-b Susques, Provincia de Jujuy. SEGEMAR Argentina.

[6] TURNER, J.C., MÉNDEZ, V., (1979) Puna. Geología Regional Argentina. Volumen I. Academia Nacional de Ciencias, Córdoba.

[7] COIRA, B.L., Recursos Minerales de la República Argentina, SEGEMAR, Anales **35** (1999) 1557–1567. Buenos Aires.

[8] ZHOU, Y., et al., Triterpane and sterane biomarkers in the YA13-1 condensates from Qiongdongnan Basin, South China Sea, Chem Geol. **199** (2003) 343–359.

[9] WENDT, C.J., LU, S.-T., Sourcing archaeological bitumen in the Olmec region, J. Archaeol Sci. **33** (2006) 89–97.

[10] MAURER, J., MÖHRING, T., RULLKÖTTER, J., Plant Lipids and Fossil Hydrocarbons in Embalming Material of Roman Period Mummies from the Dakhleh Oasis, Western Desert, Egypt, J. Archaeol Sci. **29** (2002) 751–762.

[11] BOTHE, C.I., (2007) Asphalt. In Berrie B.H. (ed) Artists´pigments. A handbook of their history and characteristics. Volume 4 Archetype Publications, London.

[12] VAZQUEZ, C., MAIER, M.S., PARERA, S.D., YACOBACCIO, H., SOLA, P., Combining TXRF, FT-IR and GC-MS information for identification of inorganic and organic components in black pigments of rock art from Alero Hornillos 2 (Jujuy, Argentina), Anal Bioanal Chem. **391** (2008) 1381–1387.

[13] VAZQUEZ, C., et al., Total reflection X ray fluorescence and archaeometry: Application in the Argeninean cultural heritage. Spectrochimica Acta Part B **63** (2008) 1415–1419.

X RAY ANALYSIS USING SYNCHROTRON RADIATION

C. STRELI, F. MEIRER, P. WOBRAUSCHEK, N. ZOEGER,
Atominstitut, TU Wien, Vienna, Austria

G. PEPPONI
Fondazione Bruno Kessler, Povo, Italy

Abstract

X ray Absorption Near Edge Structure (XANES) analysis was used in combination with Total reflection X ray Fluorescence (TXRF) and micro X ray Fluorescence (µ-XRF) analysis at different Synchrotron Radiation (SR) facilities to perform elemental analysis and speciation at trace levels. TXRF-XANES was used to perform analysis of contaminations on Silicon wafer surfaces and determine the oxidation state of Fe. Urban aerosols were sampled size fractioned and the oxidation state of Fe was determined for each impactor stage again using TXRF-XANES. Confocal µ-XRF was used to localize Pb and Zn at articular cartilage sampled from osteoarthritic human bones. The combination with XANES allowed identifying the oxidation state of Pb at the tidemark between articular and calcified cartilage. The feasibility of XANES analysis at trace levels using different SR-XRF setups was demonstrated.

1. Introduction

The X ray group of the Atominstitut in the research area "Radiation Physics" is working since years on the development of special techniques in X ray Spectrometry. Research focuses on the field of TXRF, angle resolved grazing incidence XRF for depth profiling and µ-XRF; all techniques are used with laboratory as well as synchrotron radiation sources. Due to its properties the latter is not only highly beneficial for XRF analysis in general but enables a combination of these techniques with X ray Absorption Spectroscopy (XAS) to perform chemical speciation by determining parameters related to the local atomic structure of the sample.Investigations range from environmental samples, Si wafer surfaces, medical samples to fine art samples.

Topic of the proposed research was the integration of specific analytical X ray techniques using synchrotron radiation as excitation source. It covered synchrotron radiation induced TXRF (SR-TXRF) and µ-XRF in confocal as well as conventional mode for elemental 2D and 3D X ray imaging. Both setups have been combined with absorption spectroscopy (XANES) in fluorescence mode for chemical speciation.

2. Overview of the research performed and the results obtained

2.1. *Speciation of Fe on Si wafer surfaces with SR-TXRF XANES*

SR-TXRF-XANES was used to determine the chemical state of Fe contaminations on a silicon wafer surface. The ability to characterize chemically the contamination on silicon wafers is of critical importance to the semiconductor industry. It provides information on possible unwanted chemical processes taking place on the wafer surface and helps in determining the true source of the contamination problem. This type of information is not readily accessible with standard laboratory equipment. Main purpose of the study was to test the method for a contamination issue as it could appear in a microelectronic VLSI (Very-Large-Scale Integration) production fab. This project was done in cooperation with M.A. Zaitz, IBM Microelectronics, Hopewell Junction, NY, USA.

SR-TXRF XANES measurements were performed at the bending magnet beamline L at HASYLAB using the Si(111) double crystal monochromator and a modified micro-XRF setup. The vacuum chamber was removed and the wafer mounted on an x,y,z,θ-stage. This modified setup allowed TXRF measurements with scanning capability. A laminar flow hood was used to prevent contamination during the measurement (Fig. 1). Prior to the SR-TXRF-XANES analysis the wafer has been mapped using a laboratory TXRF analyzer (Rigaku TXRF 300) to determine regions of interest showing the highest Fe contaminations (Fig. 2).

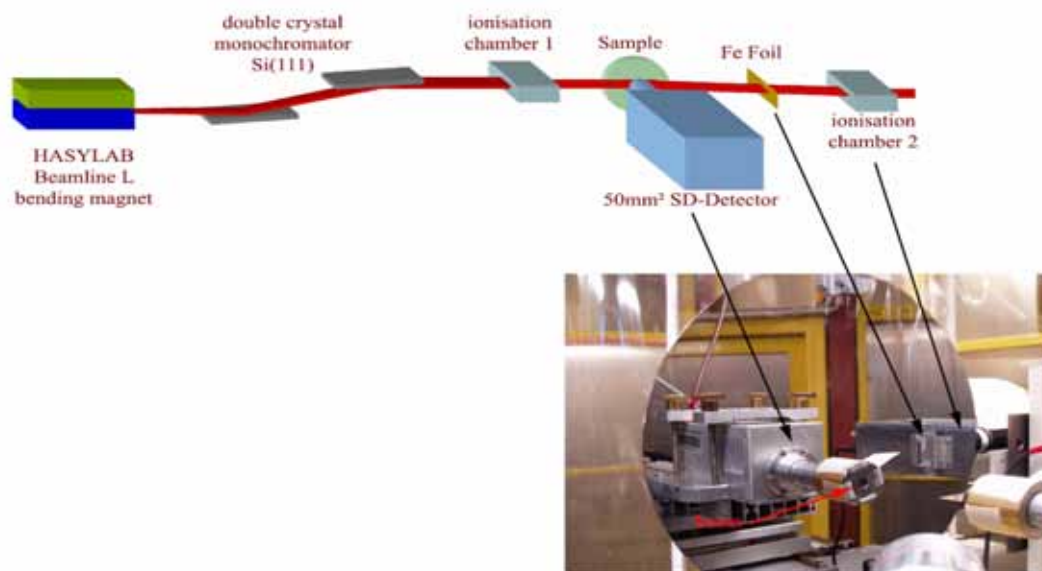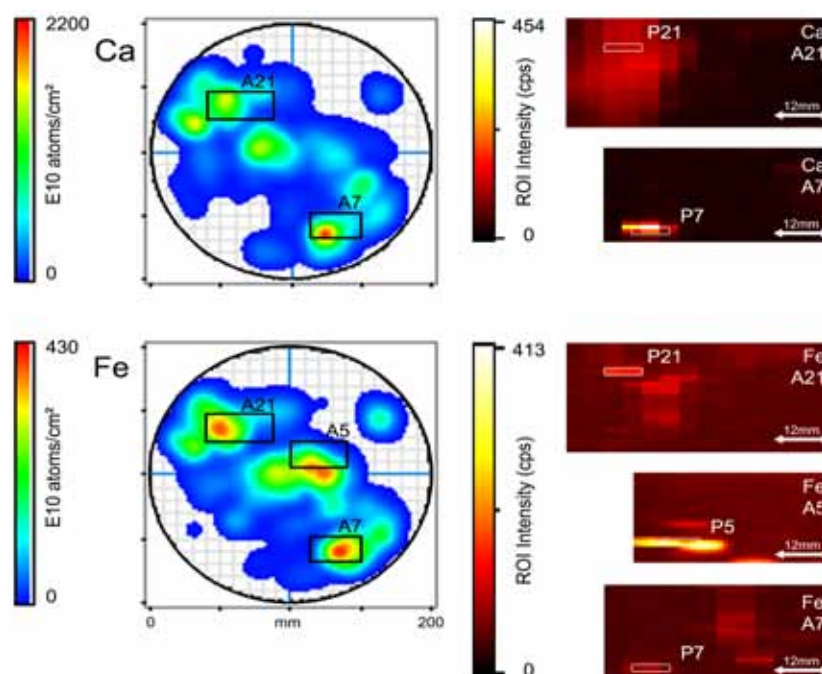*FIG. 1. Experimental setup at Hasylab, Beamline L (adapted from Ref. [1]).*

FIG. 2. Laboratory TXRF maps (left) with marked regions of the areas scanned by means of SR-TXRF (right). The marked regions on the left correspond to the areas on the right. The white boxes on the right localize the points of maximum Fe contamination which were selected for further investigations (P21, P5 and P7), adapted from Ref. [1].

It could be shown that SR-TXRF in combination with XAS enables a XANES analysis of wafer surface contaminations even in the pg region within a reasonable time frame. The setup allowed a spatially resolved multi-element analysis of the wafers surface. Additionally the type of the contamination (residual, surface layer, bulk) and the chemical state of a specific element could be determined. All these investigations can be done non-destructively using the same experimental setup. The major problem of this setup is the measurement time and the need for an intense and energy tunable X ray source. The wafer mapping and XANES scans are time consuming particularly for such low sample masses. The XANES evaluation showed, that a peak to background ratio below 10 for the element of interest in the fluorescence spectra will cause serious problems for the interpretation of the data. Within the time frame of 48 hours 3 points of interest could be investigated. A determination of the oxidation state of iron in the samples was possible (Table 1).

TABLE 1. OXIDATIONS STATES AND EDGE POSITIONS OF STANDARDS AND SAMPLES, ADAPTED FROM REF. [1]

	Compound	Edge Position [eV]
FeS	Iron(II)-sulfide	7117
FeCl2	Iron(II)-chloride	7119
FeSO4	Iron(II)-sulfate	7119.5
Fe3O4	Iron(II,III)-oxide	7119.5
FeC2O4	Iron(II)-oxalate	7120.5
(NH4)2Fe(SO4)2	Ammonium-Iron(II)-sulfate	7122.5
NH4Fe(SO4)2	Ammonium-Iron(III)-sulfate	7123
Fe2O3	Iron(III)-oxide	7123.5
Fe(NO3)3	Iron(III)-nitrate	7125
Fe2(SO4)3	Iron(III)-sulfate	7126
Wafer at P5	Fe(III)	7125
Wafer at P7	Fe(II)	7121.5
Wafer at P21	Fe(III)	7124.5

However, for the determination of the iron compound satisfactory results could be achieved for only one point (P5). The evaluation of the other points (P7, P21) using a linear

combination fit procedure was not satisfying due to the low Fe concentrations and the limited measurement time resulting in a poor signal to noise ratio of the XANES spectra.

The evaluation of the XAS data revealed that the iron contamination in point P5 was a mixture of iron compounds dominated by iron-nitrate (Table 2).

TABLE 2. RESULTS AND FIT PARAMETERS OF THE BEST FIT FOR P5 ADAPTED FROM REF. [1]

	Fe2O3 [%]	Fe(NO3)3 [%]	Fe2(SO4)3 [%]	R-factor	Chi-square
P5	26 ± 7	48 ± 8	26 ± 10	0.001424	0.1478

Although the evaluation for P5 showed a low statistical uncertainty (Fig. 3) it could not be concluded that the contamination is a mixture of iron-nitrate and iron-sulfate exclusively. Within the frame of this feasibility study it was not possible to compare the Fe contaminations with every possible Fe compound. However, the presence of iron-nitrate and iron-sulfate on a contaminated wafer shows that several chemical reactions are taking place. The iron-sulfate is particularly surprising and we are trying to better determine why or how it was formed. This will be topic of further investigations. Details can be found in Ref. [1].
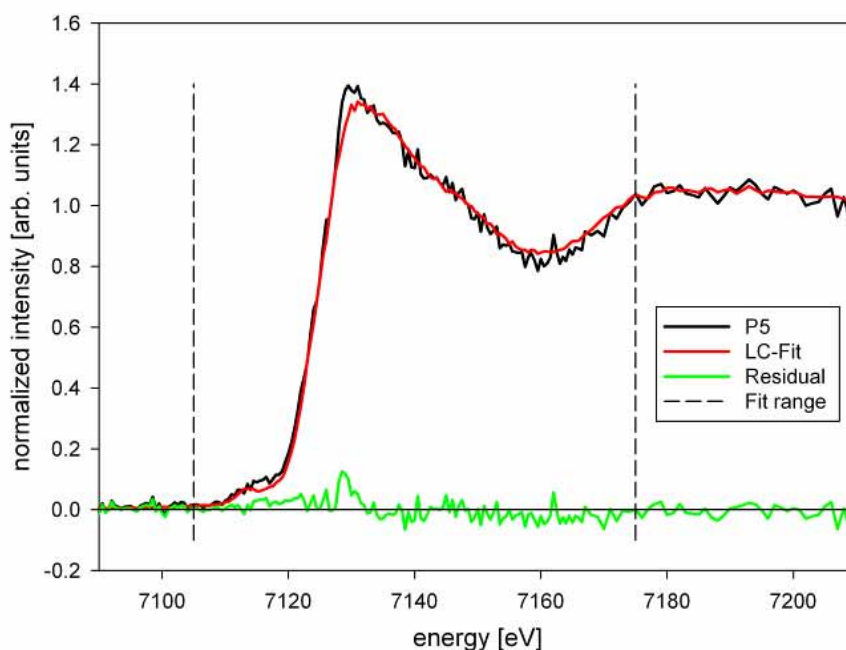

FIG. 3. Result of the best linear combination fit for sample P5, adapted from Ref. [1].

2.2. Fe K-edge TXRF-XANES of atmospheric aerosols collected in the city of Hamburg

To understand the effects of aerosols on human health and global climate a detailed understanding of sources, transport, and fate as well as of the physical and chemical properties of atmospheric particles is necessary. An analysis of aerosols should therefore provide information about size and elemental composition of the particles and - if desired - deliver information about the chemical state of a specific element of interest in the particles. Using the combination of SR-TXRF and XANES analysis it was possible to investigate the elemental composition of size fractioned atmospheric aerosols and the oxidation state of Fe in the aerosols even for small sample amounts due to short aerosol collection times. This project was accomplished in cooperation with Prof. J.A.C. Broekaert and Dr. U.E.A. Fittschen, Department of Chemistry, University of Hamburg, Hamburg, Germany.

The aerosols were collected in the city of Hamburg with a low pressure Berner impactor (Fig. 4 left) on Si carriers covered with silicone (to prevent "bounce off" effects) over time periods of 60 and 20 min each. The particles were collected in four and ten size fractions of 10.0–8.0 μm, 8.0–2.0 μm, 2.0–0.13 μm 0.13–0.015 μm (aerodynamic particle size) and 15–30 nm, 30–60 nm, 60–130 nm, 130–250 nm, 250–500 nm, 0.5–1 μm,1–2 μm, 2–4 μm, 4–8 μm, 8–16 μm. SR-TXRF measurements were performed using the setup for TXRF comprising a vacuum chamber at HASYLAB bending magnet beamline L equipped with a sample changer capable of carrying eight samples at a time.

The results from the SR-TXRF analysis of the aerosols showed that 20 min of sampling time gave still enough sample material for elemental determination of most elements. Fe K-edge SR-TXRF-XANES analysis of the samples revealed that Fe was present in the oxidation state of three (predominately in the form of Iron(III)-oxide) in all collected aerosols (Fig. 4 right).
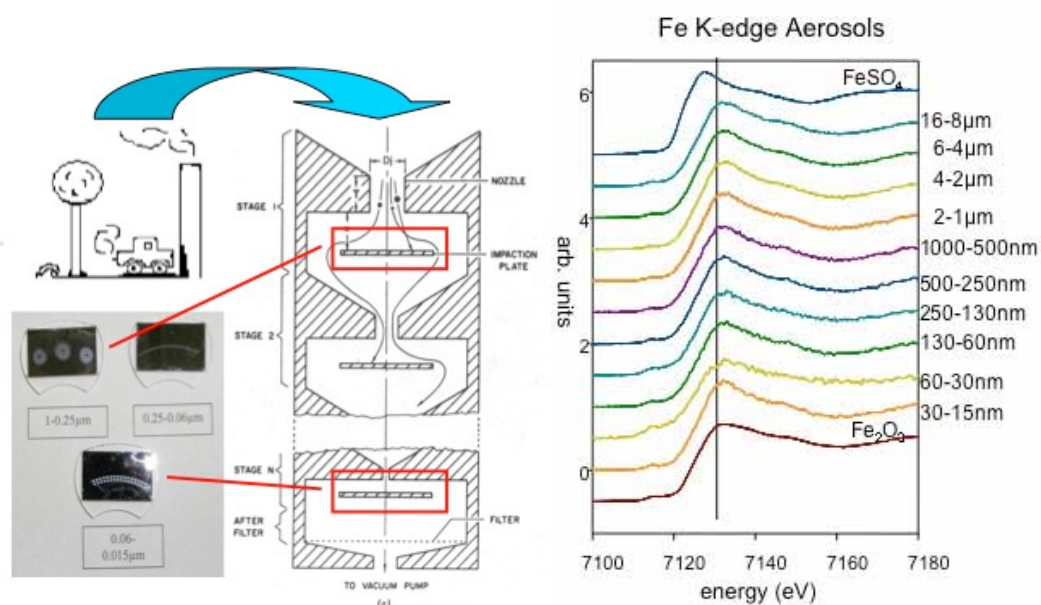

FIG. 4. Left: Principle of size fractioned direct sampling on Si wafers with a Berner impactor. Right: XANES Spectra of impactor stage. Adapted from Ref. [2].

This corresponds to other studies on the oxidation state of Fe in aerosols although in rain and cloud samples high amounts of Fe(II) were reported. Possible reasons why exclusively Fe(III) was found in the aerosols analyzed here may be the place or the height where the aerosols have been collected, or some oxidation which may have occurred during the condensation process. Finally it can not be excluded that oxidation took place during storage or sampling, even though the sampling time was kept short and the samples were stored under Argon atmosphere. Further studies will have to focus on these problems. Details can be found in [2].

One of the main threats to human health from heavy metals is associated with exposure to lead (Pb), which is associated with chronic diseases in the nervous, hematopoietic, skeletal, renal and endocrine systems. Once incorporated through ingestion or inhalation, Pb accumulates in the skeleton. However, little is known about how Pb is distributed in calcified tissue on the microscopic level. Therefore our group studied the distribution of Pb in human bones slices using synchrotron radiation induced micro X ray fluorescence analysis (SR μ-XRF) in scanning and tomographic mode. The project is performed in cooperation with the Ludwig Boltzmann-Institute of Osteology, Vienna, Austria.

Results were obtained by using the confocal microbeam setup at HASYLAB beamline L. With this setup a quasi-cubic detection volume, defined by the overlap of the focal cones of the two X ray optics (one in the primary beam, the second one in front of the energy-dispersive X ray detector) was used for analyses. Since this variant of SR μ-XRF offers the possibility to perform depth sensitive analysis it was used to determine the three-dimensional distributions of Pb and other (trace) elements in human bone with an resolution of about 10-20 μm (lateral and in depth).

2.3. Determination of the distribution of Pb in bone and cartilage of patients suffering from bone diseases

From this measurement a very local distribution of Zn and Pb at the tidemark (the border between non-mineralized and mineralized cartilage) could be detected. These novel results of the specific accumulation of Pb in the tidemark of human bone may lead to further understanding and research on the effects of Pb on cartilage, bone biology and biomineralization.

Osteoarthritis (OA), the clinical syndrome of joint pain and dysfunction caused by joint degeneration, affects more people than any other joint disease. The incidence of osteoarthritis rises precipitously with age; as a result, the prevalence and burden of this disorder is increasing rapidly. The histological disease pattern of OA in human joints includes fibrillation of articular cartilage, clefting, and cartilage loss. Besides cartilage lesions, a thickening of subchondral bone as well as tidemark duplication is observed in OA. The appearance of multiple tidemarks indicates additional cartilage calcification and it is believed to be a sign of increased turnover in the affected joint. To date very little is known about the role of trace elements in normal articular cartilage and subchondral bone and even less is known about their role in diseases such as osteoarthritis. In a recent study [3] we could demonstrate that the formation of tidemarks is accompanied by an accumulation of the trace elements lead (Pb) and zinc (Zn) at this zones of calcification in joint bones with no macroscopical signs of OA. The purpose of this study was to determine the elemental distribution, with special emphasis on Zn and Pb, in articular cartilage and subchondral bone from human femoral heads with different degrees of OA.

A pilot study with one osteoarthritic bone sample has shown that the typical duplication of the tidemark in case of OA using BSE imaging (Fig. 5). Interestingly a differential accumulation of trace elements when compared to the normal human samples as shown previously was found.
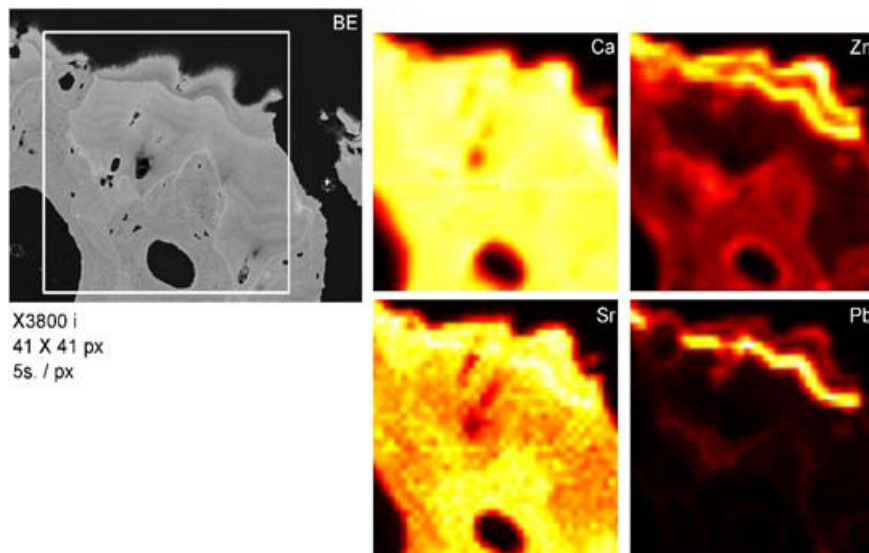
FIG. 5. BE image and elemental distribution of Ca, Zn, Sr and Pb in a human patella showing tidemark duplication. Distinct differences in the metal distribution patterns can be seen, when comparing to Figure 1 (single tidemark).

There is still a strong correlation between the distribution of Pb and Zn, but the intensity of Pb in the inner tidemark is 3-fold higher then in the outer one, while the Zn intensities are equal. The results shown suggest a correlation of the Zn and Pb intensities, but in case of double tidemark the Zn and Pb intensities are obviously not correlated. Compared to subchondral bone the Pb intensity from the inner tidemark is about 36-fold higher and Zn intensity is approximately 5-fold higher in both — the inner and outer tidemark. This shows that differences at the older and the younger tidemark can be detected with confocal SR-μXRF [4].

2.4. Determination of the oxidation state of Pb in articular cartilage

As explained the previous chapter it could be evidenced by applying SR μ-XRF in confocal mode that Pb accumulates very specifically in the tidemark. However, the mechanism of Pb storage in the tidemark is unknown. There are reports in literature, that Pb replaces Ca^{+2} ions in hydroxyapatite (HA), which could also be the mechanism of binding Pb at the tidemark. On the other hand the different chemical composition of articular cartilage (e.g. high S content) would allow for other Pb compounds, such as sulfates, sulfides, carbonates and oxides. Both, the differences in the composition, as well as the high affinity of Pb to HA motivate a study aiming the chemical speciation of Pb in the tidemark. Objective of this study was to use spatially resolved X ray absorption spectroscopy at the Pb-L_3 edge as a fingerprint method to determine the species of Pb at the tidemark. The project is performed in cooperation with the Ludwig Boltzmann-Institute of Osteology, Vienna, Austria.

Experiments have been carried out at the SUL-X Beamline at ANKA using μ-XANES in fluorescence mode. The continuous X ray spectrum from the wiggler has been monochromatized by a Si(111) double crystal monochromator. Focusing of the primary beam to a spot size of about 250×250 μm was accomplished by KB optics. μ-XRF line scans across the border between non-calcified and calcified cartilage have been performed to determine the position of the tidemark, which was the measurement position for the μ-XANES experiments. X ray absorption spectra have been recorded by tuning the excitation energy in 0.5 eV steps across the L_3 absorption edge of Pb (13035 eV) while measuring the Pb-Lα fluorescence signal with an 7-element SiLi detector. We could show that it is possible to perform Pb-LIII XANES at the tidemark of human articular cartilage. A set of standard Pb compounds, which were expected to be present in bone and cartilage have been prepared as pressed pellets and were analyzed in order to be compared with the results from the human bone sample: three Pb-substituted hydroxyapatites (one with increased carbonate content), three PbO compounds, $PbCl_2$, $Pb(NO_3)_2$, PbS, $PbCO_3$, $PbCO_3 \times Pb(OH)$, PbO_2, and $PbSO_4$. Preliminary results of the XANES analysis showed that Pb present in human bone is most likely bound to hydroxiapatite. The best agreement between XANES spectra of the sample and reference materials was found for carbonated HA (i.e. HA with increased carbonate content).

The XANES spectrum obtained at the tidemark show great similarity with XANES spectra obtained from Pb-HA (Fig. 6). But small deviations have been observed and need to be further investigated [5].
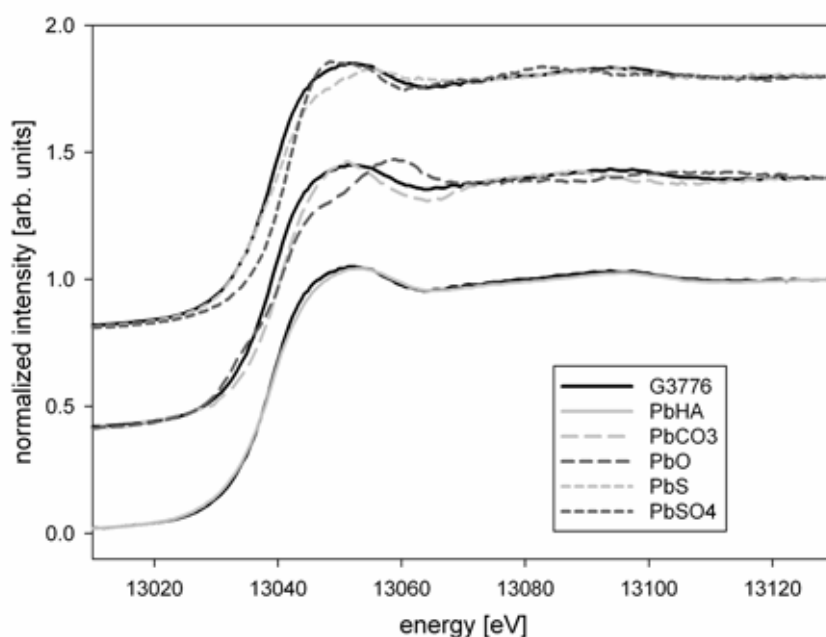
FIG. 6. Comparison of all measured reference substances and a human patella sample (G3776). The spectra are displaced vertically for clarity.

3. Conclusions

Within the frame of this CRP the successful integration of XRF using synchrotron radiation with absorption spectroscopy was demonstrated to combine the elemental analysis at trace

levels (SRTXRF) as well as with high spatial resolution (µ-XRF) with speciation (XANES). Several examples from industry, environment and medicine showed the applicability.

REFERENCES

[1] MEIRER, F., et al., Feasibility study of SR-TXRF-XANES analysis for iron contaminations on a silicon wafer surface, Surf. Interface Anal. **40** (2008) 1571–576.

[2] FITTSCHEN, U.E.A., et al., Characterization of Atmospheric Aerosols using SR-TXRF and Fe K-edge TXRF-XANES, Spectrochimica Acta Part B **63** (2008) 1489–1495.

[3] ZOEGER, N., et al., Lead accumulation in tidemark of articular cartilage, Osteoarthritis and Cartilage **14** 9 (2006) 906–913.

[4] ZOEGER, N., et al., Elemental Imaging in Osteoarthritis, Hasylab Annual Report 2006, 1283.

[5] MEIRER, F., PEMMER, B., STRELI, C., GÖTTLICHER, J., ANKA Project summary report, ENV92 Micro XANES in human bone and cartilage.

UNIFICATION OF PIXE, PIGE AND RBS ION BEAM ANALYSIS TECHNIQUES FOR USE AS A SINGLE PACKAGE FOR SAMPLE CHARACTERIZATION IN ENVIRONMENTAL AND MATERIALS RESEARCH

D. COHEN, R. SIEGELE, M. IONESCU
Australian Nuclear Science and Technology Organization (ANSTO),
Menai,
Australia

Abstract

The accelerator based ion beam analysis techniques of PIXE and PIGE using 2–3 MeV protons have been combined into one software analysis package which includes matrix corrections from PIGE for light elements being iteratively fed back into the matrix corrections for PIXE. This package can run in batch mode analysing hundreds of spectra at a time for elemental concentrations from fluorine to uranium to for concentrations from µg/g to 100%. This software package is called 'doiba' and has been published as an ANSTO external report. Future work is ongoing to include the proton Rutherford Backscattering technique as well into this doiba package particularly for carbon, nitrogen and oxide matrix corrections.

1. Introduction

ANSTO operates two accelerators: the 10 MV ANTARES accelerator (Fig. 1), and the 2 MV STAR accelerator (Fig. 2). Each of these has a number of beam lines and supporting facilities. These accelerators and their associated ion beam capabilities are the focus of the research for this particular project. ANTARES provides ion beams with energies from approximately 3 MeV to 100 MeV, depending on the ion species, with beam current intensities up to a few microamps. This facility has 3 ion sources for injection into the accelerator terminal, 3 high energy Accelerator Mass Spectrometry (AMS) beamlines and 2 high energy Ion Beam Analysis (IBA) beamlines including a state of the art world class high energy, heavy ion microprobe.

Applications include, surface and bulk analysis of solid state materials, environmental pollution monitoring, archaeological artefact elemental determinations, studies of pigment composition in paintings, biological studies using tracer elements and studies of geological material.

The STAR Tandetron accelerator can produce a wide range of light and medium ions, with energies from a few hundreds of keV to 6 MeV, and are used for a diverse range of activities in the fields of materials analysis, biological and environmental studies, as well as basic nuclear physics. The STAR accelerator also has an AMS ^{14}C beam line used for routine radio carbon measurements.

One beamline has a target chamber and data collection facility for simultaneous PIXE, PIGE and RBS. Sample holder can take up to 60 samples in vacuum and measurement of samples is automated.

A second IBA beamline is a Multi-Angle Detector Positioning System — XYZ Target Manipulator — UHV target chamber with charged particle detectors for depth profile measurements of light elements such as hydrogen, carbon and oxygen, using forward recoil and nuclear reaction techniques. These are used for measurement of water turnover in desert lizards using [18]O as a biological tracer, depth profiling of ion implanted species in semiconductors.

FIG. 1. ANTARES high energy end.
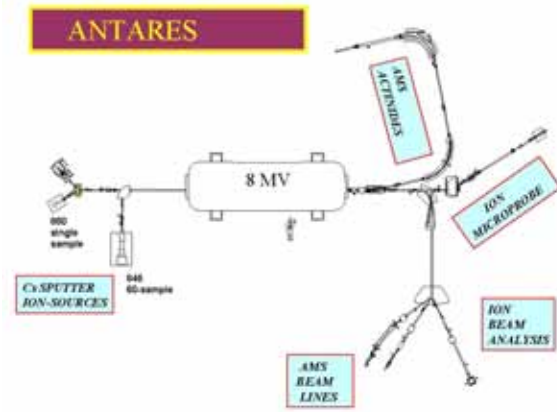
ANTARES beamline layout.

FIG. 2. STAR accelerator.

STAR beamlines.

All these techniques rely on MeV ions from low to medium positive ion accelerators. PIXE and PIGE are used for elemental analysis and RBS is used for depth profiling of elements in environmental, geological and functional materials samples. All these accelerator based ion beam analysis characterization techniques are non-destructive, have high sensitivity, are suitable for most elements in the periodic table and provide short measurement times.

It is well established that PIXE is mostly used for elements with atomic numbers above Al. For medium proton energies of a few MeV created by common ion beam accelerators, the PIGE technique is mostly suitable for light element analysis, like Li, Mg, Na and Al, where the cross sections for gamma ray production tend to be larger.

On the other hand, RBS is ideally suited for determining the depth distributions of trace elements heavier than the major constituents of the matrix or the substrate or for determining absolute matrix compositions for light elements such as carbon, nitrogen or oxygen.

We are currently developing the capability for using a combination of PIXE, PIGE and RBS simultaneously, as a single stand-alone package for quantitative elemental analysis. This integrated capability will take advantage of the strength of each individual technique, providing a better tool for characterization of materials. Each technique provides unique sample matrix information which can be iteratively fed back into the quantitative concentration estimates to produce more reliable results. In addition, this tool will be designed

to handle the analysis of a large number of samples and spectra in a batch mode, increasing the efficiency of the total analysis process.

2. Overview of results to date

ANSTO commenced this Project in January 2007. The proposed work plans for Year 1 (2007) and Year 2 (2008) are shown below.

Work plan year 1 (2007):

- Establish the main architecture of the software.
- Design the main modules of the software.
- Write the PIXE module.
- Test the PIXE module on variety of matrices.
- Establish calibration methods for PIXE and verify them using standard reference materials.
- Report results.

Work plan for year 2 (2008):

- Write the PIGE analysis module, which will consist of two modules, a basic fitting module and a module calculating concentrations using a calibration and some first order matrix correction.
- Test the individual PIGE modules on variety of matrices.
- Establish calibration methods for PIXE and PIGE and investigate if and or within which limitations a matrix independent calibrations is possible.
- Integrate the PIXE and PIGE models and use an iterative approach to calculate the matrix assuming basic oxides.
- Verify new combined module using standard reference materials.
- Report results.

To date we have successfully achieved most of the first two years' work plans by producing an analysis system called 'doiba' which combines both PIXE and PIGE nuclear analytical methods in the one package. This has been written up in an extensive Manual, which has been published as a refereed ANSTO External Report E756 [1], and can be obtained upon request from the authors.

In particular our two year achievements to date include:

- Established the range of elements and their concentrations in most matrices for PIXE
- Defined optimal PIXE backgrounds and background subtractions from theory and experiment.
- Determined typical accuracy and precision estimates for PIXE, important for later iteration criteria.
- Tested range of ways to ulitise PIGE matrix data with PIXE matrix and trace element data.
- Published a 'doiba' manual on PIXE-PIGE combinations and several journal publications on bremsstrahlung backgrounds and detector efficiencies for PIXE [2, 3].

2.1. The ANSTO 'doiba' software package

The 'doiba' software package has been developed to use PIXE and PIGE analysis without the need to provide the matrix composition for thick sample analysis. In this mode the results of both the PIXE and PIGE analysis are used to iteratively calculate the matrix composition. However, PIXE and PIGE can not determine the matrix composition completely, since a number of elements, namely light elements such as oxygen, nitrogen, carbon and hydrogen can not be measured by either technique.

As a consequence the fraction of these light elements has to be estimated independently. To estimate the matrix composition using the PIXE and PIGE results, two different modes have been implemented. In the first mode, the so called iterative mode, all the concentrations resulting from the PIXE and PIGE analysis are summed. If the sum is less then 100% the missing fraction of the composition is assumed to be made up of the light elements. Since it is not possible to know, how this fraction is divided up into the light elements one of these is chosen. This element is set by the so called Dark Matter Element. The name Dark Matter Element was chosen, because is not detected by either PIXE or PIGE. In most cases this element will be oxygen, but it can be defined by the user as any other element.

The second mode, the so called oxide mode, calculates the oxygen content from the elements measured by PIXE and PIGE using the oxide form of these elements. The particular oxide form of each element is defined by the user.

In doiba the sample analysis is a multi-step process. The first step is to fit the experimental spectra and extract peak areas (Fig. 3), while in the second step the peak areas are converted into concentrations.
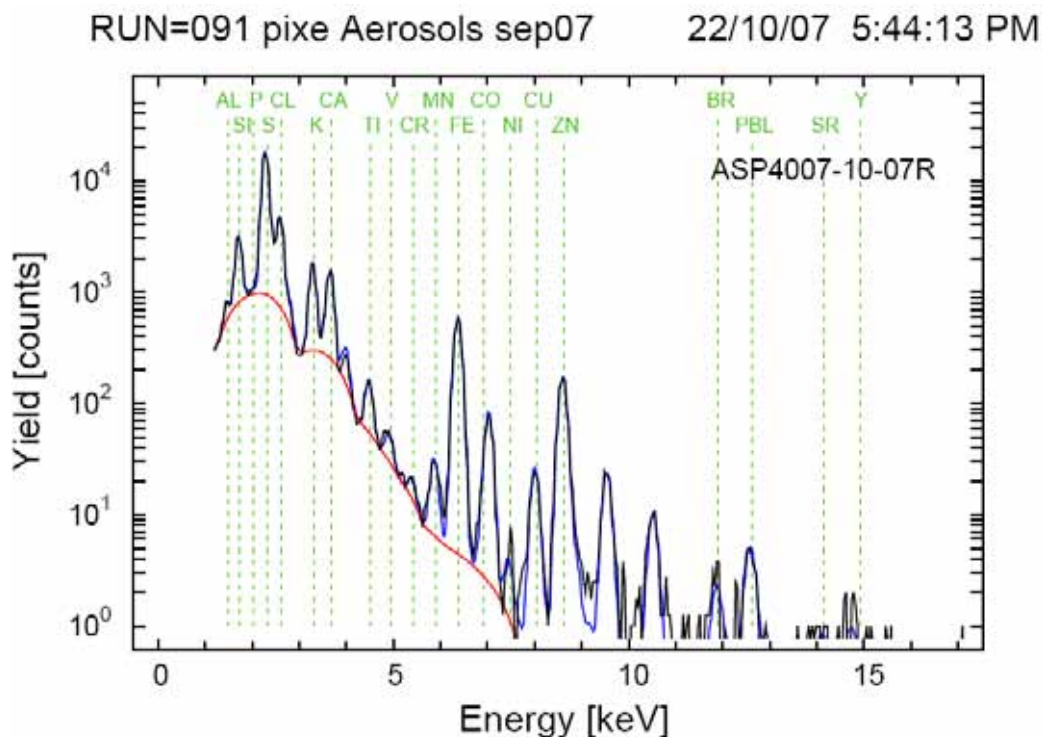

FIG. 3. Automatic fit to a PIXE spectra, both peaks and background are fitted in batch mode.

The first step is performed by the code Run Batty and the second by Run Concs. A two step process is used to allow the fitting of the spectra to be optimised first. This step may have to be performed a couple of times before the best fit to the data is found. The fit has to be optimised so that the fitted background realistically represents the bremsstrahlung background in the spectrum, but also to capture all the elements present in the sample.

Run Concs calculates concentrations from the peak areas extracted previously by BATTY. The behavior of Run Concs code changes depends on whether the PIGE analysis was turned on or off, if thin or thick targets were selected, and most importantly if an iterative calculation of the matrix composition was selected.

When PIGE analysis is turned on both PIXE and PIGE concentrations are calculated and the results are combined in a single data file. Otherwise only PIXE concentrations are calculated.

For both PIXE and PIGE results the stopping of the ion beam in the target material is taken into account, while for PIXE the self-absorption of the X ray s is included as well. In order to account for this the composition has to be known, before the calculation is performed. Although in principle the composition can be determined from the two measurements, this is not straight forward since not all elements can be measured. Hence a number of different ways can be selected in the analysis software to determine the composition. A complete explanation of doiba is provided in the Manual [1].

2.2. Silicon detector dead layer estimates

In order to properly predict backgrounds in PIXE spectra it was important to fully understand the Si(Li) detector's low energy X ray efficiency (below 3 keV). This energy region of the detector is greatly affected by the silicon detector dead layer which nominally is between 0.1 and 0.3µm thick for these types of detectors.

Figure 4 shows typical calculated efficiencies with X ray energy for 0.1 and 0.5 µm dead layers, showing how important it is to be able to accurately measure this dead layer thickness. We have developed a novel method for doing this using the secondary electron bremsstrahlung for carbon and beryllium targets. This is published in Ref. [2] and examples of the effects on PIXE secondary electron bremsstrahlung for a range of dead layer thickness are shown in Figure 5.
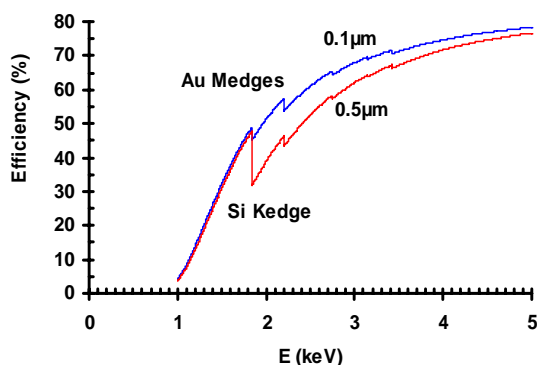

FIG. 4. Si(Li) detector efficiency, 25µm Be window, and 0.1µm and 0.5µm Si dead layers.
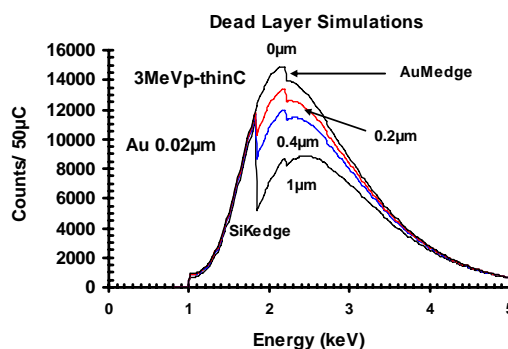
FIG. 5. Predicted PIXE bremsstrahlung for 50µC of 3 MeV protons on C.

2.3. PIXE bremsstrahlung estimates

We have also considered the three main components of bremsstrahlung background from heavy ion bombardment of solid targets in an attempt to predict X ray backgrounds for any target matrix. The three main components are quasifree electron bremsstrahlung (QFEB), secondary electron bremsstrahlung (SEB) and atomic bremsstrahlung (AB). The theoretical cross sections for these are shown in Figure 6. The total bremsstrahlung is the sum of these three components.

Figure 7 shows the calculated total bremsstrahlung form a range of light matrices bombarded with 3 MeV protons. The heavier the target the higher energy X ray s are produced. The low energy cutoff around 1–2 keV is due entirely to the Si(Li) detector efficiency in this region.

Figures 8 and 9 show the comparison of experiment with theory for 2.6 MeV protons on a thin Teflon target (CF_2) and a thin Kapton target ($C_{22}H_{10}N_2O_5)_n$. The fits are excellent with the only difference fit parameter being one scaling factor across the whole energy range 1–10 keV. There appears to be some evidence for a Bragg type summation rule as with stopping powers of ions for matrix elements below silicon and X ray energies between 1 and 10 keV. A full description of the experiment and the detailed results can be found in Ref [3].
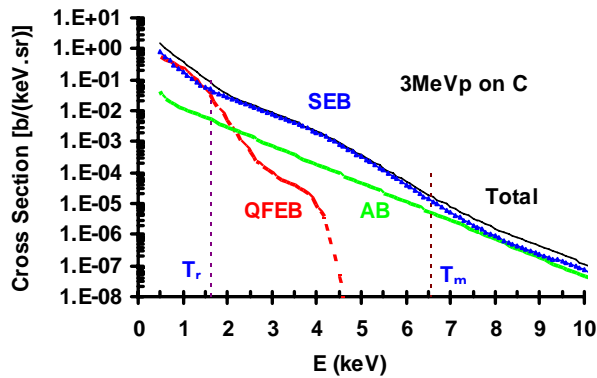
FIG. 6. Bremsstrahlung cross sections after Murozono et al Nucl. Instr. Meth., B150 (1999) 76.
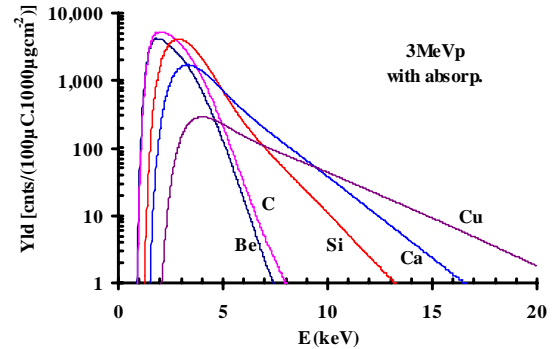
FIG. 7. Calculated bremsstrahlung yields for 100 µC of 3 MeV protons, using a detector with 80 µm Be window and 1,000 µgcm^{-2} thick targets
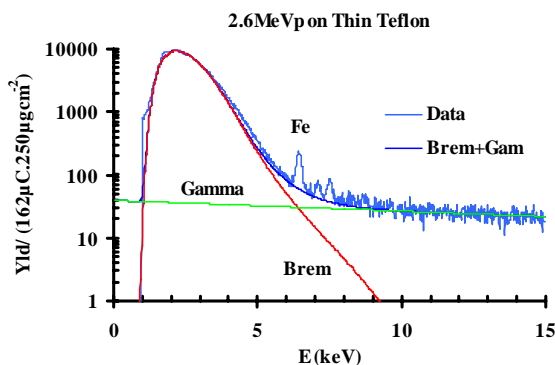
FIG. 8. Comparison of experimental and theoretical bremsstrahlung backgrounds for 2.6 MeV protons on 300 µgcm^{-2} Teflon $(CF_2)_n$ target.
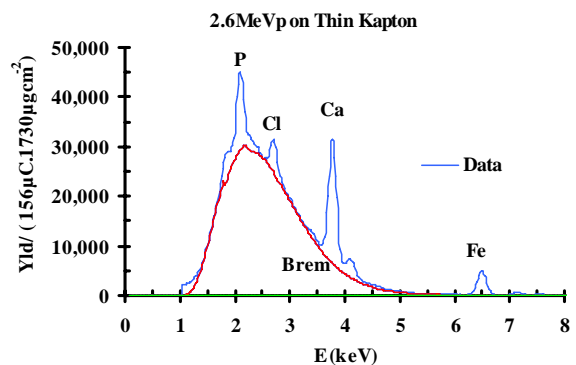
FIG. 9. Comparison of experimental and theoretical bremsstrahlung backgrounds for 2.6 MeV protons on 1730 µgcm^{-2} Kapton $(C_{22}H_{10}N_2O_5)_n$ target.

2.4. *Inclusion of Rutherford Backscattering (RBS) in doiba*

We have not yet been able to progress to the next and more difficult phase of including RBS into this PIXE-PIGE doiba combination this was planned for the final year. The workplan for the third year (2009) is shown below.

Work plan for year 3 (2009)

- Develop an RBS simulation module that simulates an RBS spectrum from the PIXE and PIGE results which can be compared with measured RBS spectrum.
- Test the individual RBS module on variety of matrices.
- Design the User Interface that facilitates the use of additional information (oxides and other boundary conditions) to constrain the results.
- Integrate the PIXE, PIGE and RBS modules.
- Test the integrated software on variety of matrices.
- Reporting of the results.

This plan will take significantly longer than anticipated to complete as the inclusion of the RBS phase into the doiba software is proving to be much more complicated than expected. Basically including PIGE into the PIXE matrix corrections has taken 30 months to complete successfully. Then putting RBS into both PIXE and PIGE matrix combinations provides many more possible solutions and combination to test and trial. Going from a two way to a three way matrix correction and making that consistent with all three techniques simultaneously is quite complicated and may not necessarily have a unique solution. So compromises have to be reached and we have not yet decided on how to best handle these compromises to produce the most likely solutions.

3. Conclusions

The two year plan has been successfully completed in about 30 months, PIXE and PIGE have been included into a doiba software package. Including the third RBS options is proofing to be much more problematic and could take another 15 months or so at least at this stage. We understand the RBS technique completely but producing results that are also consistent with PIXE and PIGE results in a batch mode operation for a very broad range of matrices is proving to be a non trivial task.

REFERENCES

[1] SIEGELE, R., IONESCU, M., COHEN, D.D., doiba Manual, ANSTO External Report No ANSTO/E765, pp1–115, April 2008.

[2] COHEN, D.D., STELCER, E., SIEGELE, R., IONESCU, M., Silicon detector dead layer thickness estimates using proton bremsstrahlung from low energy atomic number targets. X ray Spectrometry **37** (2008) 125–128.

[3] COHEN, D.D., STELCER, E., SIEGELE, R., IONESCU, M., PRIOR, M., Experimental bremsstrahlung yields for MeV proton bombardment of beryllium and carbon, Nuclear Instr. and Methods **B266** (2008) 1149–1153.

COMBINED USE OF μ-XRF, μ-XAS AND μ-XRD FOR MICROANALYSIS OF ENVIRONMENTAL AND CULTURAL HERITAGE MATERIALS IN TWO AND THREE DIMENSIONS

K. JANSSENS, W. DE NOLF, G. VAN DER SNICKT, M. ALFELD, P. VAN ESPEN
Antwerp X ray Imaging & Instrumentation Lab,
University of Antwerp,
Antwerp,
Belgium

Abstract

Various analytical techniques such as confocal μ-XRF, μ-XAS, μ-XRD, μ-Raman spectroscopy were applied for investigation of geological and environmental materials (sediments and individual particles), and cultural heritage objects (paintings, glasses, metal aretefacts). The results of selected applications are presented.

1. Proposed work plan in previous progress report

In the report prepared for the previous CRP meeting (April 2006, Vienna), the following fields of activity were put forward:

- Application of PXRF, primarily for screening purposes of 19–20th and 15–17th century paintings, in order to document better the evolution of the pigment usage in there periods of technological improvement.

- Construction of an optimized laboratory-based confocal μ-XRF and use of this instrument for non-destructive paint layer characterization in small paintings, possibly in combination with other spectroscopies.

- Application of confocal μ-XRF, in combination with μ-XAS and μ-XRD and with imaging microtomography for investigation of geological and environmental materials of various nature (mainly actinide containing sediments and particles) that have undergone partial chemical or physical changes due to interaction with the natural environment they are in contact with.

- Application of scanning μ-XRD, either in two or three dimensions for the phase distribution characterization of materials of environmental, geological or cultural heritage origin (e.g., inclusions in homogeneous minerals, paint multi-layers, corroded archaeological glass, metal artefacts covered with enameled layers or inlayer with precious materials, …).

In most of these fields, interesting results were obtained that are presented below.

2. Results

2.1. *Application of PXRF for screening purposes of 19–20th and 15–17th century paintings*

A large number of paintings by the 19th to 20th century painter James Ensor were analysed by means of PXRF (Fig. 1). The aim of this investigation was to document the relation between the pigment usage and style of painting during the different periods of activity of Ensor. During the period that he paints in a conventional manner, he also uses mainly conventional

pigment materials; however, as soon as newer pigments (such as Paris Green or Mars Yellow) become available, he start painting in what is known as the 'luminous' style.

FIG. 1. "L'intrige" by J. Ensor. The circles indicate the locations that were analyzed by means of PXRF.

The three 15th century panels showing "Angels playing music" by Hans Memling (Fig. 2), one of the painters of the so-called "Flemish primitives" school, were examined by means of a combination of different portable and non-destructive analysis methods. These included PXRF, far and mid infra red spectroscopy, UV-fluorimetry and UV-fluorescence decay measurements. Part of these measurements were performed by means of our own equipment and part of it was performed by means of the portable analysis equipment of MOLAB, University of Perugia.

The photograph below shows several of these compact instruments being used simultaneously on different panels. A remarkable result was that in the middle panel, showing Christ, the expensive blue pigment lapis lazuli was frequently employed for painting some of the jewels while in the left and right panels, these pigments could nowhere be traced. The presence or absence of this blue pigment, which does not contain any key elements that are easily detected by PXRF, was very difficult to determine by means of X ray based methods. However, by means of FTIR and the presence or absence of a characteristic CO_2 band, originating from CO_2 molecules trapped inside the lazurite crystal structure, the presence of this blue pigment/mineral could be unambiguously demonstrated.
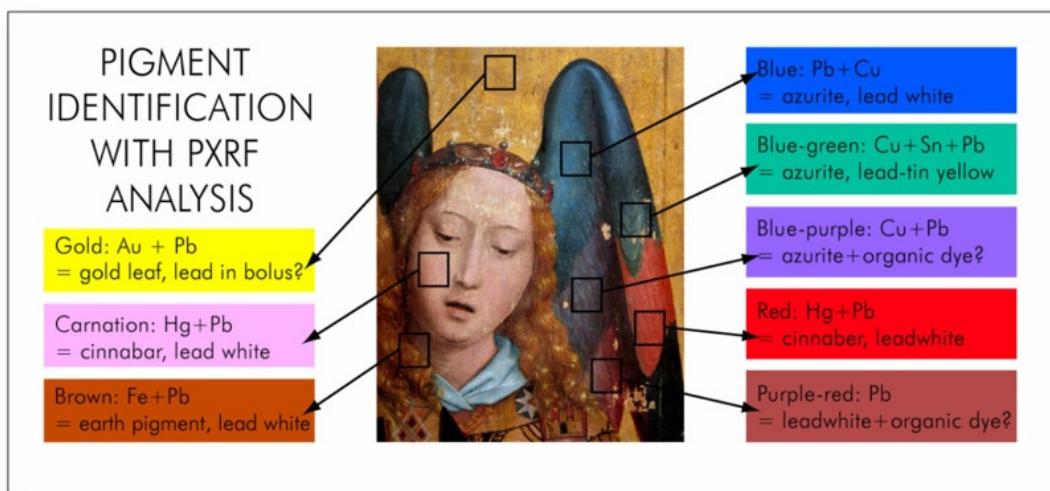
FIG. 2. Detail of one of the panels by H. Memling of "Angels playing Music" indicating the locations where PXRF analyses were performed and the names of the corresponding pigments.

More recently, a painting by Antonello da Messina (Fig. 3) in the Royal Museum of Antwerp, Belgium was investigated by means of a combination of portable XRF, far and mid infra red spectroscopy and UV-fluorimetry with the aim of elucidating the nature of the red pigments and colourants employed by Messina to render red and purple tones in the coats of both sitting figures. PXRF proved itself to be very valuable as a general screening of the painting prior to the use of other portable equipment by the MOLAB team of the University of Perugia.

FIG. 3. "The Crucifixion" by Antonello da Messina, Royal Museum of Fine Arts, Antwerp, Belgium The circles indicate the locations that were analyzed by means of PXRF.

Table 1 gives a qualitative overview of the elemental signals observed in the PXRF spectra.

TABLE 1. QUALITATIVE OVERVIEW OF THE ELEMENTAL SIGNALS IN THE PXRF SPECTRA.

	COLOR	SPOT	Si	K	Ca	Ti	Cr	Mn	Fe	Co	Ni	Cu	Zn	As	Sr	Ag	Sn	Cd	Sb	Ba	Au	Hg	Pb
1		blue sky			W				W						W								S
2		blue sky			W				W						W								S
3		blue sky retouching			W				W	W					W					W			S
4		chest of dead man			W				W						W							W	S
5		dark red blood		W	W				W						W								S
6		white trousers			W				W						W								S
7		brown tree			M				S						W							M	S
8		white sky			W				W						W					W			S
9		blue sea			W				W						W								S
10		blue sea retouching			W				W						W					W			S
11		brown tree			M				M						M							M	S
12		grey ruin			W				W						W								S
13		green tree			W				W			S			W		W						S
14		green tree			W				W			S			W		W						S
15		light green meadow			W				W			M			W		W						S
16		face madonna			W				M						W							M	S
17		red dress		W	M				M			M			W							M	S
18		lighter red		W	W				W			W			W							W	S
19		blue dress traces of purple glaze		W	W				W						W								S
20		red dress		W	W				W						W							S	S
21		red dress retouched area		W	M				M						W							S	S
22		brown foreground			W				M			M			W		W						S
23		purplegrey dress + possible glaze		W	W				W						W								S
24		edge of the painting preparation			S				W														M
25		border of the painting		W	W				W														W
26		edge + nail right		W	S				S														S
27		metal bar on top				W			S														

(W = weak; M = medium; S = strong).

2.2 Confocal μ-XRF vs. macro-XRF for visualization of hidden paint layers

While confocal XRF has the distinct advantage that it offers the possibility to obtain depth-selective information, for sensitive materials such as oil paints, the prolonged exposure to the (synchrotron) X ray beam may cause discoloration or blackening of the irradiated areas. An alternative modus operandi is to employ an energetic milli-beam of hard X ray s (E = 30 to 40 keV) and use this to quickly scan over a large area of a painting. The macro-XRF scanning technique was for the first time successfully employed to reveal the portrait of a Dutch rural lady below the upper paint layers of the painting "Patch of Grass" by V. Van Gogh (Fig. 4) in the Kroeller-Mueller Museum, Otterlo, The Netherlands [1].
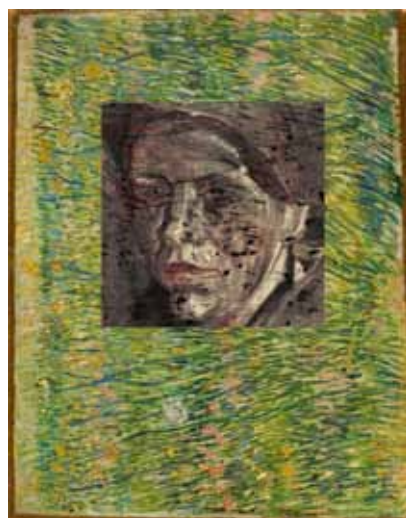

FIG. 4. "Patch of Grass" by V. Van Gogh (Kroeller-Mueller Museum, Otterlo, The Netherlands) with the woman's face as inset.

2.3. Confocal μ-XRF and μ-XAS investigation of geological and environmental materials

As an example of the combined use of μ-XRF and μ-XAS for characterization of altered materials, Figure 5 below shows S-K edge XANES spectra of different locations (indicated in C) and corresponding sulphate and sulphide maps of a partially oxidised CdS samples, scraped off a painting by J. Ensor. The oxidation process causes the yellow CdS to be transformed into the colourless $CdSO_4$.
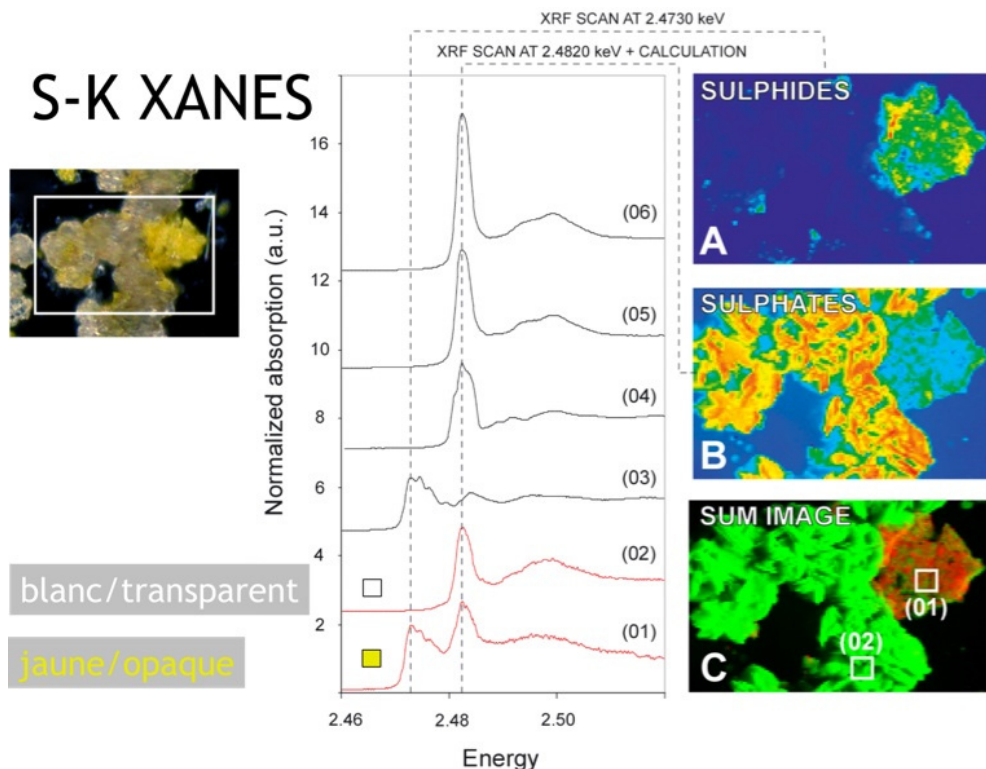
FIG. 5. S-K edge XANES spectra of different locations (indicated in C) and corresponding sulphate and sulphide maps of a partially oxidised CdS samples, in scrapings from a painting by J. Ensor.

These observations are consistent with the following, light-induced redox reaction:

$$CdS + 2O_2 \rightarrow CdSO_4$$
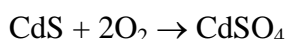
XRD measurements of the alteration product, revealed the presence of $CdSO_4.2H_2O$.

2.4. Application of scanning μ-XRD for phase characterization of materials of environmental, geological or cultural heritage origin

A combination of confocal μ-XRF and μ-XAS with scanning μ-XRD was employed for the characterization of U and Np-containing sediment and granite samples employed during migration experiments of actinides [2–4]. As an example, Figure 6 shows elemental maps while Figure 7 shows As-species specific distributions inside samples obtained by drilling at ca 40 km into geological layers at the Ruprechtov site [5]. Our study concluded that the principle cause for the capture and enrichment of U in this sediment was the presence of As^0; the latter is likely present under the form of either arsenopyrite or as As^0 absorbed to the surface of pyrite crystals (Fig. 8).
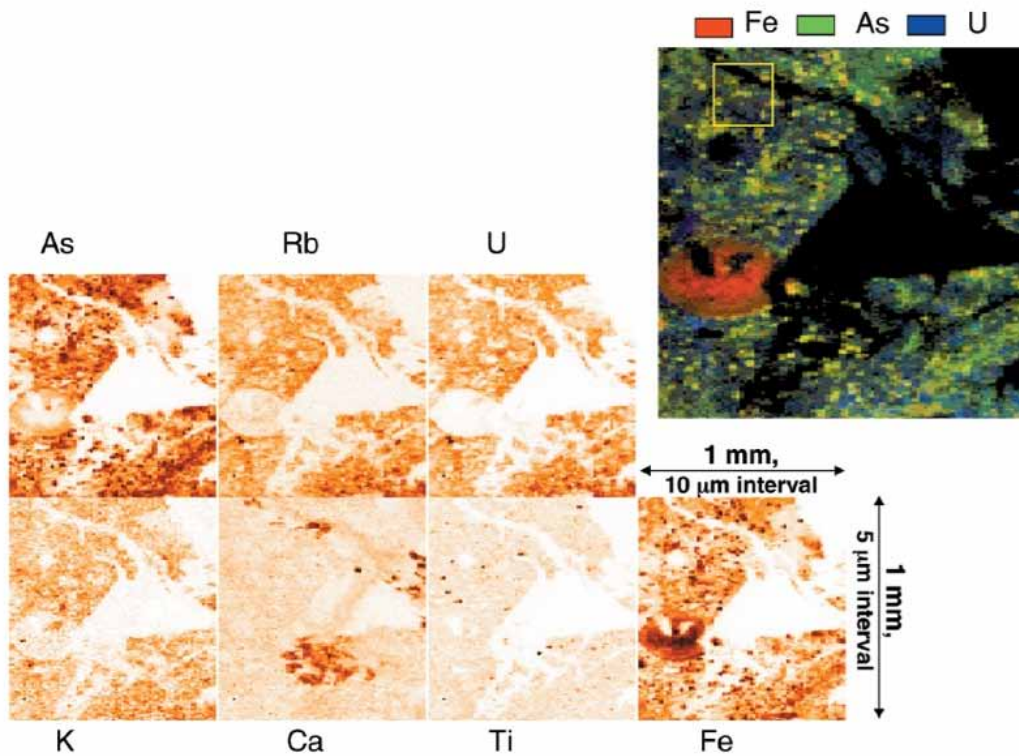
FIG. 6. Elemental distribution maps measured in fast scan mode (E_{excite} = 18 keV; 0.2 s/pixel dwell time). Gray-scale distribution images for the elements indicated are shown at the bottom and the red–green–blue RGB overlay representation for Fe, U, and As distributions at right. The area marked in yellow is shown in greater detail in Fig. 7.
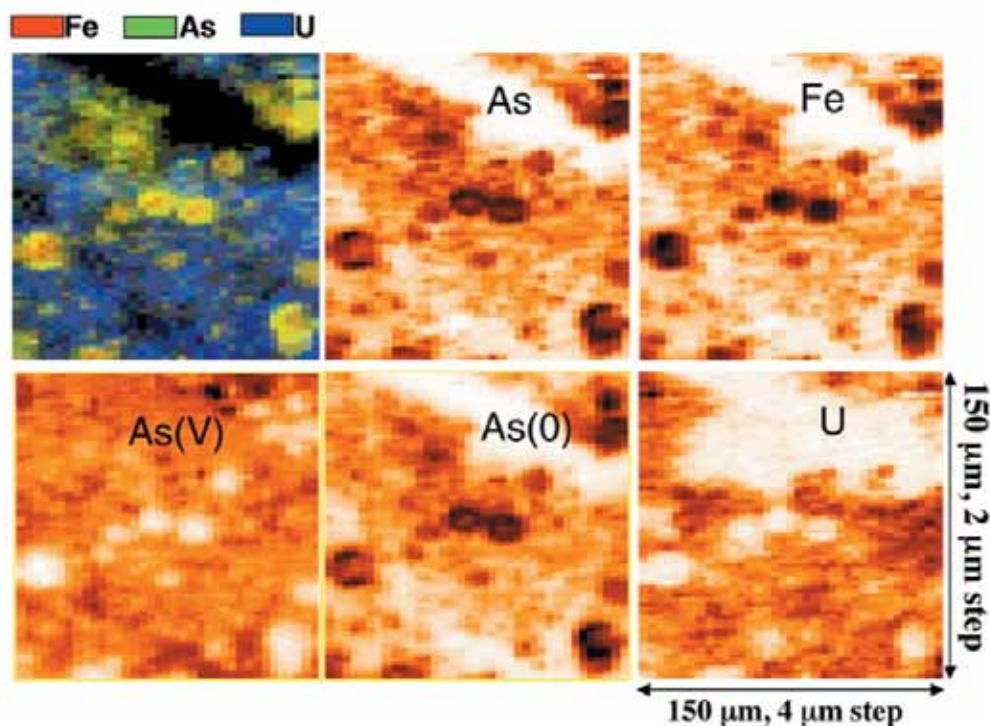
FIG. 7. µ-XRF distribution images for the total As, Fe, and U measured with E_{excite} = 18 keV and 1 s counting time in the area marked in the RBG map in Figure 6 and arsenic chemical state distribution of As^V and As^0 of the same area measured.
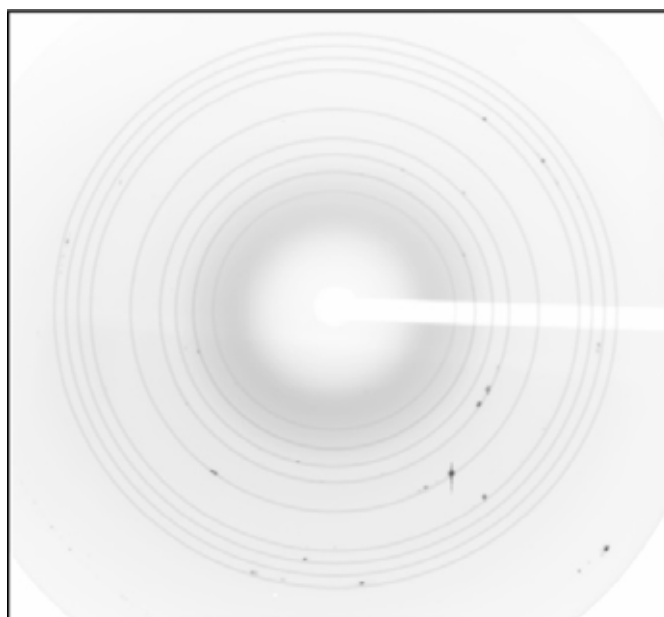
FIG. 8. μ-XRD diffraction pattern collected over the same six As^0 rich pixels used to measure the μ-XANES shown in Figure 7b. E =18 keV, λ = 0.6888 Å; 10 s illumination. Reflections appear as dark dots, characteristic d-spacing pattern calculated for FeS$_2$ up to 2θ = 29° as gray circles.

2.5. Combined μ-Raman and μ-XRF analysis vs. μ-XRF / μ-XRD analysis of pigments in illuminated manuscripts

A small device was constructed incorporating the possibilities to perform localized molecular and atomic spectrometry [6]. An excitation-detection scheme was designed to allow both Raman and XRF spectroscopy to be performed simultaneously on the same location of a macroscopic sample. The layout of the instrument is shown in Figure 9.
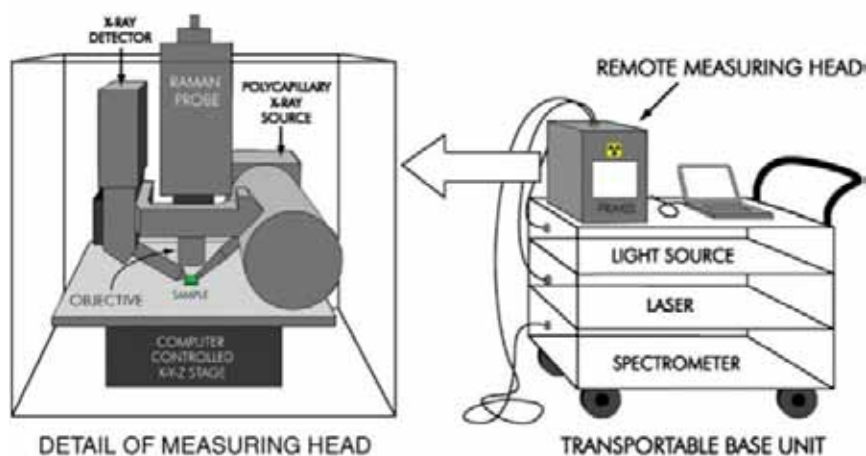
FIG. 9. Schematic representation of PRAXIS, the combined μ-XRF and μ-RS instrument. On the left a detail of the remote measuring head. Dimensions of the transportable head are ca. 25×25×40 cm^3.

In Figures 10–12 some examples of results obtained with this instrument in the field of pigment identification are compared to those obtained by scanning μ-XRD for the specific case of a 16th century illuminated manuscript, a so-called 'Book of Tides'.
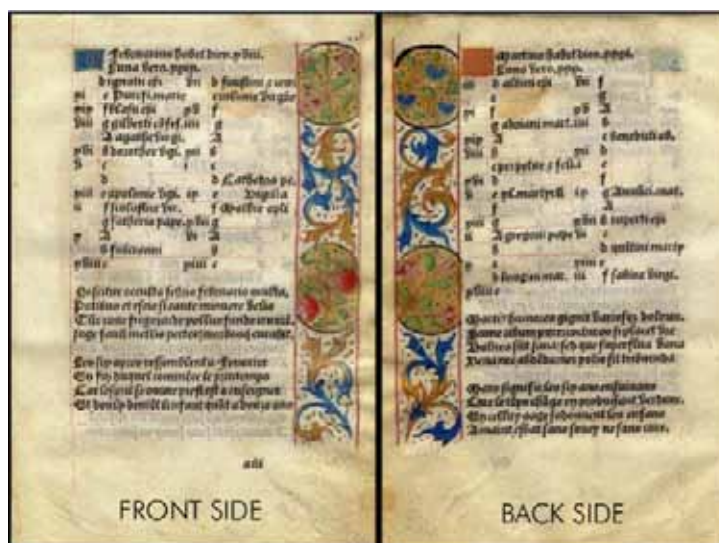
FIG. 10. Front and back side view of the analyzed sheet of parchment.
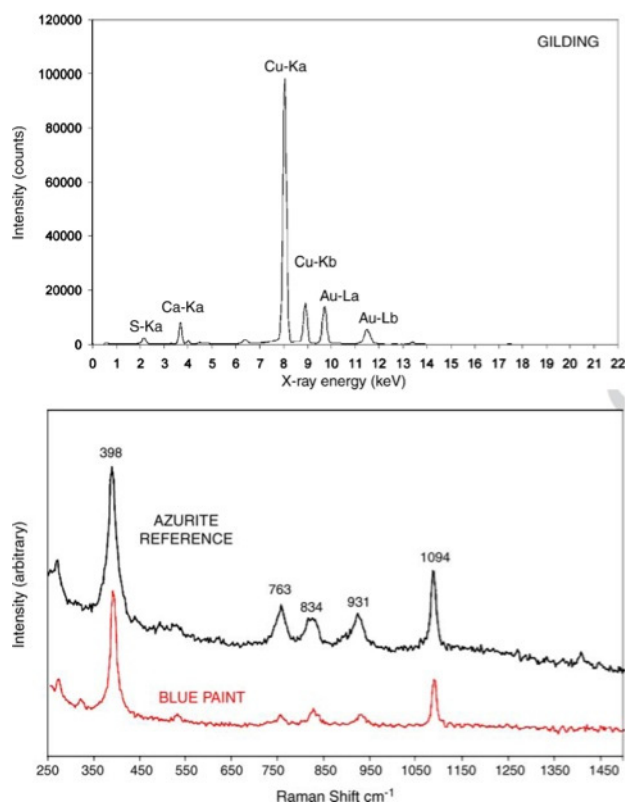
FIG. 11. (Upper panel) XRF spectrum of blue/gildered areas of the MS shown in Fig. 10, showing the presence of Ca, Cu and Au and (lower panel) Raman spectrum of the blue pigment azurite (basic copper carbonate) compared to a reference spectrum.

50
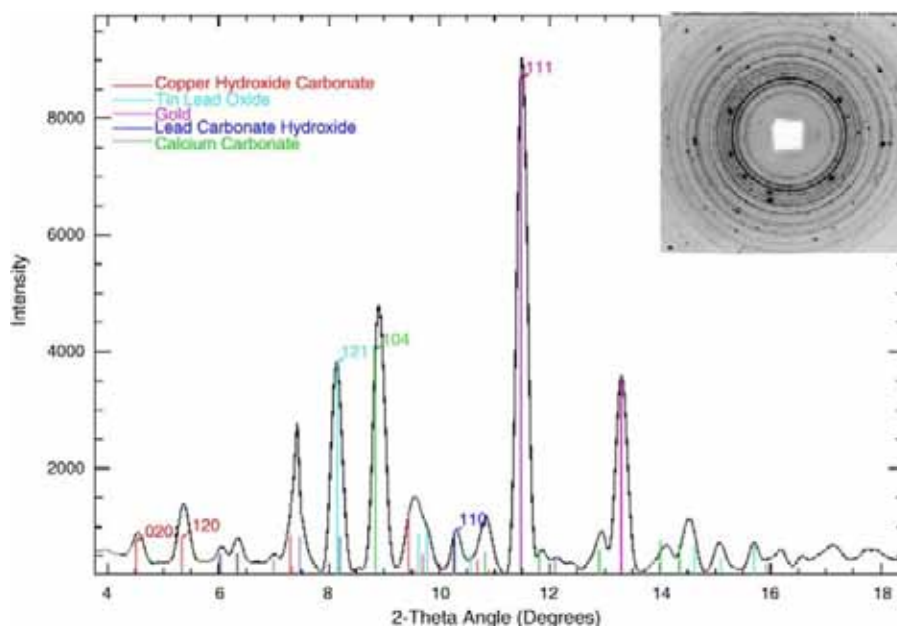
FIG. 12. X ray diffractogram and corresponding 2θ-spectrum of a blue area in the MS shown in Fig. 10. Next to gold and azurite, also other compounds can be identified, present on the back side of the folio.

REFERENCES

[1] DIK, J., et al., "Visualization of a Lost Painting by Vincent van Gogh Using Synchrotron Radiation Based X-ray Fluorescence Elemental Mapping", Analytical Chemistry **80** (2008) 6436–6442.

[2] VAN DER SNICKT, G., et al., "Characterization of a Degraded Cadmium Yellow (CdS) Pigment in an Oil Painting by Means of Synchrotron Radiation Based X-ray Techniques", Analytical Chemistry (2009). DOI: 10.1021/ac802518z

[3] M. A. DENECKE, K. JANSSENS, K. PROOST, J. ROTHE, U. NOSECK, "Confocal micro-XRF and micro-XAFS studies of uranium speciation in a tertiary sediment from a waste disposal natural analogue site", Environmental Science and Technology **39** (2005) 2049–2058.

[4] DENECKE, M.A., et al., "Microanalysis (micro-XRF, micro-XANES and micro-XRD) of a tertiary sediment using micro-focused synchrotron radiation", Microscopy and Microanalysis **13** (2007) 165–172.

[5] M.A. DENECKE, et al., "μ-X ray fluorescence and μ-X-ray diffraction investigations of sediment from the Ruprechtov nuclear waste disposal natural analog site", Spectrochimica Acta B **63** (2008) 484–492.

[6] VAN DER SNICKT, G., DE NOLF, W., VEKEMANS, B., JANSSENS, K., "μXRF/μ-RS vs. SR μ-XRD for pigment identification in illuminated manuscripts", Applied Physics **A 92** (2008) 59–68.

INTEGRATION OF ANALYSIS TECHNIQUES OF DIFFERENT SCALES USING X RAY INDUCED AND ELECTRON INDUCED X RAY SPECTROMETRY FOR APPLICATIONS IN PREVENTIVE CONSERVATION AND ENVIRONMENTAL MONITORING

R.VAN GRIEKEN, L. DARCHUK, V. KONTOZOVA, S. POTGIETER-VERMAAK, K. VAN MEEL, E. STEFANIAK, A. WOROBIEC.
Environmental Analysis Group, University of Antwerp,
Antwerp,
Belgium

Abstract

In the past years, and also within the framework of this CRP, we have used a combination of several nuclear and non-nuclear techniques in fundamental research and especially in various applications. Most work has been done with energy-dispersive X ray fluorescence in combination with electron probe X ray microanalysis, but several other more common analysis techniques have been used as well. The applications have included mostly preventive conservation (e.g. characterisation of damaging atmospheric particles in many museums) and environmental monitoring (e.g. for atmospheric particles in relation to their health effects in outdoor and especially indoor environments). Fundamental aspects have been in the optimising of interfaced electron microprobe and Raman microprobe analysis and the evaluation of the potential of such an instrument for atmospheric aerosols; quite a few unexpected and unpredicted problems have appeared in the latter study.

1. Introduction

X ray spectrometry (XRS), in its various forms, has been very useful for broad analytical applications, since many years. Electron probe X ray microanalysis (EPXMA) is well known for analysis with microscopic spatial resolution, albeit with local detection limits in the 1000-ppm range; it is a very common technique and available in many institutes in the Member States, although it is not often used or well known by the direct beneficiaries of IAEA funding. Our EPXMA units have been upgraded to include low-Z element detection and quantification (using thin-window detectors and Monte Carlo simulations) for chemical speciation at the single micro-particle level, analyses at liquid nitrogen cooling conditions to assess also more volatile particles, and analyses of surface and in-depth layers of single particles (using variable energy electron excitation followed again by quantification calculations). X ray fluorescence (XRF), and especially the more nuclear-related energy-dispersive version (EDXRF), allow bulk analysis at the sub-ppm level. Unifying, e.g. for atmospheric aerosol studies (and for environmental particles in general), bulk XRF with single particle EPXMA allows to identify much more straightforwardly the sources of such particles and to predict their fate. Analysis with single particle and size information is important for assessing the potential of these particles to penetrate deep into the lungs and to be deposited on works of art, but bulk analysis with much better sensitivity allows obtaining information about e.g. heavy metals.

One scope was to evaluate, during the course of this CRP, the value of the unification of the various nuclear spectrometries, much more than we would have done without the initiative of his CRP. This implied demonstrating and proving the added value of using simultaneously different nuclear and other techniques, from bulk to the micro- or nano-scale, on the same samples. The necessary software applied for quantitative analysis in EPXMA (quantifying the enormous matrix effects for low-Z elements) and for handling the large amount of data generated by automated or high throughput techniques, was to be refined and finalised.

Another purpose was to demonstrate further the added advantages of simultaneously using various nuclear and non-nuclear techniques for applications in the field of conservation and environmental research, with an emphasis on atmospheric particles.

2. Overview of the research performed and the results obtained

2.1. Instrumentation used

The instrumentation that was invoked during this CRP included as "nuclear techniques": for bulk-EDXRF: Epsilon-5 of PANalytical, a high-energy polarized-beam secondary-target system; for single-particle EPXMA: a JEOL-733 electron microprobe and a JEOL-6300 scanning electron microscope (SEM) with energy-dispersive X ray (EDX) attachment. For supplementary "non-nuclear" bulk analysis, we applied a Varian ion chromatograph (for ion determinations), passive diffusion tubes for the accumulation of gaseous pollutants to be analysed later by ion chromatography or UV/Vis spectrophotometry, an on-line Magee soot monitor, gravimetry for aerosol mass determinations, and for additional micro analyses, we used a Renishaw InVia micro-Raman spectrometer (MRS). All these instruments are located in and belong to the Micro and Trace Analysis Centre the University of Antwerp.

Additionally, specific interfaced EPXMA-MRS instruments were used, in the Department of Industrial Chemistry, University of Bologna, Italy, namely a Renishaw SEMSCA unit interfaced with an EVO.Zeiss SEM, and a Renishaw SEMSCA unit interfaced with an advanced JEOL SEM-EDX within Renishaw plc in Wolten-on-Edge, UK. Towards the end of this CRP, also use was made of a state-of-the-art JAMP 9500F JEOL instrument, of IntellectAnalytics in Kiev, Ukraine, which combines EPXMA with both micro-XRF and Auger electron spectrometry.

This CRP does not provide our group with any specific additional funding for research; hence; the work that pertains to this project is, in fact, funded by other projects, financed by various sources. We refer to the Appendix for the publications that were generated from the applications of various techniques in the context of these studies during this CRP.

2.2. Applications in preventive conservation

Preventive conservation refers to the study of e.g. the atmospheric conditions (including micro-climate or chemical pollution) around a work of art or in a museum, with the intention to improve these conditions and hence to improve the cultural heritage conservation. We have used a combination of instruments, always including XRF and/or EPXMA, mostly in combination with other techniques, in preventive conservation studies of: the Royal Wawel Castle Museum in Krakow, Poland, the Metropolitan Museum of Art in New York, the Rubens' House Museum in Antwerp, the Plantijn-Moretus Printing Museum in Antwerp, valuable mountain churches in Rocca Pietore, Italy and Szalowa, South-eastern Poland, and (in the context of the effect of protective glazing in front of medieval stained glass windows) in: the Basilica St. Urban in Troyes, France, the Dom in Cologne, Germany, and the Sainte-Chapelle church, Paris, France, etc. Some of these subprojects are evident from the list of relevant publications in the attached Appendix.

In the more general field of cultural heritage research, we want the mention the collaboration, within the framework of this CRP, with Prof. C. Vazquez from CNEA and the University of Buenos Aires, in which we studied, by a combination of EDXRF, EPXMA and MRS, some Argentinean artefacts, rock paintings, ancient bones and other archaeological findings.

Other environmental applications, which have been finalised and studied, using a combination or integration of analysis techniques are: particulate atmospheric matter in schools, residences, elderlies' service flats and offices in Belgium, North Sea air aerosols, Hungarian Tisza river sediments, heavy mineral sands from South Africa, welding aerosols, Amazon Basin aerosols, lime industry pollutants, air pollution in the border region of Germany-Poland-Czechia, uranium in soils, etc. Most of these studies are again reflected in the published articles, shown in the Appendix.

2.3. Methodological advances

Methodological advances concerning the integrated methods of analyses will be discussed here in a bit more detail, namely for the interfacing of EPXMA and MRS in one instrument, and the interfacing of EPXMA with micro-XRF and Auger electron spectrometry in another, always in view of aerosol particulate matter characterisation. While the applicability of stand-alone EPXMA or SEM-EDX and MRS instruments is undisputed, although not without restrictions, a hybrid instrument combining these techniques will transform the EPXMA into a powerful material characterisation tool. Such combination of two well-established technologies allows morphological, elemental, chemical and physical analysis without moving the sample between instruments. The "two-in-one-unit" offers a number of doubtless advantages.

The EPXMA/MRS hybrid provides a solution for several fundamental and analytical problems. Some companies provide now an interfaced instrument (e.g. Renishaw plc.), but there is no literature yet concerning their use for individual environmental particles, and we found that the combined measurements are less obvious than originally expected. Especially in the case of analysis of individual fine particles, this analytical approach needs a further and more sophisticated optimisation. The most important aspects regard the following: (a) beam damage and molecular changes; (b) stability of image in case of very fine features (1–4 μm) and (c) the success of relocating a particle correctly. The damage of individual particles with the EPXMA/MRS interface seems to be more problematic than in stand-alone instruments. Some electron beam sensitive particles appeared resistant to the laser beam (e.g. ammonium nitrate and –sulphate are not damaged during MRS analysis) and as long as one works with a "cold stage" to collect X ray and MRS spectra of these particles, there is no problem during measurement with the EPXMA/MRS interface. On the other hand, we determined that some particles stable under the electron beam are being damaged by the laser beam, so their analysis was obstructed. The physical and chemical phenomena that lie underneath the damage with a laser still remain unclear. The successful relocation of the same particle is also connected with the compatibility of the two spots, laser and electron beam, as well as the probing depth. In other words, this is a problem of x-, y- and z-resolution. The diameter of the electron beam has to be correlated with the laser spot size, in order to cover precisely the same area of interest. The laser spot can be smaller than 0.5 μm, which makes it comparable with the area analysed by the electron beam. If the object has been relocated correctly, we can assume that the excited area is also covered by both beams. Another aspect inseparable from the spot size is the probing depth. In case of EPXMA, it is controlled by the energy of the beam electrons and the nature of the sample. For MRS, the collected volume of scattered light can be limited by a high-magnification objective and also by applying the confocal mode. With an appropriate instrument setup, the probing depth can be controlled, but it is always achieved at the expense of the quality of the optical image. Objectives of a large magnification are characterized by a small depth of field, which can cause loss of details in the particle morphology and – consistently – lead to the incorrect recognition of the object. In

other words, there has to be a (not always trivial) compromise between the successful relocation of the spot and the compatibility of the two beams.

The preliminary work with the advanced field-emission EPXMA, micro-XRF and Auger electron spectrometry (AES), combined in one novel instrument, lead to the following preliminary conclusions: (1) the high resolution SEM enables to obtain high quality images of both submicrometer and nano scale size with their fine details revealed, (2) the micro-XRF technique can not be reasonably applied to single aerosol particle analysis because its spatial resolution does not match the size of relevant atmospheric particles, and (3) the Auger electron escape depth does not exceed 2 nm while the sharply focused electron beam has a lateral diameter of 2–3 nm, thanks to the superbly performing electron-optical column. In other words, the instrument is a unique Auger 3D-nanoprobe. The local AES technique can be successfully applied for the composition test of particles of any size and for obtaining the element distributions along a line (line profile), in an area (Auger mapping) and in depth with the help of ion etching (depth profile). The preliminary aerosol samples were all urban aerosols, and AES indicated e.g. a strong enrichment of N in the surface nm layers, undoubtedly the result of interactions with gaseous NO_x in the air. The quantification of the results should be studied further.

3. Conclusions

As expected, the combination of EDXRF with EPXMA and with other bulk and microanalysis techniques appeared to be much more powerful than using only one individual technique, in various applications, mostly preventive conservation and atmospheric aerosol characterisation. Unexpectedly, several problems were encountered in the application of a commercial interfaced EPXMA/MRS instrument and these led to a need for further optimisation and evaluation of the procedure.

INTEGRATION OF THE PIXE AND XRF SPECTROMETRIES FOR SIMULTANEOUS APPLICATIONS

V. DESNICA, M. JAKŠIĆ, S. FAZINIĆ, M. BOGOVAC, Ž. PASTUOVIĆ
Ruđer Bošković Institute, Laboratory for Ion Beam Interactions,

V. DESNICA
Laboratory for Science and Technology in Art, Academy of Fine Arts,

Zagreb,
Croatia

Abstract

Within this CRP two nuclear spectroscopic methods, PIXE and XRF, were integrated into a single set-up and the unification of techniques was investigated. For that purpose the vacuum chamber of the PIXE line of the IAEA experimental line at the Rudjer Boskovic Institute in Zagreb was used. A new chamber top flange was constructed, which allowed mounting of a small, low power X ray tube within the chamber. Parameters for achieving optimal signal to noise ratio of the X ray fluorescence from typical soil samples were determined for this set up. The benefits of this CRP were twofold. Firstly, by using the detection system and the positioning mechanism of the existing PIXE line, a fully operational XRF system was acquired without much further investment. This allows material characterization measurements when the ion beams from the accelerator are not available. Secondly, this integration exploits the complementarities of the two methods, and by broadening the sensitivity for low and high Z elements depending on the method used, it allows even wider elemental characterization of a sample under investigation.

1. Introduction

The respective benefits of XRF and PIXE have been eagerly debated in many fields of application and in recent years a number of papers comparing the results of the two isolated experimental set-ups were published [1–5]. A general agreement seems to have been reached that the two modes of excitation of characteristic X ray s are indeed complementary rather than competitive.

X ray fluorescence (XRF) is a mature, routine, extremely versatile instrumental technique for rapid analysis of major, minor and trace elements in solids, powders and liquids, and in commercial use for the past ca. 50 years. Particle induced X ray emission (PIXE) is a somewhat newer, fast, simultaneous, quantitative, multi-element technique with low limits of detection, in use for the past 35 years. One of the major differences between XRF and PIXE lies in the excitation of X ray s in the sample. It has been shown by many authors that in particle induced excitation the ionization cross sections of the elements decrease with increasing atomic number, while in X ray photon excitation the cross sections increase with the increasing atomic number. That means that in XRF and PIXE the background intensity distributions follow those of the excitation cross sections, i.e. they are opposed. Consequently, XRF should exhibit higher sensitivity for heavier elements, whereas PIXE should be more sensitive for analysis of light elements. Furthermore, the penetration depths and irradiated areas, and hence analytical volumes, are rather different in PIXE and XRF, with the XRF penetration depth relatively larger. This can be very important especially when investigating very old artistic objects and objects found in excavations, where a degree of corrosion in the surface layer can be very high. Moreover, PIXE exhibits relatively straightforward and, compared to XRF, simpler quantification calculations in unknown matrices. However, a

serious problem in the use of PIXE in art and archaeology is the energy deposition which may damage the object as well as the possibility of charge buildup in the non-conducting samples and subsequent spectrum-distorting sparking. XRF does not suffer from these effects. Due to all these differences, it was interesting to investigate the integration of the two methods into one set-up and to study their specific advantages and disadvantages in the controlled environment. This project was carried out at the Laboratory for ion beam interactions of the Rudjer Boskovic Institute (IRB) in Zagreb. The Laboratory utilizes two particle accelerators - the larger one is EN Tandem Van de Graaff and reaches a maximum voltage of 6 MV at the terminal. The second, Tandetron accelerator, reaches a maximum voltage of 1 MV at the terminal (for accelerated protons up to 2 MeV). The RBI accelerator facility consists of several dedicated beam line end-stations for ion beam analysis (IBA), including in-air PIXE and nuclear microprobe (Fig. 1).
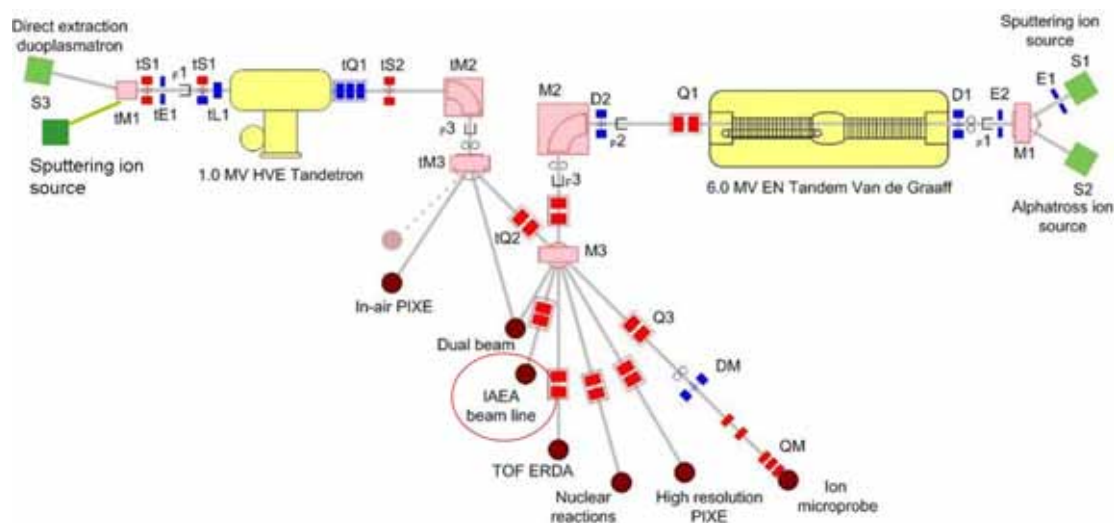
FIG. 1. Layout of the RBI accelerator facility, showing the two accelerators and the beam line end-stations. System elements are labeled as: S, ion source; L, electrostatic lens; D, electrostatic or magnetic deflector; M, dipole magnet; Q, quadrupole magnet; F, Faraday cup. The activities within this CRP were carried out at the IAEA beam line (red circle).

Most of the beam lines can be used independently, using the ion beams from both accelerators. The Tandetron accelerator is also equipped with the computer control system developed in the Laboratory. It can be controlled remotely through the computer network as well. More details about the RBI accelerator facility and the data acquisition and analysis software may be found in [6]. The IAEA beam line, where the integration PIXE-XRF was carried out, is a general purpose IBA end-station, equipped with a vacuum chamber and detectors for PIXE, PIGE and RBS measurements. The ion beam has a diameter between 1 and 5 mm.

2. Overview of the research performed and the results obtained

2.1. Construction of the chamber

In order to unify the XRF and PIXE spectrometric methods into one single set up the vacuum chamber of the PIXE end station of the IAEA experimental line is used and modified. A new top covering flange is constructed, on which a small power X ray tube is mounted so its X ray exit window is located within the chamber. This chamber cover is interchangeable with the

existing PIXE top flange and the modular design gives possibility to an independent utilization of the XRF and PIXE methods, depending on the specific needs. To control the temperature of the X ray tube an NTC thermistor sensor was mounted to the part of the tube within the chamber. The tube temperature control is especially important when using the X ray tube in a vacuum environment, as the tube relies on air cooling and air convection. The geometry of the setup is shown in Figure 2.

(a)   (b)
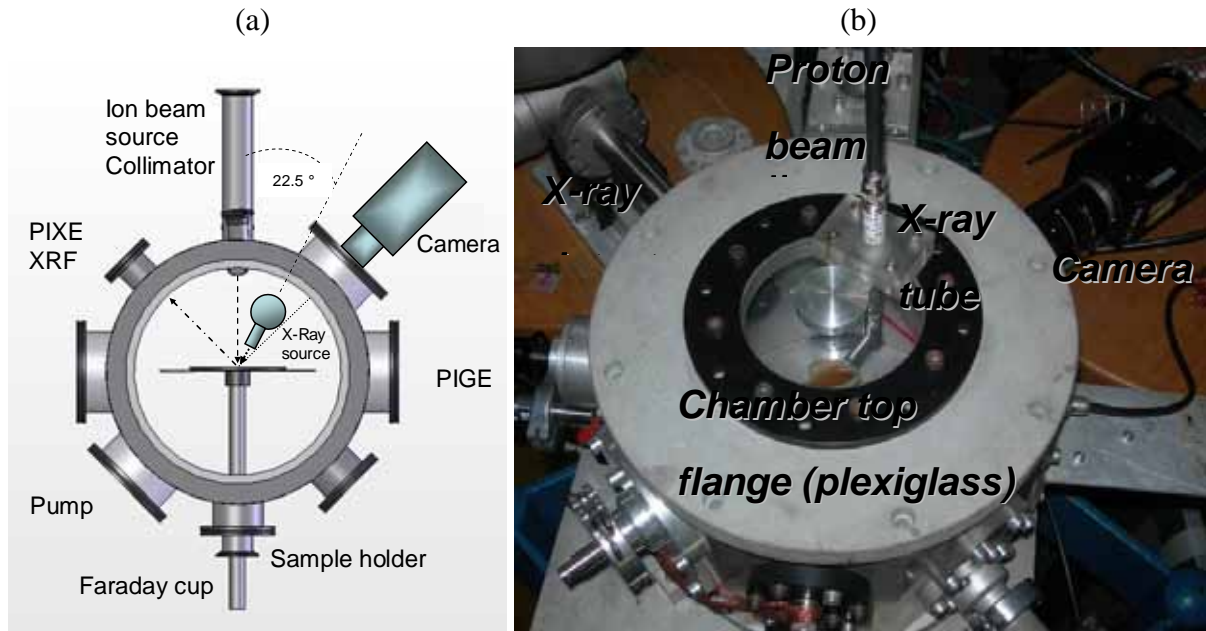
FIG. 2a and 2b. Integrated PIXE-XRF set up at the IAEA beam line.

The angle of the incident X ray beam to the sample is 22.5 degrees (measured from the normal to the sample plane), the distance of the tube anode to the sample is 35 mm. Two different collimating systems were tested and compared — a simple aluminum pin-hole collimator and a collimator made of a combination of aluminum and graphite. It was opted for the latter, shown in Figure 3a. In order to minimize the effects of possible secondary radiation from the cylinder material itself the materials chosen for the collimator were aluminum and graphite, which, beside Al, contains mostly light elements [e.g. Mg, Si as minor components (traces)] and whose characteristic radiation does not affect the XRF measurements in great extent. The collimator is 20 mm long, with a 2 mm graphite aperture at the exit end (Fig. 3b).

(a)   (b)

FIG. 3a) Photo of the pin-hole collimator mounted on the "pencil" X ray tube. The aperture defining the exiting beam size is 2 mm. 3b) Cross-section of the pin-hole collimator showing its components.

2.2. Sample positioning and initial beam alignment

The sample positioning for both XRF and PIXE applications are carried out using an in-house developed LOCATOR software. For determining the irradiated spot on a sample during a measurement a system of a video-camera monitoring was developed. It allows digital m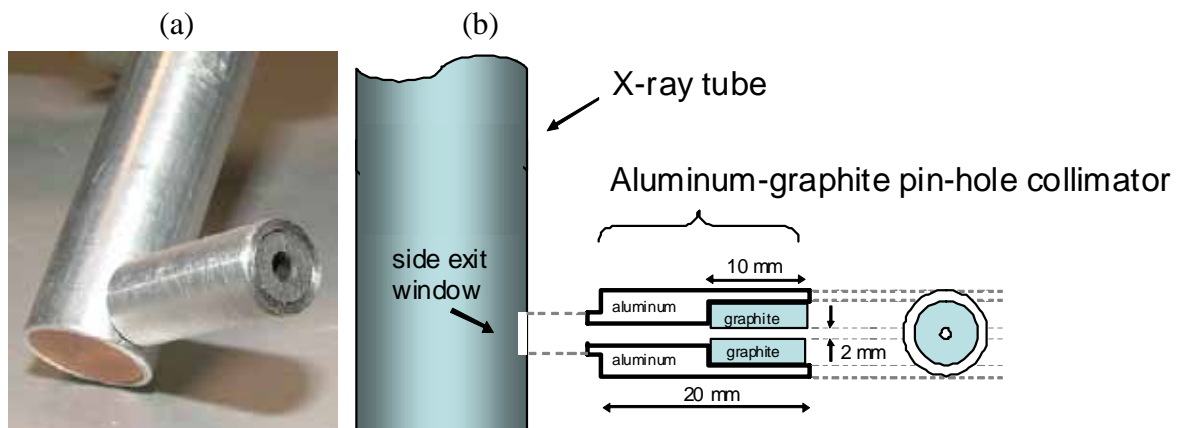arking of the investigated area by clicking on the display with a mouse. The actual position of the X ray beam is defined during preliminary beam alignment by irradiating a fluorescence paper inserted in the target plane, which allows "seeing" the X ray beam and marking its on-the-sample position (Fig. 4). The same positioning system is used for defining the proton beam irradiation spot needed for PIXE measurements (by illuminating a quartz target). The revolving sample holder can hold up to 16 targets.
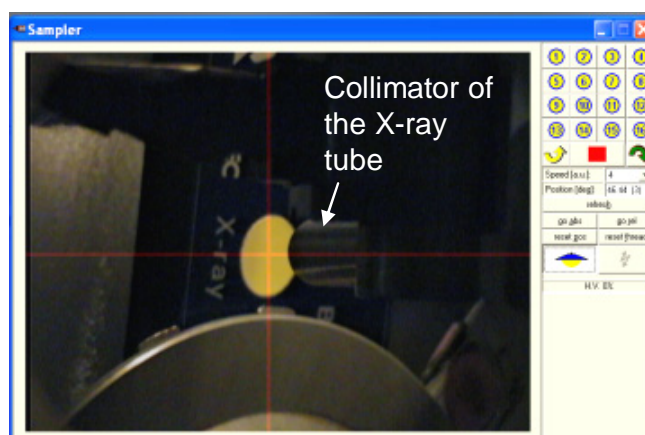
FIG. 4. User interface window of the developed positioning program, showing the X ray tube with the collimator pointed at the fluorescence shield. The X ray s illuminate the irradiated area of the shield and the intersection of the red marker lines are moved to pin-point this position for subsequent measurements. Due to the strong ambient light needed to make this photo the fluorescing area, clearly seen under typical working conditions, is hardly seen on this photo.

2.3. Software

For data acquisition a multi-parameter software SPECTOR is utilized, employing up to 8 ADCs and therefore allowing simultaneous combination and integration of different spectroscopic techniques (i.e. detection systems). As a new generation of hardware and software, the SPECTOR data acquisition and sample/beam control unit has been developed at our laboratory in cooperation with the IAEA Seibersdorf Laboratories and is constantly being refined and adapted to changing needs. The SPECTOR and LOCATOR programs have been recently integrated into a new program TERMINATOR, which allows simultaneous controlling possibilities during the measurement, all in one window (Fig. 5).
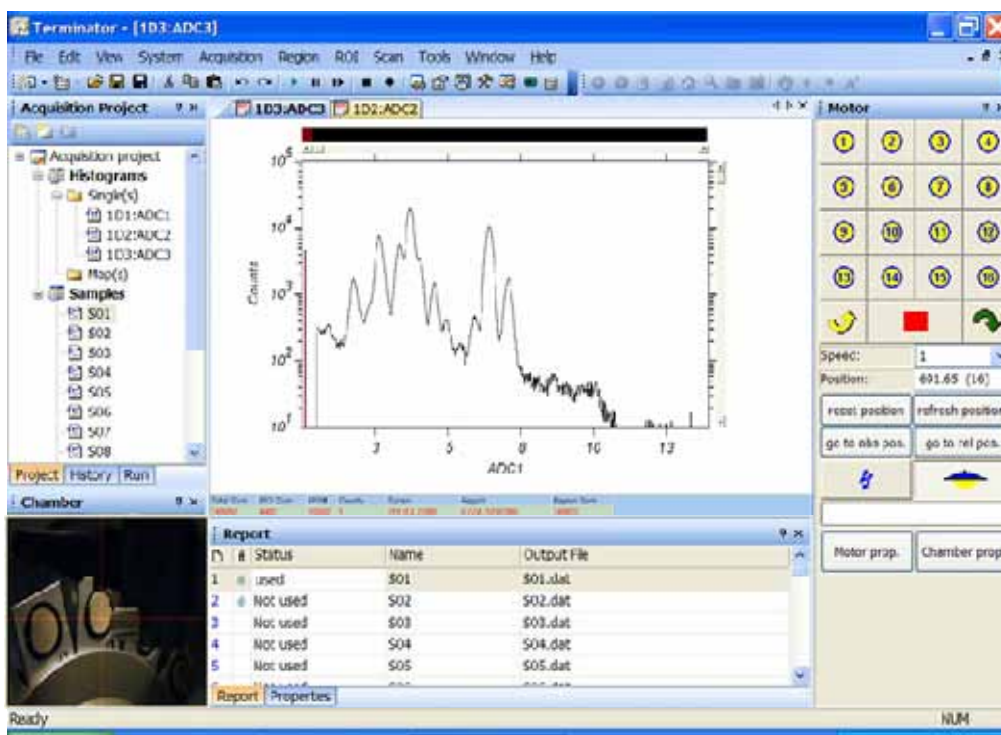
FIG. 5. Data acquisition and control program (Terminator) running during a measurement on the PIXE-XRF integrated system at the IAEA beam line. Spectrum is displayed in the middle of the screen; to the left one can choose to open old spectra or start a new acquisition; below one can control the area which is being analyzed; at the right a subroutine providing control of the stepping motors for sample positioning is displayed.

2.4. Hardware and software development

In the present work the MCA/MPA unit compatible with NIM ADCs has been designed. Virtually all nuclear laboratories has peak detect ADCs as a NIM module. There are several vendors on the market that offer such ADCs. All available ADCs have an external connector for connection with MCA/MPA unit. Although NIM is a standard that defines electrical and mechanical (size) properties of the modules, not all ADCs have exactly the same control and data pins on their external MCA connector. The present MCA/MPA unit is pin to pin compatible with Canberra 8075, 8077 or equivalent ADCs. Fortunately the main difference among different ADC models is in the pin names and their position on the external ADC connectors (connects ADC with MCA). Therefore only a simple connector should be built to use ADCs that are not compatible with Canberra 8075 or 8077 ADCs.

The system hardware is enclosed in a stand alone box that contains switching power supply, general purpose field-programmable gate array (FPGA) board with static RAM (SRAM) and USB/Ethernet modules and eight 26-pin connectors to connect eight NIM ADCs via 5V to 3.3V level translators (Fig. 6).

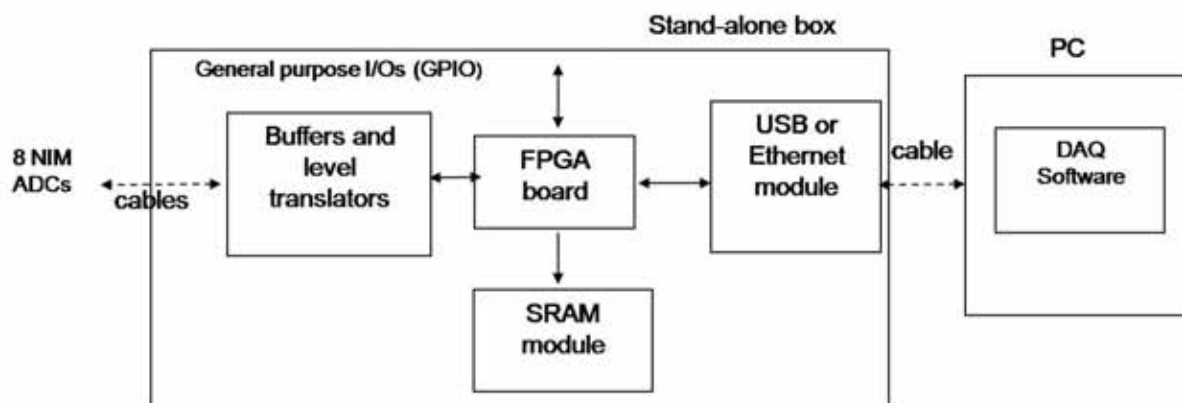*FIG.6. Basic components of the data acquisition system.*

MCA/MPA software for data acquisition, which is a MS Windows application, is called Spector and has been written in MS Visual Studio C/C++. The application performs several tasks including: hardware initialization via set of dialog boxes (measurement time, number of ADC channels, number of active ADCs, polarity of ADC signals …), start/stop measurement, data transfer and visualization during measurement. The communication with FPGA on PC side is done via driver and set of software routines (dynamic link libraries) provided by the vendor of the FPGA board.

2.5. Measurements results

Test measurements were carried out on various standard reference materials (1249 Inconel 718, NIST 2710 Montana soil, ISE 954 Clay, ISE 983 Marine sediment) using both systems and the results were analyzed. For XRF analysis, measurements using different excitation parameters were tested and the peak to background ratio for various elements were calculated (Fig. 7). For a typical thick soil sample optimum excitation energy for reaching good broad range results with this set up seems to lay around 25 keV. Of course, here one must be aware of the fact that a tradeoff will exist between the demand for broad range elemental analysis and the optimum choice for attaining the lowest possible detectable level for a given element. When comparing these results with the results obtained through PIXE measurements on a same sample, generally higher peak to background ratios are observed. In order to conclude on the sensitivity differences between the methods the minimum detection limits (MDL) achieved with each of the two techniques were calculated from XRF and PIXE spectra (Table 1) and the results were plotted versus the atomic number of the emitting target element (Fig. 8). The commonly accepted three-sigma criterion was used to evaluate the MDL. It says that an X ray peak is statistically significant with a 99.87% confidence level, when its peak count N_P satisfies the condition $N_p \geq 3(2N_B)^{1/2}$, where N_B is the background count. When directly compared, overlaid PIXE and XRF spectra show considerable differences in sensitivity, where PIXE clearly exhibits more sensitivity for light elements (low energy X ray emitters) and XRF is more sensitive for heavier elements (Fig. 9). These spectra of a reference standard NIST 2710 Montana soil were recorded under typical measuring conditions, using 25 keV and 50 µA for XRF, and 3 MeV for PIXE.

62
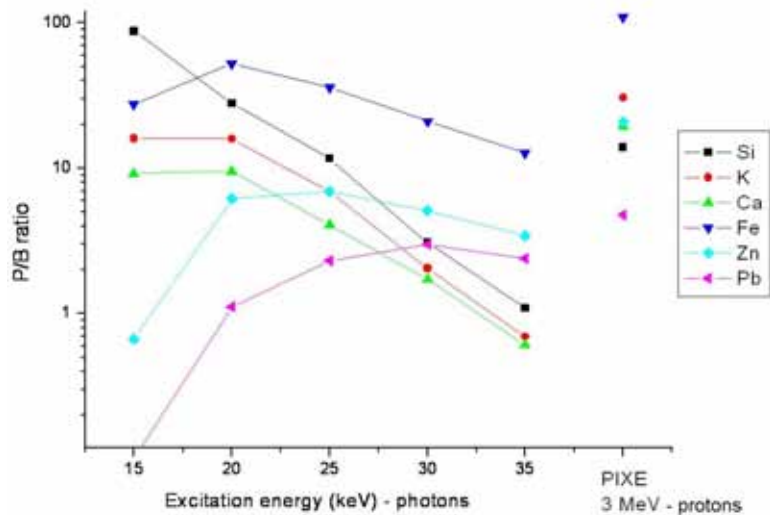
FIG. 7. Experimentally obtained peak to background ratios for several elements of a typical soil sample, in dependence of the excitation energy and excitation mode. The photon energies for XRF ranged from 15 to 35 keV, the PIXE measurements were carried out using 3 MeV protons.

TABLE 1. CALCULATED MINIMUM DETECTION LIMITS (MDL) FOR SOME ELEMENTS FROM THE MONTANA SOIL STANDARD

Element	Certified concentration ($\mu g/g$)	XRF MDL ($\mu g/g$)	PIXE MDL ($\mu g/g$)
Si	289000	1915	1481
K	21100	255	35
Ca	12500	196	29
Ti	2830	127	26
Fe	33800	49	20
Zn	6952	48	36
Pb	5532	98	160
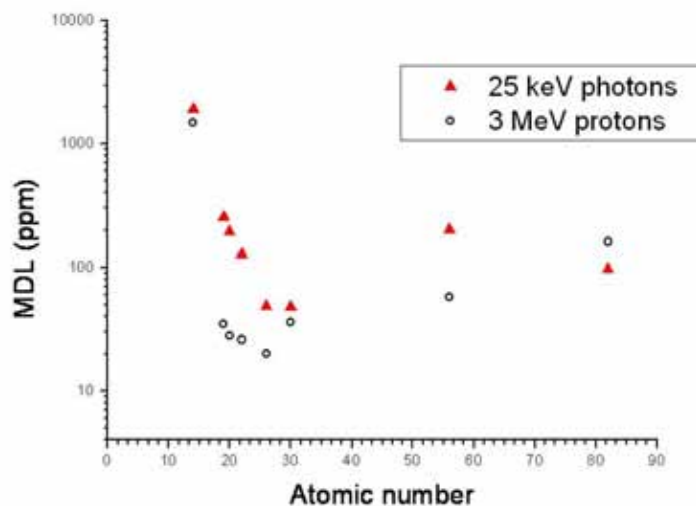
FIG. 8. Variation of the MDL versus the atomic number of the emitting target element, extracted from XRF (triangles) and PIXE (circles) spectra, for elements Si, K, Ca, Ti, Fe, Zn, Ba and Pb. The MDLs for Ba and Pb were calculated for L lines.
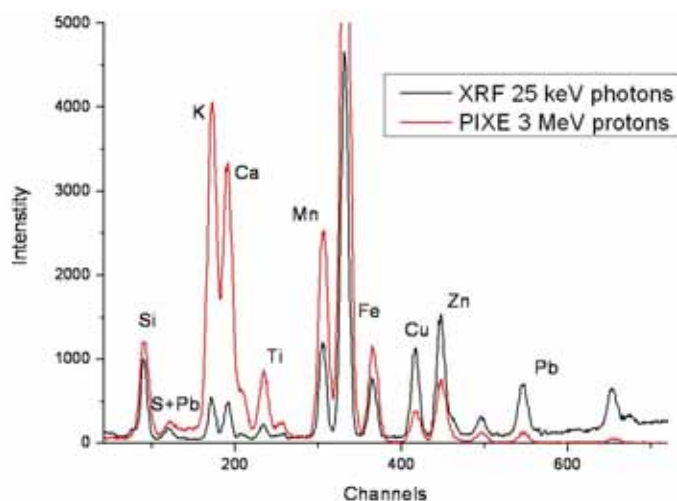
FIG. 9. Overlaid PIXE and XRF spectra (acquired measuring using typical experimental parameters) of a reference standard NIST 2710 Montana soil. It is obvious that PIXE exhibits more sensitivity for lighter elements and XRF for heavier.

3. Conclusions

PIXE and XRF offer both high analytical potential for multi-elemental investigations and material characterization. The main objective of the Project, to exploit the possibilities of integrating these two nuclear techniques into one set up, was successfully fulfilled.

Measurements on standard reference materials using both methods showed that they exhibit differences in experimentally obtained peak to background ratios and show complementary behavior in elemental sensitivities. PIXE exhibits more sensitivity for light elements (low energy X ray emitters) and XRF is more sensitive for heavier elements. Therefore, when the

two methods are unified into one integrated set up, these complementarities can be used to enhance the analytical capabilities of the measurement system. Depending on the analytical needs, choice of a most suitable method and experimental conditions, or a combination of the two complementary techniques can be utilized to improve the analytical results. Furthermore, by mounting an X ray source within a PIXE chamber, and using the existing PIXE detection system and electronics, a reliable and rather inexpensive XRF analysis station was acquired. This set up allows easy and fast preliminary screening and bulk analysis of the samples prior to a PIXE measurement, or simply provides an alternative technique when ion beam from the accelerator is not available.

REFERENCES

[1]   MALMQVIST, K.G., Comparison between PIXE and XRF for applications in art and archaeology, Nucl. Instrum. Methods **B14** (1986) 86–92.
[2]   WILLIS, J.P., XRFS and PIXE: Are they complementary or competitive techniques? Nucl. Instrum. Methods **B35** (1988) 378–387.
[3]   ARAUJO, M.F., ALVES, L.C., CABRAL, J.M.P., Comparison of EDXRF and PIXE in the analysis of ancient gold coins, Nucl. Instrum. Methods **B75** (1993) 450–453.
[4]   BENYAICH, F., MAKHTARI, A., TORRISI, L., FOTI, G., PIXE and XRF comparison for applications to sediment analysis, Nucl. Instrum. Methods **B132** (1997) 481–488.
[5]   L. PAPPALARDO et al., Complementary use of PIXE-alpha and XRF portable systems for the non-destructive and in situ characterization of gemstones in museums, Nucl. Instrum. Methods **B239** (2005) 114–121.
[6]   M. JAKŠIĆ et al., New capabilities of the Zagreb ion microbeam system, Nucl. Instrum. Methods **B260** (2007) 114–119.

DEVELOPMENT OF 3D MICRO-PIXE

B. KANNGIESSER, R. SCHÜTZ, W. MALZER, I. MANTOUVALOU, T. WOLFF
Technical University of Berlin, Institute for Optic and Atomic Physics,
Berlin,
Germany

D. SOKARAS, A.-G. KARYDAS
Institute of Nuclear Physics, NCSR "Demokritos",
Athens,
Greece

N. GRLJ, P. PELICON, M. ŽITNIK
Jožef Stefan Institute,
Ljubljana,
Slovenia

I. REICHE, S. RÖHRS, J. SALOMON
Centre de Recherche et de Restauration des Muse´e de France,
French Ministry of Culture,
Paris,
France

Abstract

A novel experimental technique, 3D Micro-Particle Induced X ray Emission (3D micro-PIXE) has been developed during the past three years and is described in this report. 3D micro-PIXE is realized by using an X ray optic in front of the X ray detector, thus creating together with the focused proton micro-beam a probing volume from which information on elemental distribution is obtained. By moving the sample across the probing volume, the emission of spatially resolved characteristic X ray s is recorded. The first 3D micro-PIXE measurements confirmed the potential of the technique to resolve elemental depth distribution in surface layers overcoming the depth analytical limitations of standard ion beam techniques, whereas combining the fine microbeam scanning mode in the lateral plane with the sample movement parallel to the beam axis, three-dimensional (3D) element-specific distributions can be achieved. In the present report, the theoretical and experimental work undertaken up to now will be reviewed and characteristic applications will be presented. The advantages and limitations of the 3D micro-PIXE analysis will also be discussed in comparison with other nuclear analytical techniques aiming to depth resolved elemental analysis.

1. Introduction

Particle and X ray induced fluorescence radiation techniques (PIXE, XRF) have been developed over the last thirty years to provide multi-elemental quantitative analysis with sensitivity even down to 'ppb' or 'ppt' region. Analysis is being carried out for a variety of samples with interest in various disciplines. The quantitative analysis is generally considered as quite accurate, if the elements are homogeneously distributed within the analyzed volume. With the help of new X ray optics lateral spatial resolution has been also attained at the micrometer regime during the past fifteen years. However, in order to reach similar depth or 3D elemental specific resolution the problem is still tackled by the scientific community. So far, near-surface depth resolved analysis in the range of a few micrometers is also possible for specific elements by means of complementary application of other nuclear analytical techniques such as Rutherford Back-Scattering (RBS) and NRA (Nuclear Reaction Analysis).

Nevertheless, the potential of ion beam methods to provide full characterization is significantly hampered by the fact that materials often exhibit inhomogeneities or a layered

structure extending far below the surface. Several important attempts have been reported aiming to provide analytical methods for depth resolved analysis based on nuclear spectroscopic techniques. All these efforts, up to now, use PIXE or XRF analysis at variable incident energy or variable incident angle. For PIXE the strong dependence of the X ray ionization cross section on the proton energy, as well as the possibility to vary continuously the proton energy and subsequently the range of protons in matter, may result in the successive tuning of the average PIXE production depth deeper inside the analyzed material. These fundamental physical properties triggered and motivated the development of the so-called differential PIXE analysis. Since 1996 various analytical strategies have been developed and implemented by different groups [1–4].

The development of polycapillary X ray s lenses during the last decade opened a new era in the field of X ray microscopic analysis. Among the first applications of X ray lenses in the field of X ray fluorescence analysis was the formation of X ray micro-beams with diameters of the order of a few micrometers. Later, the polycapillary X rays lenses were introduced also in the detection channel to form a confocal geometry. Laboratory or synchrotron induced 3D-XRF spectroscopy provides nowadays an advanced characterization of materials with depth resolving capability together with probing of the elemental composition of individual structures [5–10].

Three years ago, we transferred the concept of the confocal set-up successfully to the field of the micro-PIXE technique by implementing a polycapillary half lens in front of the X ray detector and taking advantage of an excellent spatial resolution of an ion micro-beam. The first applications using a proton microbeam in vacuum [11] and under atmospheric pressure [12] have clearly demonstrated the potential of the technique in the analysis of stratified materials to resolve elemental depth profiles. The particular advantage of an ion microbeam for fast lateral scanning has driven 3D elemental investigations. M. Žitnik et al. [13] have presented 3D element selective imaging of aerosol micro particles captured in thick quartz filters with a micron spatial resolution aiming finally to deduce concentration depth profiles for the strong emitters of the sample (Fe, Ca and S).

Theoretical models that may simulate 3D micro-PIXE intensities for various experimental parameters, sample structure, local compositions and scanning modes have been recently proposed [14, 15] enabling a systematic assessment of the analytical potential of the technique. In this report the experimental and theoretical work undertaken up to now for the development of the 3D micro-PIXE technique is reviewed. Furthermore, characteristic applications and examples will be presented and discussed revealing in that way the advantages and the limitations of the 3D micro-PIXE analysis in respect to other nuclear analytical techniques aiming to depth elemental analysis.

2. Overview of research performed and results obtained

2.1. *Basic principles and experimental setup of 3D micro-PIXE*

The basic principle for the realization of the 3D micro-PIXE technique is the creation of a confocal geometry. The confocal setup is defined through the intersection of a focused proton microbeam, formed by a nuclear microprobe, and the sensitive detection field of an X ray polycapillary lens, placed in front of an X ray detector (Fig. 1). When a sample is irradiated, this common intersected volume, the so-called probing microvolume, restricts spatially the irradiated area being under detection with respect to the whole area producing the total PIXE

yield. In that way, when sample's position is sequentially changed with respect to this volume, laterally as well as into depth three-dimensionally resolved information can be extracted with spatial resolution of some tens of micrometers. The spatial resolution which can be obtained depends on the corresponding performance of the nuclear microprobe and the X ray lens.

Nuclear microprobes can provide proton microbeams in vacuum below 2 μm in size; while 10–20 μm are achieved when the beam is extracted in air (external microbeams). Microbeam cross section is defined through a pair of perpendicular slits. Thus, the beam can be suitably described as a rectangular with a constant flux density. Furthermore, experimental findings indicate that the beam size does not change noticeably along its propagation direction for about 100–150 μm around its optimum focal point [11].
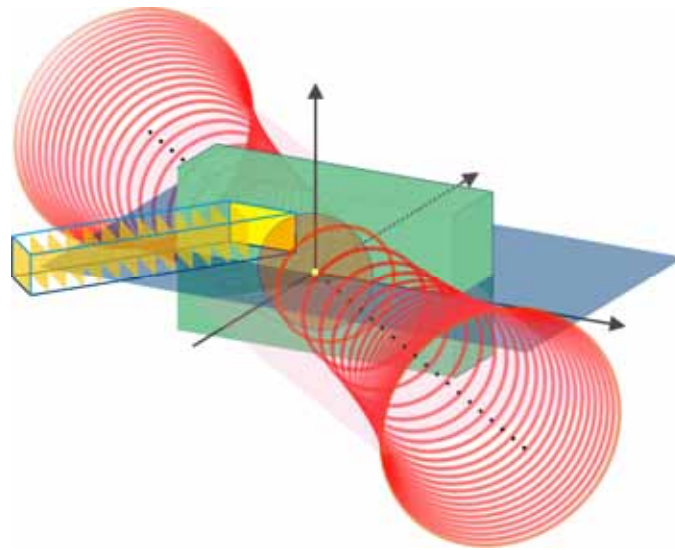
FIG. 1. Graphical representation of typical confocal micro-PIXE geometry. A rectangular ion microbeam (yellow) irradiates a sample which is observed though the sensitive detection-volume of a polycapillary lens (the red surface represents an isosurface of the lens acceptance for a given X ray energy).

With respect to characterization of the X ray optics, several authors have investigated the flux density distribution of X ray beams formed by polycapillary lenses [16–19]. The spatial distribution of the focused X ray micro-beams has been examined experimentally by means of knife edge or wire scan methods. It came out that the spatial distribution is very well represented by a Gaussian function. Therefore, it has been suggested [20] that a two-dimensional Gaussian bell function is the best candidate for the description of the profile of a focused X ray micro-beam. T. Wolff et al. [21] have recently provided a thorough experimental investigation of the energy dependence of the polycapillary half-lens spot size and its transmission function, when it is utilized either in the focusing or collecting mode, namely when the incoming or outgoing X ray beam is parallel, respectively. In both cases, the spatial distribution of the focused beam or of its acceptance function can be described by a Gaussian-like function. However, in the latter (collecting) mode, much larger spot sizes are produced and the differences increase as the energy of the transmitted X ray s is decreased. Thus, it will finally be adopted that in this case (collecting mode) the spatial resolution of the lens exhibits the same shape like the flux density distribution of a focused X ray micro-beam.

Modern polycapillary lenses can provide spatial resolution with a FWHM down to 15–20 μm at 8 keV while usually exhibit an inverse (E^{-1}) functional dependence with the transmitted X ray energy due to the dependence of critical angle for total external reflection on energy.

For the confocal micro-PIXE setups using proton microbeams of very small dimensions (with respect to the FWHM of the polycapillary half-lens), the probing microvolume characterization is actually based on the dominant influence energy-dependent, Gaussian response function of the X ray lens. Therefore, the setup's spatial sensitivity function exhibits a 'Gaussian' shape along propagation of the microbeam.

3D micro-PIXE measurements aim to scan sequentially this spatial sensitivity function over the sample's surface, as well as along the depth below the surface in order to provide complete 3D resolved information. The experimental implementation of the sample scanning across the probing microvolume is attained by means of proper stepping motors with accuracy at the micrometer regime. Furthermore, ion micro-beam focusing devices (nuclear microprobes), can provide reproducible scanning of the micro-beam with sub-micrometer accuracy in the plane perpendicular to its propagation axis. This experimental possibility adds considerable flexibility, precision and speed towards elemental depth profiling in a confocal geometrical setup as well as 3D profiling when it is combined with the sample scanning mode [13, 14].

2.2. Current developments and applications of 3D micro-PIXE

For investigating the performance and potentials of 3D micro-PIXE several experimental efforts have already been accomplished. As a first demonstration, an artificial multilayer target has been examined [11] in order to evaluate the depth resolving capacity of the method (Fig. 2). The investigated multilayer sample had the following layer sequence: Ag/Kapton/Au/Kapton/ Ni/Kapton/Cu with nominal foil thickness of 3 μm/12.5 μm/1 μm/12.5 μm/1 μm/12.5 μm/7 μm, respectively. It was prepared by simply attaching one foil onto the other one and packing all of them together in an aluminum frame.

(a)   (b)
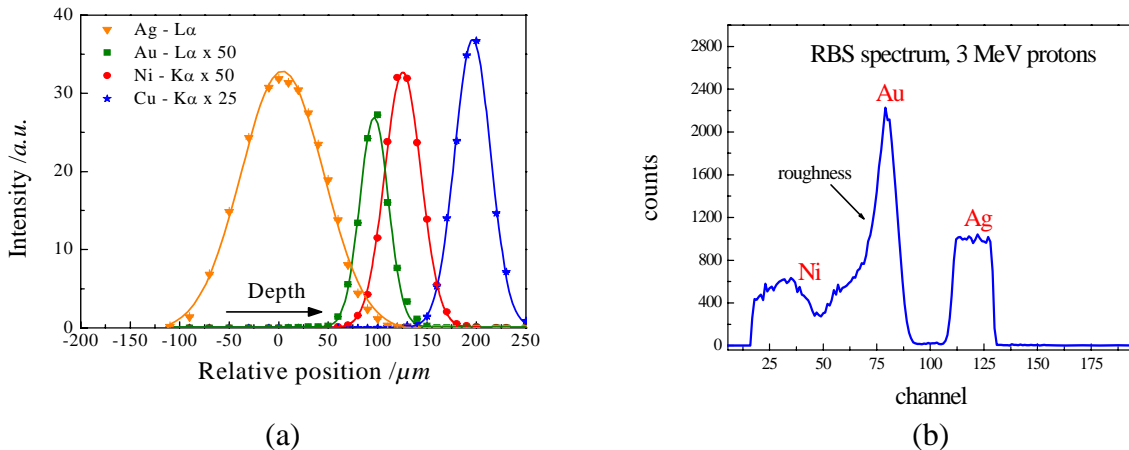
FIG. 2. a) Intensity depth profiles of a multilayer sample with the following structure: Ag (3μm)/ Kapton (12.5μm) /Au (1μm) /Kapton (12.5μm) /Ni (1μm)/Kapton (12.5μm) /Cu (7 μm) obtained by means of the 3D micro-PIXE analysis. The solid lines represent corresponding Gaussian fits. 2b) Spectrum from a simultaneous RBS measurement, but even using 3MeV protons the last layer of the sample could not be probed.

Although simple, this preparation technique does not allow a full control of the foil's positions, since the non-flatness of material may lead to in-between spaces and, consequently, to a displacement of their surfaces from a close-packed arrangement. This can be observed in the measured intensity profiles shown in Figure 2a. The ability of measuring the intensity profile of the copper foil at the bottom of the multilayer stack proves the potential of the new technique for depth resolved studies, which are not feasible by traditional ion beam techniques. For example, RBS and NRA can supply information only from a few micrometer into the depth (Fig. 2b). Furthermore, the most important aspect of 3D micro-PIXE analysis of the multilayer sample is that the uncertainties in the determination of the intensity profiles centroids are relatively small, close to 0.5 μm. The potential of the 3D micro-PIXE technique is therefore evident to provide in a rather straightforward manner qualitative analysis of a multilayered sample, provided that the layer thickness is small compared to the corresponding spatial resolution of the setup.

For the implementation and pilot evaluation of the confocal micro-PIXE setup in the characterization of a real layered structured material, an archaeological sample was examined. The sample is an attic ceramic small fragment (TH/CL-AKROP-34, 5cent. BC, Makrygianni, Acropolis), recently (2000–2003) excavated at the Akropolis area in Athens and dated back to the Classical period [11]. A SEM micrograph, of a freshly fractured cross section produced with secondary electrons is shown in Figure 3. In principle, the fragment consists of two basic layers, one black gloss layer on the top with a typical thickness ranging between 20–25 μm. The black gloss layer is fairly well adhered to a second layer, the ceramic porous body.
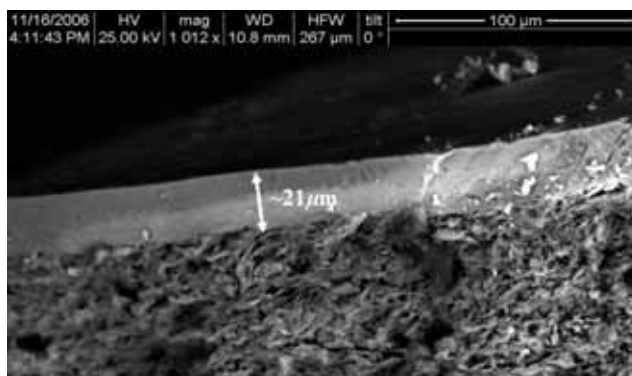
FIG. 3. SEM micrograph of a freshly fractured cross section of the Attic ceramic fragment with the code TH/ CL-AKROP-34, 5cent. BC, Makrygianni, Acropolis (magnification 1012x). The estimated black gloss layer thickness is 21 ± 2 μm.
Micrograph by courtesy of E. Aloupi.

The measured 3D micro-PIXE intensity depth profiles for Al, Si, K, Ca and Fe are presented in Figure 4. In order to simulate in a first attempt the obtained intensity depth profiles, PIXE intensities produced by a layer of infinitesimal small thickness located at various depths were convoluted with a Gaussian profile using the proper FWHM's after calibrating the experimental setup [11].
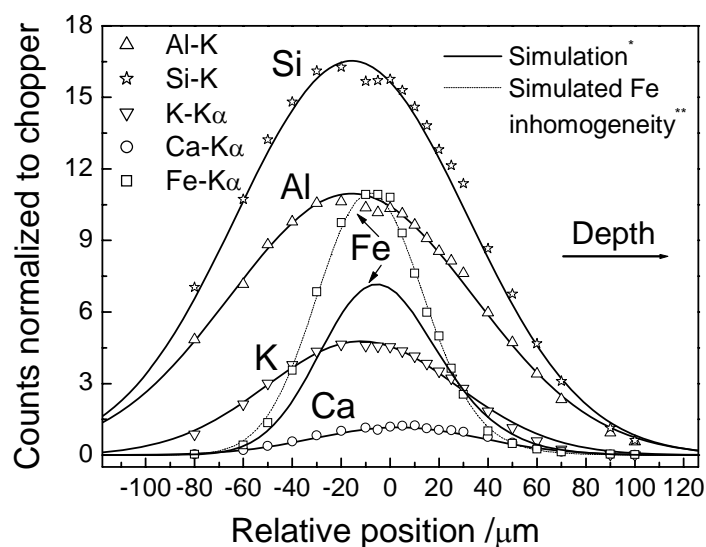
FIG. 4. Comparison between simulated and measured depth profiles obtained from the Attic ceramic fragment.

In Figure 4 the various solid lines represent simulated intensity profiles calculated using a black gloss layer thickness of 19 μm (that mainly affects the Ca profile) and the following concentrations for the gloss/body (g/b) two layer system: Al_2O_3 (33.0%) and SiO_2 (53.3%) for the black gloss layer only, K_2O (3.8/3.8%, g/b), CaO (0.40/16.7%, g/b) and Fe_2O_3 (16.8/11.4%, g/b). Initial values for the concentrations were extracted through Electron Probe Micro-Analysis (EPMA) and XRF techniques. EPMA was used to determine major and minor elements of the black gloss layer at a flat point of the surface, whereas XRF complemented the quantitative characterization of the black gloss surface layer and of the clay body at a section area [11].

The experimental 3D micro-PIXE profiles. However, they deviate about 10% with the corresponding ones of XRF and EPMA [11], which is an acceptable deviation for single spot analysis of such a complex sample. It is remarkable, however that the simulated Fe profile based on the results of XRF and EPMA fails to describe the Fe profile (Fig. 4). This might be attributed to the presence of Fe inhomogeneities in the proton beam path. The dotted line of Fig. 4 presents the result of a simulation of the experimental Fe profile by introducing at a depth of 8 μm a particle rich in Fe (~72%) with a size of about 1.2 μm, whereas the Fe concentration at the rest of the gloss layer was kept at a level of 16.3%.

A confocal micro-PIXE model aiming to reconstruct 3D element-specific local distributions has been proposed by M. Žitnik et al. [13, 14] and demonstrated just recently by the same authors [22]. To achieve 3D spatial resolution both scanning modes have to be applied. For the reconstruction of elemental concentrations the sample is divided in microscopic cubic cells. The model offers in quantitative terms the contribution of each cubic cell to the element specific intensity recorded per pixel from sequential 2D-images produced at each sample position by the microbeam scanning mode. The authors have applied this formalism in the case of PM10 aerosol particles immersed into a very low density matrix (quartz filter)

[13, 14]. The aerosol sample was obtained during the regular air quality monitoring at the open air bulk terminal of Port of Koper Slovenia. An air flow of 15 l /min was pumped for a week through a high purity quartz filter aerosol particles were preselected by an impactor with 10 μm aerodynamic cutoff diameter [13, 14]. The analysis of the raw 3D micro-PIXE data offered the element-specific concentrations of individual PM10 aerosol particles together with their respective positions with a micron spatial resolution. The penetration depth of Fe rich particles was found to be smaller than the one for Ca and S (Fig. 5) since iron is present in the dust in the form of larger particles than Ca and S. The concentration depth profiles are properly described by exponentially dumped function with penetration depth depending on the aerosol particle size.
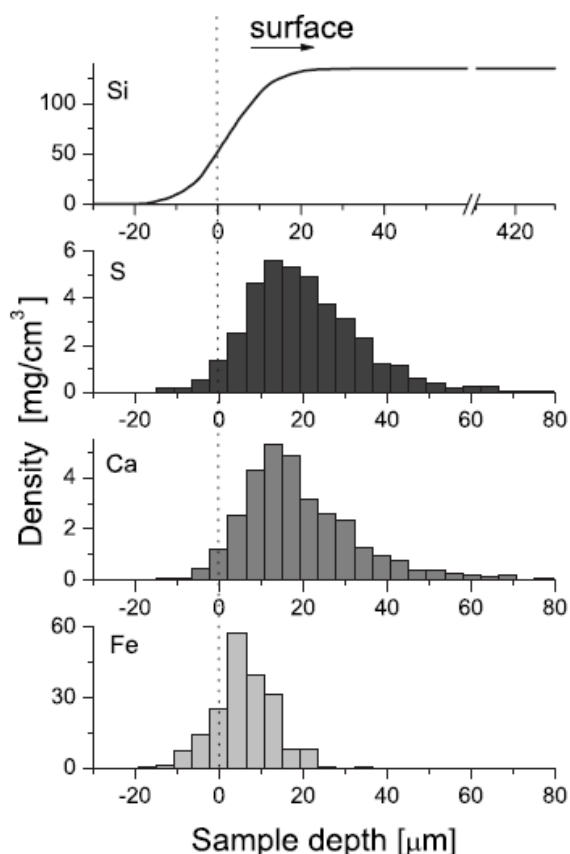
FIG. 5. *Concentration depth profiles of loaded quartz sample as generated from the local atomic densities. The profiles are normalized to surface mass densities determined by previous PIXE analysis.*

Just recently, the demonstration of true 3D composition analysis of an extended object where energy loss of protons and self-absorption effects cannot be neglected was accomplished by M. Žitnik et al. [22]. The spatial distribution of hematite in an irregular particle composed of hematite dust was reconstructed by a single sweep of the proton microbeam through the acceptance volume of the polycapillary lens. While the lateral resolution is determined by the proton microbeam cross section (~2 μm), the depth resolution was about 10 μm. The limiting factor for the latter is the field of view of the polycapillary lens. Although the object's material was known, the method could be effectively used for reconstruction of submillimeter objects containing a known share of light elements and an unknown share of 'visible' elements (Z>10). Larger objects can also be reconstructed but with an elaborate sample movement.

2.3. Discussion- advantages and limitations

3D micro-PIXE presents a new experimental method to look into the depth of a sample by combining an ion microprobe and X ray spectroscopy. In particular, when different elements are present in separate layers having a small thickness in the micrometer regime, 3D micro-PIXE reveals a powerful potential. The analysis of basic features of measured depth profiles provides in a direct way the distribution and the approximate depth position of the elements present in the sample. In a more general case, i.e. when elements are mixed in different layers or a concentration gradient exists in one or more layers, the analytical signal at various depth positions represents a rather complex concept. The 3D PIXE signal that emanates from various depths is convoluted with the setup's spatial resolution. This feature exhibits, as far as it concerns its complexity, some similarities with the differential PIXE analytical signal. However, 3D micro-PIXE depth profiles include additional information about local inhomogeneities that provide a more detailed knowledge of the elemental distribution and composition in the depth. Apart from the absolute scale of the intensity profile, its centroid position, FWHM and shape (if it is pure Gaussian or an asymmetric one towards the depth) may be considered as additional parameters supporting substantially the quantitative description.

The implementation of the confocal geometry at an ion-microprobe beamline has certain advantages with respect to 3D Micro-XRF setups. For 3D micro-PIXE only one X ray lens in front of the detector is required taking advantage of the excellent intrinsic spatial resolution of the ion microprobe. Also the beam scanning possibilities play an important role not only for the relative ease and fast alignment of the confocal setup, but also for deducing intensity depth profiles. On the other hand, the decrease of the proton ionization cross sections with increasing depth, in contrast to the fluorescence cross sections which are depth independent, is certainly a disadvantage and a limiting factor for depth analysis. Higher proton energies (greater than 3 MeV) and relative low atomic number matrices (organic, aluminum-silicate) increase the penetration depth of protons to more than 100 μm, thus, improving the information depth for elements emitting characteristic X ray s with energies above about 5 keV. It should also be pointed out that for metal alloys the 3D micro-PIXE information depth could be even larger than the corresponding one for 3D Micro-XRF analysis with X ray tubes. Hence, the magnitude of the X ray production cross sections and the proton penetration depth for a specific matrix are the decisive factors which method is more suited for a three dimensional elemental analysis.

A first comparison of 3D micro-PIXE with differential PIXE [1–4] has been accomplished by means of a theoretical quantitative model which describes 3D micro-PIXE intensities for stratified materials [15]. The model incorporates the effect of the finite ion micro-beam dimensions and the restricted spatial resolution of an X ray lens to generate the sensitivity function of the probing microvolume in a closed form. For comparison two samples having a quartz matrix with 1% of Fe concentration were selected. A lamina of 3 μm thickness with increased Fe concentration (3%), placed at depth of 5 μm and 30 μm, respectively, was also assumed. In Figures 6a and 6b the relative contribution of Fe Kα radiation (from the 3μm lamina) with respect to the total PIXE Fe yield is indicated versus the sample position and versus the ion impact energy.

74

It is obvious and very characteristic that the Fe 'anomaly' in the case of 3D micro-PIXE affects the measured Fe yield with higher sensitivity. More specifically, the partial contribution from the 3 μm lamina with 3% Fe concentration provides more enhanced but also localized contribution (with respect to the sample position) to the total Fe yield. In comparison with differential PIXE, in principle, 3D micro-PIXE seems to exhibit an enhanced sensitivity in respect to the spatial resolution that should be proved in practice by the analysis of the same real sample by both techniques in the future.
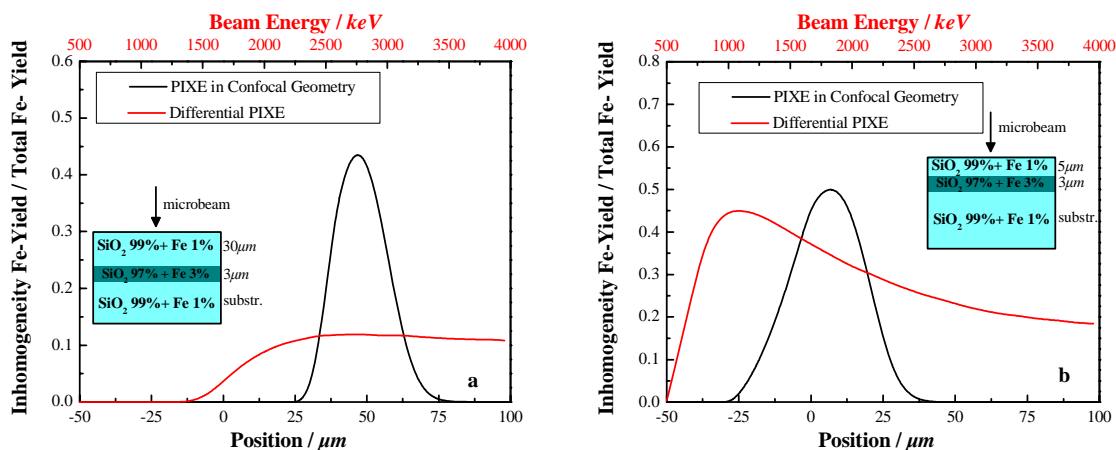

FIG. 6. Comparison of the depth probing sensitivity for 3D micro-PIXE and differential PIXE by estimation of the contribution of a local Fe inhomogeneity (3% in a lamina of thickness 3μm) to the total Fe yield. (Sample: quartz matrix with 1% Fe concentration, $E_0 = 3MeV$, $FWHM_{FeK\alpha} \sim 20\mu m$).

3. Conclusions

The use of a polycapillary half lens in a typical micro-PIXE setup renders the conventional micro-PIXE technique into a new tool for depth resolved elemental analysis. 3D micro-PIXE provides the possibility to resolve elemental distribution in separate layers in a complex structure. The information depth can range even up to 40–50 μm, overcoming in some cases the analytical capabilities of standard ion beam techniques for elemental depth profiling.

The significant potential of the new method to provide direct three-dimensional information on the elemental distribution has been shown so far for a complex, archaeological sample as well as for an aerosol PM10 filter. In general, 3D micro-PIXE may be used for the investigation and determination of structure and composition of layer systems and of elemental concentration gradients. Furthermore, it is suitable to select individual micrometer sized objects which are within a probing depth beneath the surface. In comparison to 3D Micro-XRF analysis, the confocal micro-PIXE setup will be more suited for depth analysis of light elements at a probing depth below 5–10 μm. With its non-invaisive and depth-resolving properties, 3D micro-PIXE seems especially suited for investigations in the field of environmental studies, biology and cultural heritage and for thick samples with light Z matrix in general.

4. General remark

A large part of this report has already been reported by us for the IAEA under the title "3D micro-PIXE, a new development for the micro-PIXE Technique- Analytical applications and perspectives". It was a contribution to the IAEA Technical Meeting (G4-TM-34787) "Special Configurations and New Applications of Micro-analytical Techniques Based on Nuclear Spectrometry" which took place in Vienna, Austria, on the 20th to 24th October 2008.

REFERENCES

[1] NEELEMEIJER, C., WAGNER, W., SCHRAMM, H.P., Depth resolved ion beam analysis of objects of art, Nucl. Instr. and Meth. **B118** (1996) 338.
[2] DEMORTIER, G., RUVALCABA-SIL, J.L., Differential PIXE analysis of Mesoamerican jewellery items, Nucl. Instr.and Meth. **B118** (1996) 352.
[3] NEELEMEIJER, C., MÄDER, M., Quantitative analysis in confocal micro-PIXE general concept and layered materials, Nucl. Instr.and Meth. **B189** (2002) 293.
[4] WEBER, G., DELBROUCK, J.M., STRIVAY, D., KERFF, F., MARTINOT, L., Use of a variable incidence angle PIXE arrangement for studying pigment multilayers, Nucl. Instr.and Meth. **B139** (1998) 196.
[5] KANNGIEßER, B., MALZER, W., REICHE, I., A new 3D micro X ray fluorescence analysis set-up – First archaeometric applications, Nucl. Instr. and Meth. **B211–212** (2003) 259.
[6] KANNGIEßER, B., MALZER, W., FUENTES RODRIGUEZ, A., REICHE, I., 3D micro-XRF Investigations of Paint Layers with a tabletop set-up, Spectrochim Acta **B60** (2005) 41.
[7] KANNGIEßER, B., MANTOUVALOU, I., MALZER, W., WOLFF, T., HAHN, O., In-Situ Analysis of Corrosion Layers of Historical Glass Objects by 3D Micro X-ray Fluorescence Analysis, J. Anal. At. Spectrom., 2008. DOI:10.1039/B717286A.
[8] WOLL, A.R., et al., Development of confocal X ray fluorescence (XRF) microscopy at the Cornell high energy synchrotron source, Appl Phys **A83** 2 (2006) 235.
[9] JANSSENS, K., PROOST, K., FALKENBERG, G., Confocal microscopic X-ray fluorescence at the HASYLAB microfocus beamline: characteristics and possibilities, Spectrochim Acta **B59** (2004) 1637.
[10] PATTERSON, B.M., HAVRILLA, G.J., Three-dimensional elemental image using a confocal X-ray fluorescence microscope, American Laboratory **38** 8 (2006) 15.
[11] KARYDAS, A.G., et al., 3D Micro-PIXE – a new technique for depth-resolved elemental analysis, J. Anal. At. Spectrom. **22** (2007) 1260.
[12] KANNGIEßER, B., et al., 3D Micro-PIXE at atmospheric pressure: A new tool for the investigation of art and archaeological objects, Nucl. Instr. and Meth. **B264** (2007) 383.
[13] ŽITNIK, M., et al., Three-dimensional imaging of aerosol particles with scanning proton microprobe in a confocal arrangement, Appl. Phys. Lett. **93** (2008) 094104. DOI:10.1063/1.2976163.
[14] ŽITNIK, M., et al., Element-selective three-dimensional imaging of microparticles with a confocal micro-PIXE arrangement, X-ray Spectrom. **38** 6 (2009) 526–539.
[15] SOKARAS, D., et al., Quantitative analysis in confocal micro-PIXE – general concept and layered materials, J. Anal. At. Spectrom. **24** (2009) 611–621.
[16] PROOST, K., et Al, Characterization of a polycapillary lens for use in micro-XANES experiments, X-ray Spectrom. **32** (2003) 215.

[17] GORMLEY, J., JACH, T., STEEL, E., XIAO, Q.-F., Adv. X-ray Anal. **41** (1997) 239.

[18] GAO, N., PONOMAREV, I., Polycapillary X-ray optics: manufacturing status, characterization and the future of the technology, X-ray Spectrom. **32** (2003) 186.

[19] HASCHKE, M., HALLER, M., Examination of poly-capillary lenses for their use in micro-XRF spectrometers, X-ray Spectrom. **32** (2003) 239.

[20] MALZER, W., KANNGIEßER, B., A model for the confocal volume of 3D micro X-ray fluorescence spectrometer, Spectrochim Acta B **60** 9–10 (2005) 1334.

[21] WOLFF, T., et al., Performance of a polycapillary halflens as focussing and collecting optic – a comparison, J. Anal. At. Spectrom., DOI:10.1039/B817828C (2009).

[22] ŽITNIK, M., et al., 3D-reconstruction of an object by means of a confocal micro-PIXE, J. Anal. At. Spectrom. **25** 1 (2009) 28–33.

DEVELOPMENT OF A MULTIPURPOSE PIXE INDUCED XRF TECHNIQUE

D. SOKARAS, A.-G. KARYDAS, C. ZARKADAS, A. LAGOYANNIS
Institute of Nuclear Physics, NCSR "Demokritos",
Athens,
Greece

B. BECKHOFF, R. FLIEGHAUF
Physikalisch-Technische Bundesanstalt,
Berlin,
Germany

Abstract

The development, installation and research undertaken with a multi-functional PIXE induced XRF scattering chamber at the Demokritos Tandem VdG 5.5MV TN accelerator are reported. The set-up combines optimally the advantages of particle and photon interactions with matter supporting research in the following topics: Quantitative sub-keV X ray fluorescence spectrometry and the study of the X ray resonant Raman scattering for elements not sufficiently studied previously. The work undertaken within the three years of the CRP life will be overviewed including the developed integrated PIXE and XRF software and first measurements of fundamental parameters related with Fe inner shell de-excitation processes and the X ray resonant Raman scattering on Al, as well as with quantification related topics.

1. Introduction

The Particle Induced X ray Emission (PIXE) and X ray Fluorescence (XRF) are well established analytical techniques providing simultaneous multi-elemental analysis of a variety of samples with interest in various fields, ranging from material, biomedical and earth sciences, to environmental, archaeometrical, forensic and industrial applications [1,2]. The minimum detectable concentrations that can be attained by both methods are in the low ppm (µg/g) region or below [in SR-XRF, 3] for the most of the analyzed elements and for a wide range of matrix sample compositions. The particular advantages of the two methods are based on the high ionization cross sections of inner atomic shells by either X ray s or charged particles [4] and the much lower background production, being mainly attributed for PIXE in the sample induced bremsstrahlung radiation [5] and for XRF in various detector contributions [6, 7].

Within this CRP a dynamic utilization of the advantages of the PIXE and XRF methods was proposed by means of the development of a multipurpose integrated X ray spectrometric PIXE induced XRF technique for materials research. The PIXE mode can be used at first to provide an intense X ray source by irradiating a pure thick target (with an atomic number Z=13–30) with few MeV protons [8, 9]. The incorporation of an appropriate filter between the primary target and the sample improves considerably the spectrum purity and quality of the exciting X ray beam, i.e. attenuating the low energy bremsstrahlung background component and absorbing completely the backscattered particles, respectively [10]. The XRF mode of excitation can be accomplished next by positioning the sample of interest between the primary target and detector in the usual two orthogonal axes geometry.

The concept of proton induced almost monochromatic X ray s has been utilized in the past in various studies related with the impurities or minor elements quantitation in pure metal matrices [11–15], as well as for X ray resonant Raman scattering (RRS) studies [15–19].

However, the experimental set-ups, developed up to now, did not allow a full exploitation of the analytical possibilities of the PIXE induced XRF technique. The developed within this CRP novel multifunctional scattering chamber at the Demokritos Tandem 5.5 MV TN accelerator opened a new area of research and applications, in particular in the soft X ray energy region.

2. Overview of the research performed and the results obtained

2.1. Development and installation of the integrated PIXE induced XRF experimental *set-up*

The specifications and the main part of the multifunctional PIXE induce XRF scattering chamber design was accomplished by Demokritos group and then a specialized company (BESTEC GmbH, Berlin-Germany) finalized the mechanical drawings and constructed all the mechanical parts. In Figure 1 and in the appendix figures, final drawings of the various parts of the scattering PIXE-XRF chamber are presented.

The PIXE-XRF chamber was designed in an optimized geometry ensuring maximum solid angles combined with efficient collimation (in both the excitation and detection channel). In summary, the experimental setup incorporates the following instrumentation and characteristics:

- Two level chamber (low level: primary targets, upper level: samples).
- Two rotatable feedthroughs for positioning six primary targets and six samples.
- Primary target feedthrough electrical isolated & liquid cooled.
- Filter wheel with 8 positions enabling the stopping of the backscattered ions and filtering of the exciting X ray beam.
- All excitation/detection angles are set at 45 degrees.
- Oil-free vacuum system composed by a turbo-molecular pump with carbon-free backup vacuum pump.
- An X ray UTW Si(Li) detector with a AP1.7 window (Gresham/e2v Sirius®).
- Dose monitor through charge integration or/and an X ray Si PiN detector (Amptek®).

2.2. Development of combined PIXE-XRF software

A new software was developed in C++ language including appropriate data bases to account for: (i) the K-shell and L-subshell proton ionization cross sections (up to 4 MeV) of all the elements of the periodic table (ii) K and L- subshell fluorescence cross sections, (iii) stopping power of protons in matter and (iv) mass attenuation coefficients of X ray s in matter.

(a)

(b)
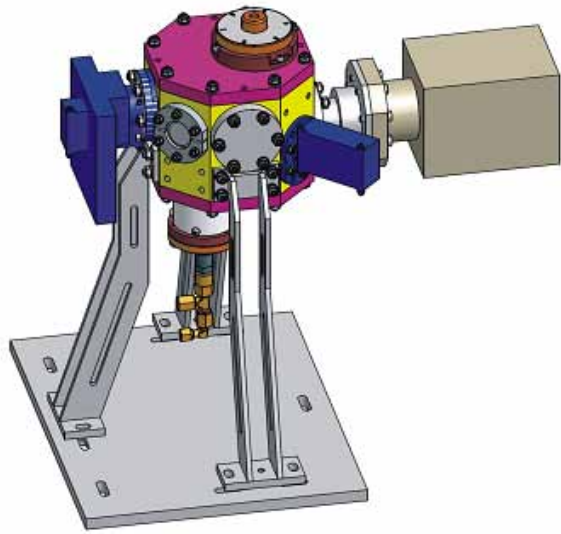
(c)

FIG. 1. (a) The PIXE induced XRF experimental setup on the R2 beam line at Tandem VdG Laboratory of INP (Institute of Nuclear Physics), (b) 3D mechanical drawing of the PIXE induced XRF chamber, and (c) close-up view indicating the geometry of the primary target and sample irradiation.

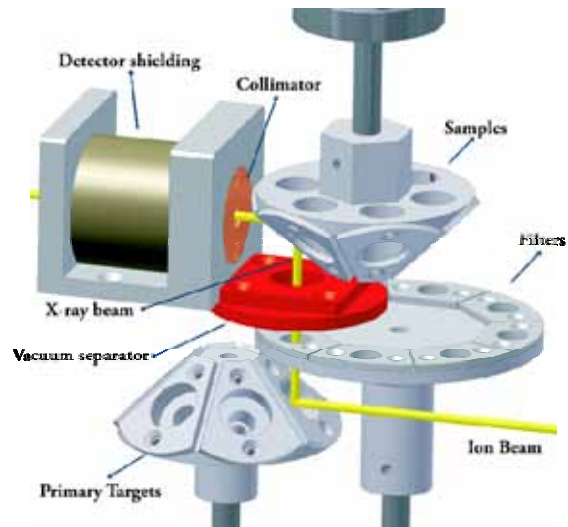By this way, integrated simulations of the PIXE induced XRF intensities can be carried out. In Figure 2 an example of the application of the new software is shown.
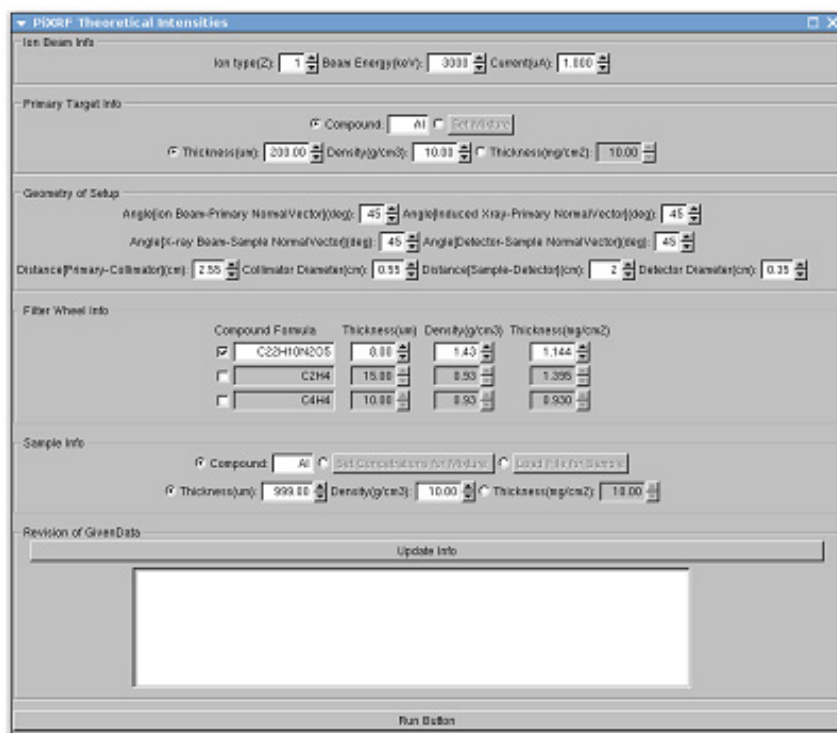
FIG. 2. The GUI of the developed software that simulates PIXE induced XRF intensities.

As an example of the developed software, calculations for the total X ray distribution emanating from a Cu thick target when 3MeV protons bombarding its surface are displayed in Figure 3. Using proper filtering for the resulted X ray beam, the relative intensity of the total continuum radiation with respect to the characteristic X ray lines can be well below 1%. The calculation of the bremsstrahlung emission by the Cu target was based in a parameterization proposed by Murozono et al. [20].

FIG. 3. X ray energy intensity distribution induced by 3 MeV protons an a Cu pure target.

For a well defined solid angle (4.7msr), a total X ray flux up to ~10^8 photons per second is feasible (Fig. 4). It is evident that the proton induced monochromatic X ray intensities despite of their lower specifications with respect to the one produced at a synchrotron facility (for example at BESSY II X ray intensities of about ~ 2–5 10^{10} s^{-1} are feasible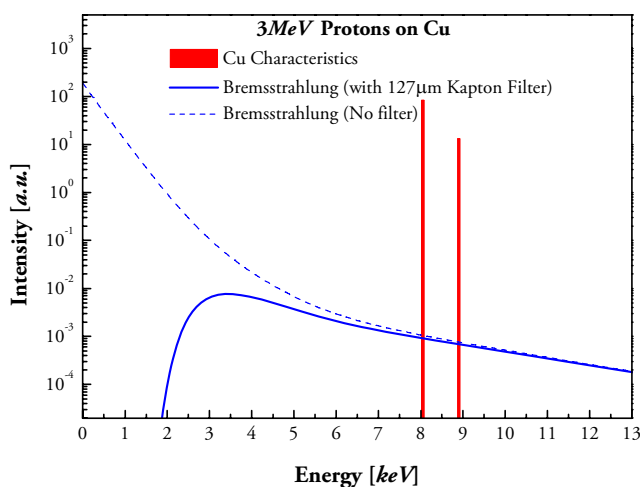 exhibiting also sub-millimeter spatial resolution and polarization properties), can be still considered as an alternative, in particular low X ray energy source for dedicated experiments.
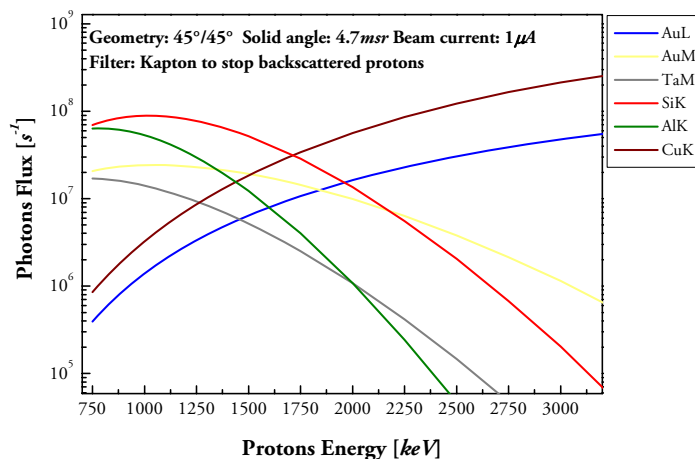
FIG. 4. Photons Flux from various targets vs. proton energy.

An additional stand alone software application has been also developed towards the quantification of PIXE induced XRF analyses. The software is also applicable for the quantitation of individual PIXE or XRF analyses including any mode of X ray excitation. The spectrum deconvolution procedure and the determination of unknown concentrations are linked simultaneously in an iterative manner leading thus to more accurate analysis of the spectrum intensities. An example of the relevant GUI is shown in Figure 5.
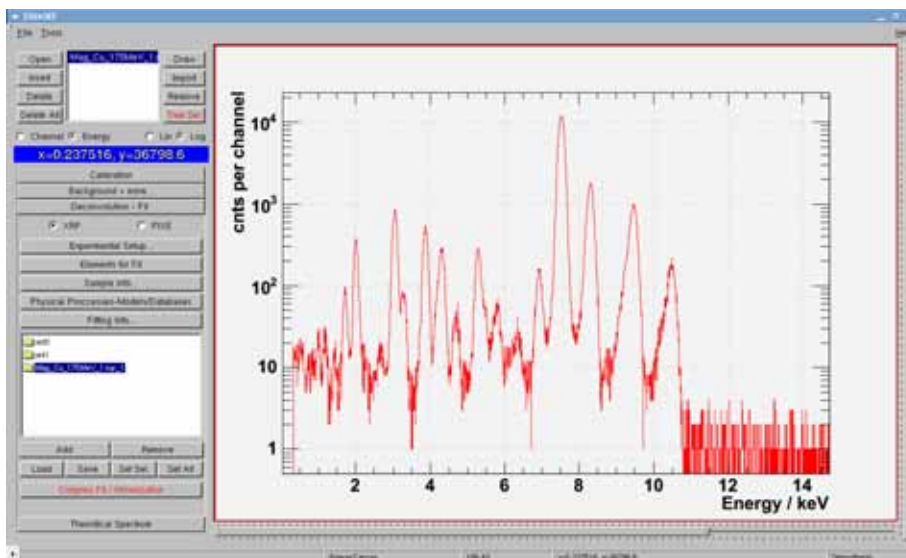
FIG. 5. GUI of the developed software for quantification analysis in combination with spectra deconvolution.

2.3. X ray Resonant Raman Scattering on Al

Experimental measurements of the Resonant Raman scattering (RRS) on aluminium (Al) at 1.5 keV (Al-Ka) incident X ray beam have been performed. Analysis for the absolute RRS cross section determination is under evaluation in order to be compared with corresponding unpublished measurements performed in PTB laboratory at BESSY II synchrotron radiation facility. In this way, the behaviour of the phenomenon with respect to the polarized and un-polarized type of incident radiation will be studied. In Figure 6 the acquired RRS spectrum is presented together with the least squared fit based on the theoretical description of experimental RRS intensities [18]. The absolute RRS cross section will be resulted based either on the fluorescence K– emission of lighter than Al elements (F, Na, Mg), or based on the respective RSS cross section of Si by Si-K incident X ray beam. It should be noted that up until now experimental light element RRS cross sections have been reported only for silicon and in particular, apart the work performed by Hall et al. [21], only the very recent publications [22, 23] are relevant.
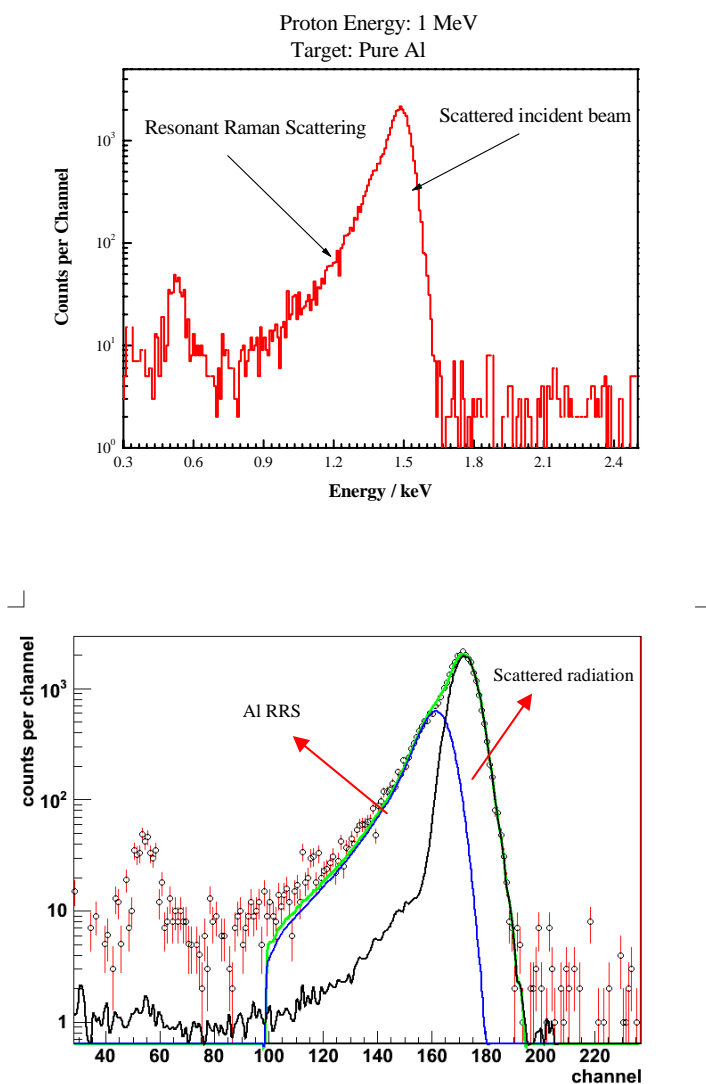
FIG. 6. Resonant raman scattering on aluminum induced by Al-K lines.

2.4. Study of cascade effect in Fe-L lines

A detailed study for the enhancement of the intensity of Fe-L fluorescence lines due to the cascade effect triggered by the K-shell hole de-excitation process has been accomplished. Using a wide range of primary targets, an extended energy range of primary X ray beams was produced, both above and below Fe-K shell binding energy (7.11keV). In this way, the relative jump of the Fe-L lines intensity when the energy of the incident X ray beam exceeds the Fe-K shell binding energy has been determined (Fig. 7).
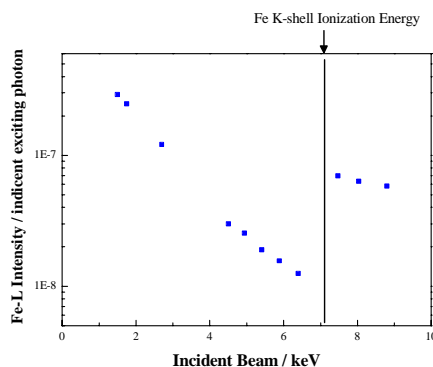
FIG. 7. Experimental Fe-L intensities normalized per incident photon measured by means of different proton induced X ray beams. The abrupt jump of the Fe-L intensity above Fe-k shell energy indicates the K to L cascade effect.

2.5. Selectable energy excited X ray Fluorescence analysis of geological samples

Using different proton induced X ray beams (Al-K, Ti-K, Cu-K), a selectable energy XRF analysis was performed for geological origin standard reference materials (IAEA-SL1, USGS-MAG1) (Fig. 8).
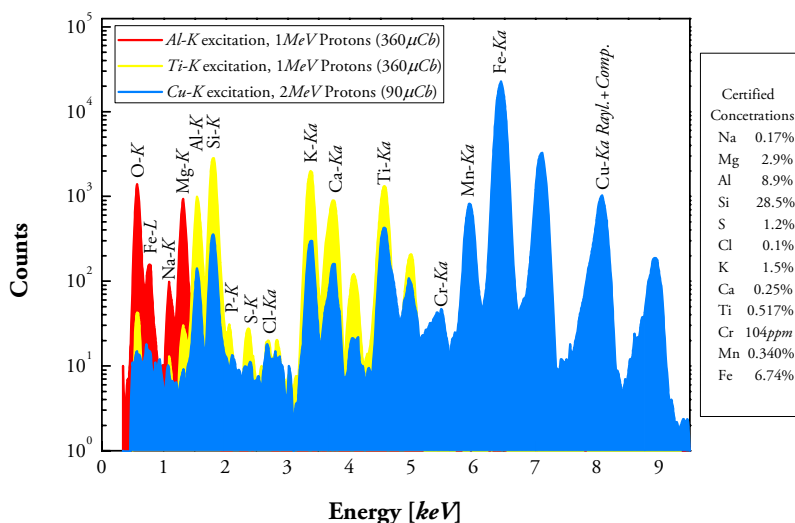
FIG. 8. The IAEA reference material SL-1 analyzed by means of three different proton induced X ray beams

For particular elements, respective minimum detection limits were determined presenting the analytical potential of the proton induced XRF technique (Table 1).

TABLE 1. MINIMUM DETECTION LIMITS EXPRESSED IN PPM FOR THE SL-1 AND MAG-1 STANDARD REFERENCE MATERIALS FOR DIFFERENT EXCITING X RAY BEAMS (CU-K, TI-K AND AL-K)

Proton beam dose 150uCb (~300s with 0.5uA proton beam current).

	Element	Concentration (ppm)	Minimum detection Limit (ppm)		
			Cu-K	Ti-K	Al-K
SL-1	Na	1720	nd	nd	202
	Mg	29000	nd	6638	287
	Ca	2500	186	20	nd
	Ti	5170	48	nd	nd
	Mn	3460	33	nd	nd
MAG-1	Al	86760	8783	2439	
	Si	235800	4405	1414	
	Cl	31000	230	57	
	Ca	9590	189	34	
	Ti	4500	89	nd	
	Mn	760	49	nd	

3. Conclusions

A PIXE induced XRF scattering multi-functional chamber has been successfully designed and installed at the 5.5MV Tandem VdG accelerator of Institute of Nuclear Physics at N.C.S.R. "Demokritos", Athens, Greece. It has been demonstrated that through an electrostatic (Tandem VdG) accelerator, research can be conducted related to the basic interactions of X ray s and atoms (Resonant Raman Scattering), as well as for atomic de-excitation processes (K to L-shell cascade effect in Fe). Furthermore, a general-purpose quantification software for XRS has been developed applicable not only for the PIXE-induced XRF technique but also for general X ray spectrometric purposes.

The first experimental results obtained so far have showed optimum analytical performance (analytical range, sensitivity) in the low and sub-keV energy region, a critical development in comparison with the conventional tube excited XRF and PIXE modes. The perspectives for further applications are numerous and significant towards: Systematic measurement of RRS cross sections, the improvement of the detection limits for certain trace elements in metallic matrices, evaluation of secondary processes in XRF spectrometry and for applying and assessing reference-free quantitation using unpolarized excitation.

REFERENCES

[1]   JOHANSSON, S.A.E., CAMPBELL, J.L., P.I.X.E. A novel Technique for Elemental Analysis, John Wiley and Sons, 1988.

[2]   Handbook of X ray Spectrometry, Eds. R. Van Grieken and A. Markowicz, Marcel Dekker Inc., 1993.

[3]   SPARKS, Jr., C.J., X ray fluorescence Microprobe for Chemical Analysis, In Synchrotron Radiation Research (h. Winick and S. Doniach, eds) pp. 459–512, Plenum New York 1980.

[4]   PAUL, H., An analytical cross section formula for K-production by protons, Nucl. Instr. Meth **B3** (1984) 5.

[5]   ISHII, K., MORITA, S., Continuous Background in PIXE, Int. J. PIXE **1** (1990) 1.

[6]   CAMPBELL, J.L., MAXWELL, J.A., PAPP, T., WHITE, G., Si(Li) Detector Lineshpaes: Contribution from Atomic Physics and Detector Properties, X-ray Spectrometry **26** (1997) 223–231.

[7]   PAPP, T., On the response function of solid-state detectors, based on energetic electron transport processes, X-ray Spectrometry **32** (2003) 458–469.
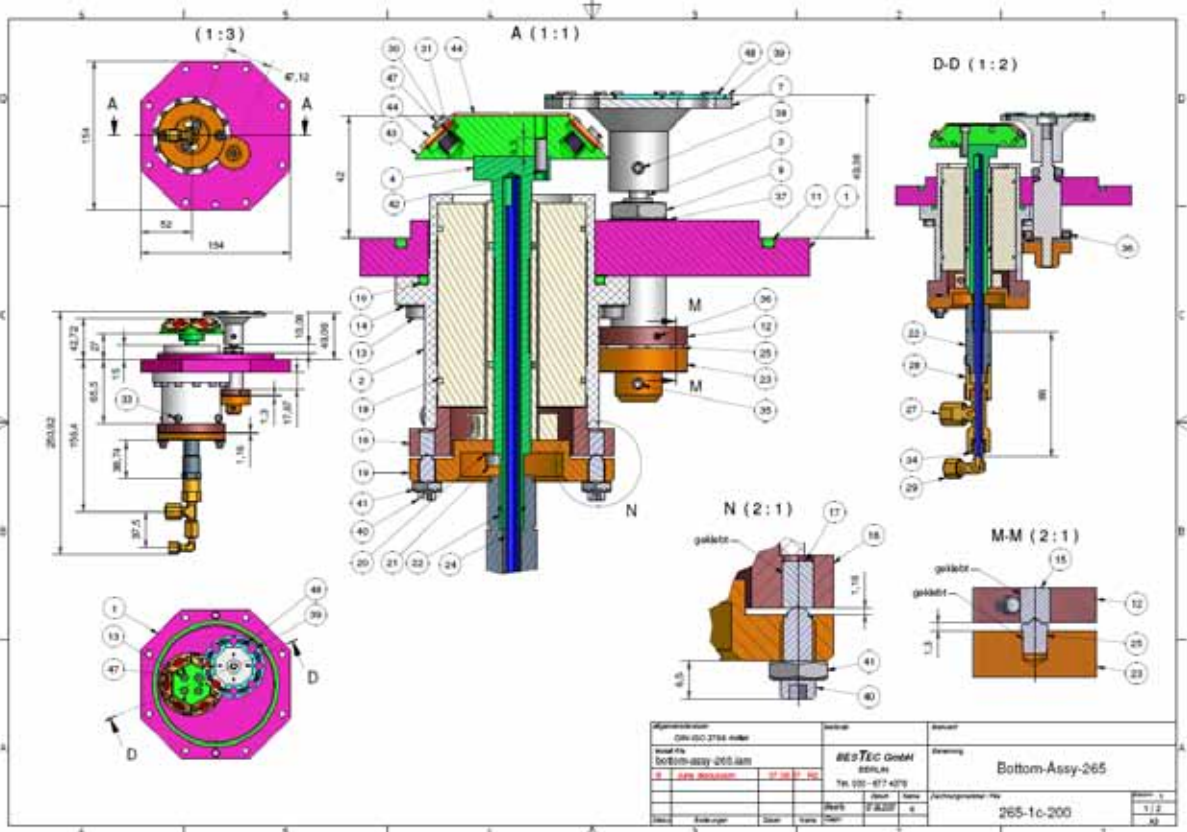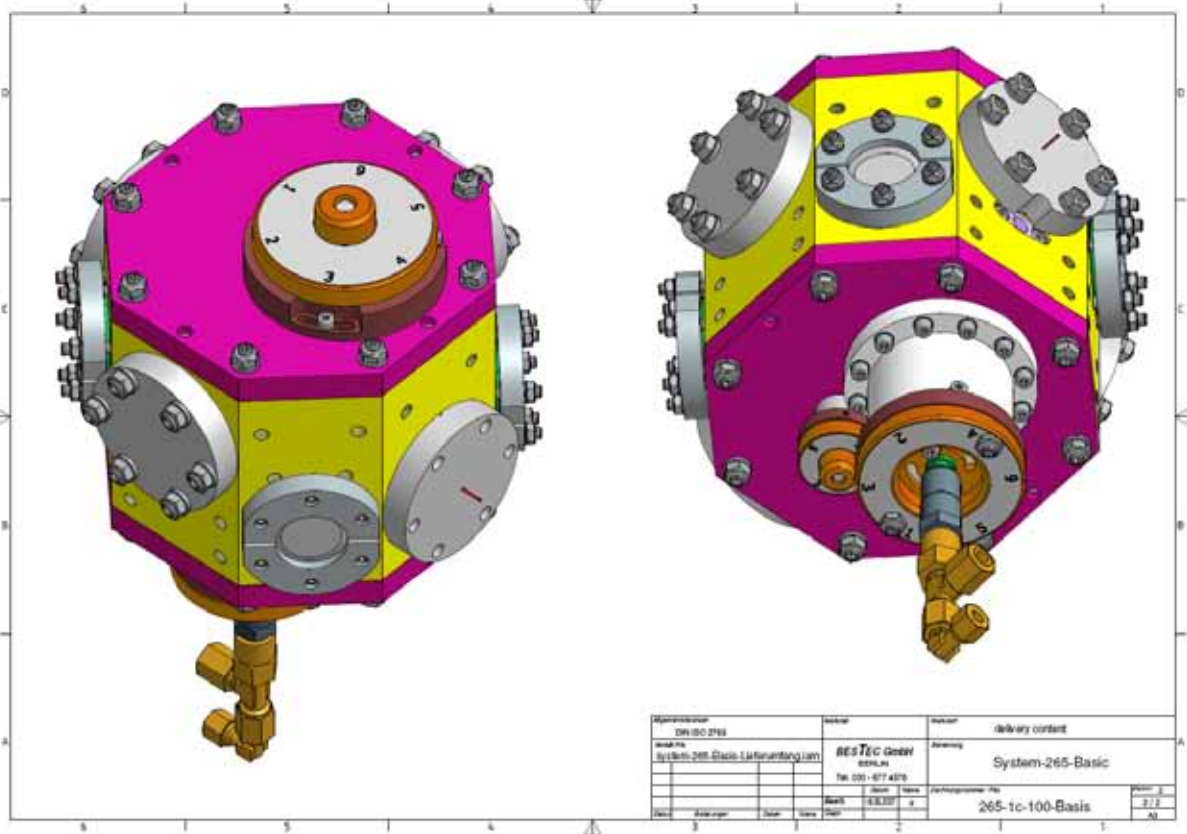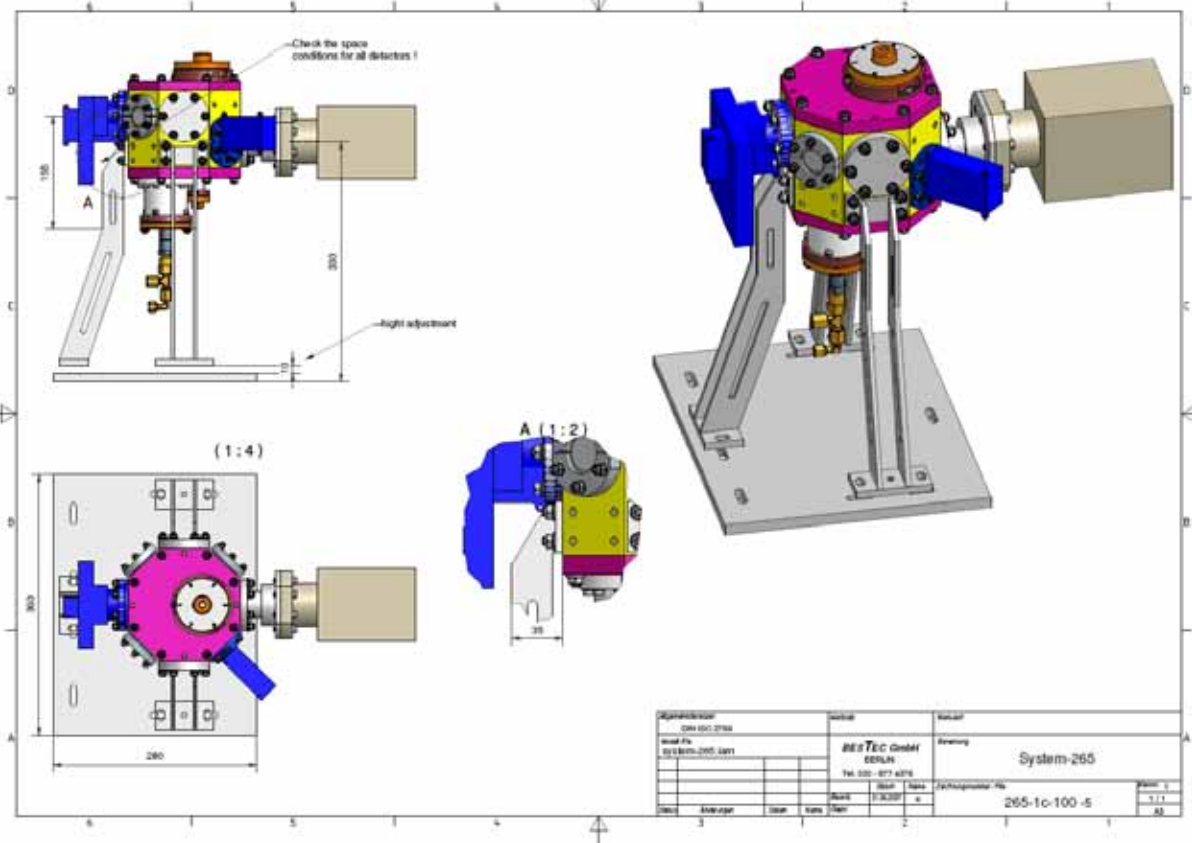
[8]   GRODZINS, L., BOISSEAU, P., Ion Induced X-Rays for X-ray Fluorescence Analysis, IEEE Trans. Nucl ScI. NS **30** (1983) 1271.

[9]   KARYDAS, A.G., PARADELLIS, T., Proton Induced Monochromatic X-ray Beams, X-ray Spectrometry **22** (1993) 252–259.

[10]   AVALDI, L., BASSI, S., MILAZZO, M., SILARI, M., Intense sources of monochromatic X-ray s for XRF analysis from cyclotron beams, Nucl. Instr. Meth. **B49** (1990) 24–28.

[11]   QUYNH, L.H., DEMETER, I., SZÖKEFALVI-NAGY, Z., PIXE induced XRF analysis of trace amounts of iron in pure copper matrix, Nucl. Instr. Meth. **B49** (1990) 566–568.

[12]   KOTANI, T., NAGASHIMA, S., KATO, M., MORITO, K., UDA, M., Interference peak intensities due to the Raman scattering in PIXE induced XRF, Nucl. Instr. Meth. **B109/110** (1996) 28–30.

[13]   NISHIDE, Y., SASA, Y., UDA, M., PIXE-induced XRF analysis of trace amounts of Mn, Cr, V, and Ti in low-steel alloys, Nucl. Instr. Meth. **B94** (1994) 271–276.

[14]   GUERRA, M.F., Fingerprint ancient gold with proton beams at different energies, Nucl. Instr. Meth. **B226** (2004).

[15]   G. DEMORTIER, S. MATHIOT, B. VAN OYSTAEYEN, PIXE Gadgets, Nucl. Instr. Meth. **B49** (1990) 46.

[16]   KARYDAS, A.G., PARADELLIS, T., Measurement of KL and LM resonant Raman scattering cross sections with a proton-induced Cr-Kα X-ray beam, J. Phys., B At. Mol. Opt. Phys. **30** (1997) 1893–1905.

[17]   KARYDAS, A.G., BUDNAR, M., SMIT, Z., ZARKADAS, Ch., PARADELLIS, T., Proton induced monochromatic X-ray beams: a versatile source for resonant Raman scattering studies, Nucl. Instrum. Methods **B189** (2002) 43–48.

[18]   KARYDAS, A.G., GALANOPOULOS, S., ZARKADAS, Ch., PARADELLIS, T., KALLITHRAKAS-KONTOS, N., Chemical state speciation by resonant Raman scattering, J. Phys., Condens. Matter **14** (2002) 12367–12381.

[19]   ZARKADAS, Ch., KARYDAS, A.G., MÜLLER, M., BECKHOFF, B., X-Ray Resonant Raman Scattering (RRS) on Ni employing polarized and unpolarized exciting radiation, Spectrochimica Acta Part **B61** (2006) 189–195.

[20]   MUROZONO, K., ISHII, K., YAMAZAKI, H., MATSUYAMA, S., IWASAKI, S., PIXE spectrum analysis taking into account bremsstrahlung spectra, Nucl. Instrum. Meth. **B150** (1999) 76–82.

[21] HALL, J.M., JAMISON, K.A., WEAVER, O.L., RICHARD, P., ABERG, T., Internal resonance Raman scattering of characteristic target K X-rays in thick silicon targets, Phys. Rev. **A19** (1979) 568.

[22] M. MULLER, BECKHOFF, B., ULM, G., KANNGIESSER, B., Absolute determination of cross sections for resonant Raman scattering on silicon, Phys. Rev. **A74** (2006) 012702.

[23] SZLACHETKO, J., et al., High-Resolution Study of X-ray Resonant Raman Scattering at the K Edge of Silicon, Phys. Rev. Lett. **97** (2006) 073001.

APPENDIX

A SET OF TECHNICAL DOCUMENTS FOR THE
PIXE-XRF SCATTERING CHAMBER

90

Check the space conditions for all detectors !

Right adjustment

A (1 : 2)

(1 : 4)

System-265

265-1c-100 -5
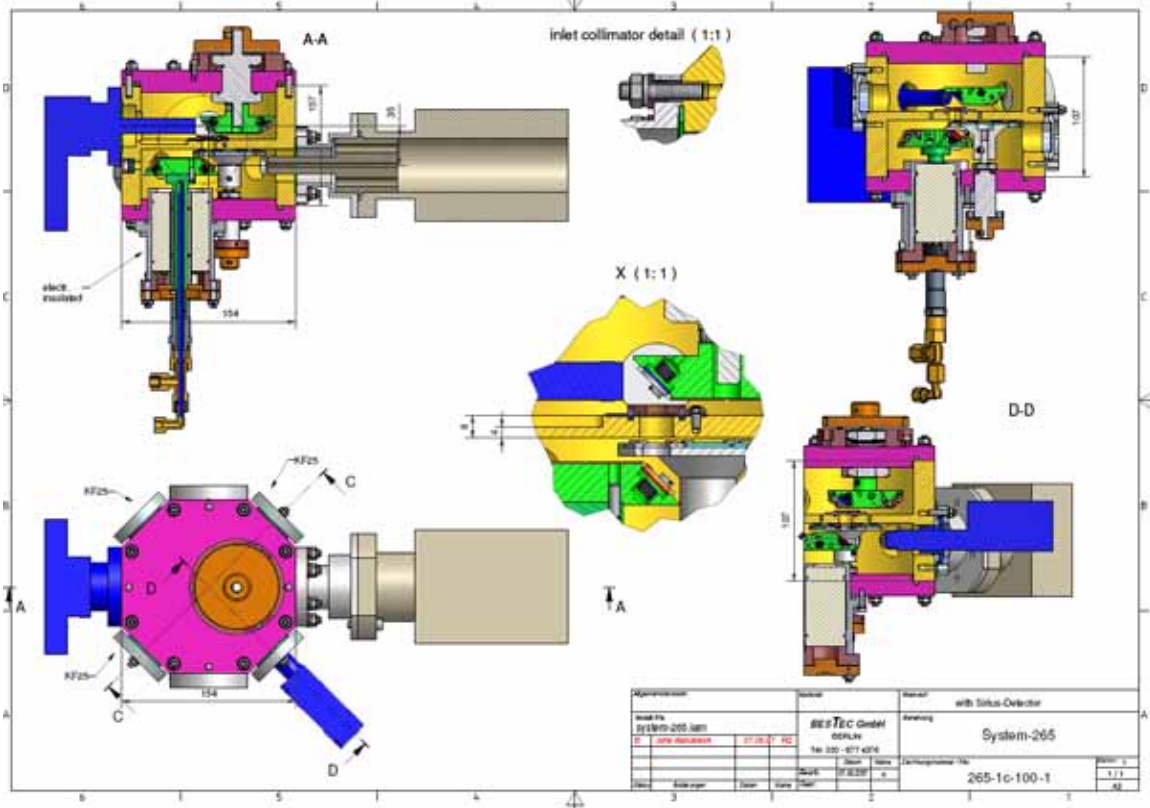
ANALYSIS OF PRE-COLUMBIAN AND CONTEMPORARY GOLD ALLOYS AVAILING OF EDXRF EQUIPMENT

R. CESAREO
Dipartimento di Matematica e Fisica, Università di Sassari,
Sassari,
Italy

S. RIDOLFI
Ars Mensurae,
Roma,
Italy

Abstract

Gold alloys of moderate to high fineness do not corrode under natural conditions, and consequently the problem of their analysis is not complicated by the presence of corrosion products. EDXRF-analysis is therefore ideal for gold analysis, because bulk and surface analysis are mainly coincident. For a systematic analysis of many areas of the same object, and for the analysis of many precious metal objects, only absolutely non-destructive and non damaging techniques may be proposed, and among them, Energy-Dispersive X ray Fluorescence (EDXRF) analysis is the most suited, because it is not only absolutely non-destructive, but also multi-elemental, reliable and rapid. The fact that reliable EDXRF can be used in a portable set up adds much to the above important statements. EDXRF-analysis is a surface analysis, in the sense that the thickness of the alloy involved in the analysis is of the order of microns to a maximum of tens of microns; because of this peculiarity, which can be considered negative from the analytical point of view, EDXRF-analysis is able to distinguish a gold alloy from gilded copper or silver alloys by using the internal ratio of Cu and Ag-lines. Around 500 B.C., in the Mediterranean region, a process for purifying native gold come into use, and the practice to alloying native gold first with silver and later with copper was introduced and this method is still in use nowadays. At the contrary the practice to alloy native gold with copper was practiced already in the prehistoric civilizations of Central and South America where gilded methods were extensively used. In this memory we are going to report the results of the non destructive in-situ campaign on pre-columbian alloys from the royal tombs of Sipán with a portable EDXRF equipment together with the protocol established to choose a proper bench-top XRF instrument for the set up of a laboratory dedicated to the analysis of contemporary gold alloys. In the first case the goal was to give archaeometric results on more than 50 golden objects from the Royal Tombs of Sipán and especially on their gilding procedure. In the second case the goal was to determine, with reduced uncertainty, the fineness of the raw material and semi-finished goldsmiths objects and to compare the results with cupellation.

1. Pre-Columbian gold alloys from the royal tombs of Sipán (Perù)

1.1. Introduction

On the north coast of present-day Peru flourished between 50 and 700 AD approximately, the Moche civilization, which metalworking ability was impressively demonstrated when Walter Alva and co-workers discovered in 1987 the "Tumbas Reales de Sipán" [1, 2].

Spectacular gold, silver and copper funerary ornaments were excavated, and are now exposed in the namesake Museum, in Lambayeque, close to Chiclayo.

Important information could be deduced from the EDXRF these measurements, i.e.:

- Moche metalworking was based primarily upon objects made of hammered metal sheet.

- Besides native gold and native gold-silver alloys (with some copper), gold and silver were already intentionally alloyed at that time.

- The Moche developed very low carat gold (typically 80% Cu, 15% Ag, 5% Au) or silver alloys appearing from outside as gold (or silver) by depleting the surface from copper (this alloy is called tumbaga, i.e. depletion gilded or silvered alloy); the low carat alloy was burned and/or treated with acids extracted from plants, which produced a copper oxide which could be removed mechanically, leaving the surface covered with a thin film of almost pure gold (or silver). In the case of gold the object was then placed in an oxidizing solution containing, it is believed, salt, and ferric sulfate. This process removed through oxidation the silver from the surface of the object leaving only gold.

Only objects made of gold (gold + silver + copper alloy), or tumbagas, containing a high concentration of gold at the surface, preserved their gold aspects during the 1500 years burial in the adobe pyramids. Other objects, made of copper, or silver-copper alloy, or gilded copper, were found covered with green patinas containing copper corrosion products.

EDXRF-analysis also gives the value of the thickness of gold in the case of gilded copper or tumbaga (the surface-behaviour of these two cases is similar, and an "equivalent" gold thickness can be measured for tumbaga-gold).

To analyse Sipán alloys, a portable EDXRF-equipment was transferred to the Museum "Tumbas reales de Sipán", to systematically analyse the most important objects [3].

1.2. Experimental set-up

The portable equipment employed for analysis of Sipán alloys is composed of a X ray tube (Eclipse II by AMPTEK-Oxford [4]), which is characterised by a Ag-anode, and works at 30 kV and 100 μA maximum voltage and current.

The portable equipment and the geometrical arrangement are shown in Figure 1.

FIG 1. Experimental set-up, showing, on the left, the Eclipse II X ray tube (with a brass collimator), and the Si-PIN detector (also collimated with a brass cylinder), during measurements on the golden mask, in the Museum "Tumbas Reales de Sipán", in Lambayeque, Peru.

To reduce the X ray output of the tube the X ray beam is collimated with a brass cylinder 2 cm long and with an internal hole of 2 mm diameter. Further, to excite silver in an efficient manner, the X ray tube output is also filtered with about 0.1–1 mm Al, to better "form", and to partially monochromatize the X ray beam. In such a manner the radiation protection problem is negligible, and the low energy tail of the X ray spectrum, which is not useful to excite copper, silver and gold, is strongly reduced [5].

The X ray detector is a thermoelectrically cooled Si-PIN, with a 300 μm, 7 mm^2 Si-crystal, and a thin Be-window, with about 180 eV energy resolution at 6.4 keV[4] .The detector is also collimated with a brass cylinder 3 cm long and with an internal hole of 2 mm diameter to limit background and scattered photons.

To measure gilding thickness of gilded gold or silver, the Cu(Kα/Kβ)-ratio or Ag(Kα/Kβ)-ratio and the (Au-L$_α$/Cu-K$_α$) or (Au-L$_α$/Ag-K$_α$)-ratios were employed [6].

1.3. Results

A large number of objects from the "Tumbas Reales de Sipán" were analysed, on gold, gilded copper, tumbaga, silver and copper alloys. The majority of them originates from the tomb of the "Señor de Sipán"; several are from the tomb of the "Sacerdote" and other tombs.

1.3.1. Gold objects composition

Several objects from the "Tumbas Reales de Sipán" are made of gold, i.e. characterised by the presence of Au, Cu and Ag as main components. In some samples traces of Fe, Zn and Br are also visible.

1.3.2. Gilded copper: analysis and thickness measurement for gold

Only a few analysed objects from the "Tumbas reales de Sipán" are on gilded copper; they were identified by the visible presence of deteriorated areas, and presence of only copper in some of these areas. In the case of gilded copper it was possible to determine the composition of the gilding layer, and its thickness was found from the (N_{Au-L}/N_{Cu-K})-ratio; the Cu- $K_α/K_β$ - ratio could not be employed, because of the very reduced Au-thickness.

The mean gilding composition of various objects on gilded copper was determined to be: Au~97.5%, Ag~2.5% (Cu, if present in the gilding, was not determined, because of the high Cu-contribution from the support), while the gilding thickness was measured to be ~0.6 μm.

1.3.3. Tumbaga gold alloy: average composition and "equivalent" gold thickness

The majority of the gold alloys from the "Tumbas reales de Sipán" are made of "tumbaga". From the point of view of EDXRF-analysis, i.e. from the X ray spectra, "tumbaga" behaves in a similar manner as gilded copper, the gold-equivalent surface thickness can be determined both from Cu-Kα/Kβ – ratio and from (N_{Au-L}/N_{Cu-K})-ratio. They refer, in any case, to a very superficial alloy depth, of the order of 10 μm.

1.3.4. Copper objects

Only parts a few objects are made of copper. All are composed of about 99% Cu, and traces of Fe and/or Ni.

1.3.5. Composite objects

Many objects from the "Tumbas Reales de Sipán" are interesting also for the variety of composition. In the earrings n. 27 (Fig. 2), for example, the external spheres are made of gilded copper; the gilding thickness was measured to be ~1 μm, and the composition about 60% Au, 40% Ag. The external rings are of "tumbaga", which thickness is of ~2.6 μm. The internal rings and the heads are of gold, with the following composition: Au=76%, Ag=16%, Cu=8% and Au=65%, Ag=25% and Cu=10% respectively.
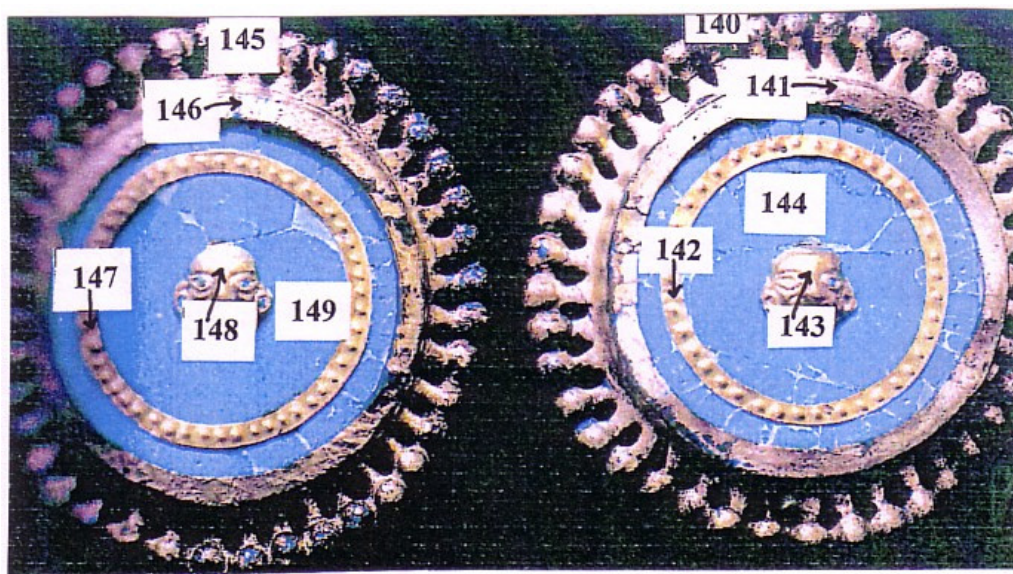

FIG. 2. Earrings made of gold (heads in the middle, areas 143 and 148, and internal rings, areas 142 and 147), gilded copper (external spheres, areas 140 and 145) and "tumbaga" (external rings, areas 141 and 146).

2. Contemporary gold alloys

2.1. Introduction

For the selection of a bench top instrument, it is not an easy task to compare among different commercial EDXRF instruments and settle their behaviours and performances in order to determine which might be the best suited to the project needs. To support an accurate comparison of the instruments, we assessed a protocol of analysis taking into account only hardware performances, since the factory's software may have precluded a proper survey. The instruments could stay at our laboratory only for 3 days. The procedure had to be concluded in this time interval.

To guarantee homogeneous results, the analyses were performed on samples expressly created for the tests and the deconvolutions on raw spectra were performed with the aim of the software WinAxil (Camberra Inc.). The commercially available instruments that we analysed were the Spectro "MIDEX", the Thermo Fisher "Fischerscope XAN" and the Italstructures "Gold X". The companies released little or nothing information about the hardware set-ups. The only information available was that the Spectro MIDEX was using a SDD detector while the other two were using a S-PIN detector.

To fulfill homogeneous results with instruments sometimes quite different one from each other, it was necessary to set up an analytical procedure to be applied as strictly and as scrupulously as possible so that all the equipment might be tested under identical ambient conditions. This meant examining the same samples in the same order and to reduce the geometrical factor, having the same operator handling and positioning the samples to be tested.

The factors that were evaluated were: stability, linearity, MDL, energy resolution and easiness of employ. In this memory we are going to report the results of the linearity and energy resolution trials.

2.2. Results

As far as linearity is concerned the samples reported in Table 1 were analysed with the three instruments under identical conditions. The samples were chosen for their percentage composition in copper and silver ranging from zero up to 15% for the former and 35% for the latter. The measures lasted 300 seconds each.

TABLE 1. COMPOSITION OF THE SAMPLES OF YELLOW GOLD ALLOYS USED FOR THE LINEARITY TRIALS

Sample	Au (‰)	Ag (‰)	Cu (‰)
1s	950	50	0
2s	780	70	150
3s	770	100	130
4s	750	150	100
5s	730	200	70
6s	710	250	40
7s	700	300	0
8s	650	350	0

The instruments were used as the operational manual of the producer was suggesting for the warm up and calibration procedures. Several measurements were made for every sample and a correlation line was drawn with copper and silver concentrations versus experimental peak counts. In Figure 3 and 4 we report the results for copper and silver.

In the graph, the instrument represented by a violet square has a SDD detector while the other two have a S-PIN detector. The differences in results are mainly connected to the very different count rate that characterise the SDD detector.
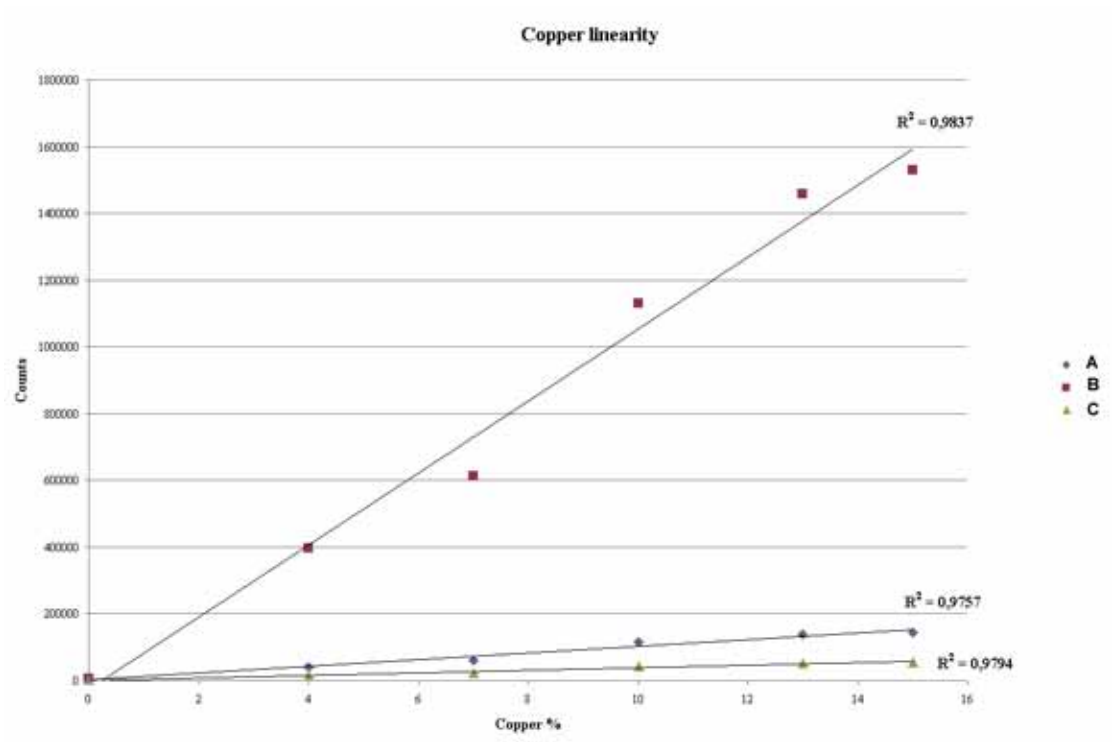
FIG. 3. Linear correlation for Copper concentrations and counts for the three instruments. Instrument B as a SDD detector.
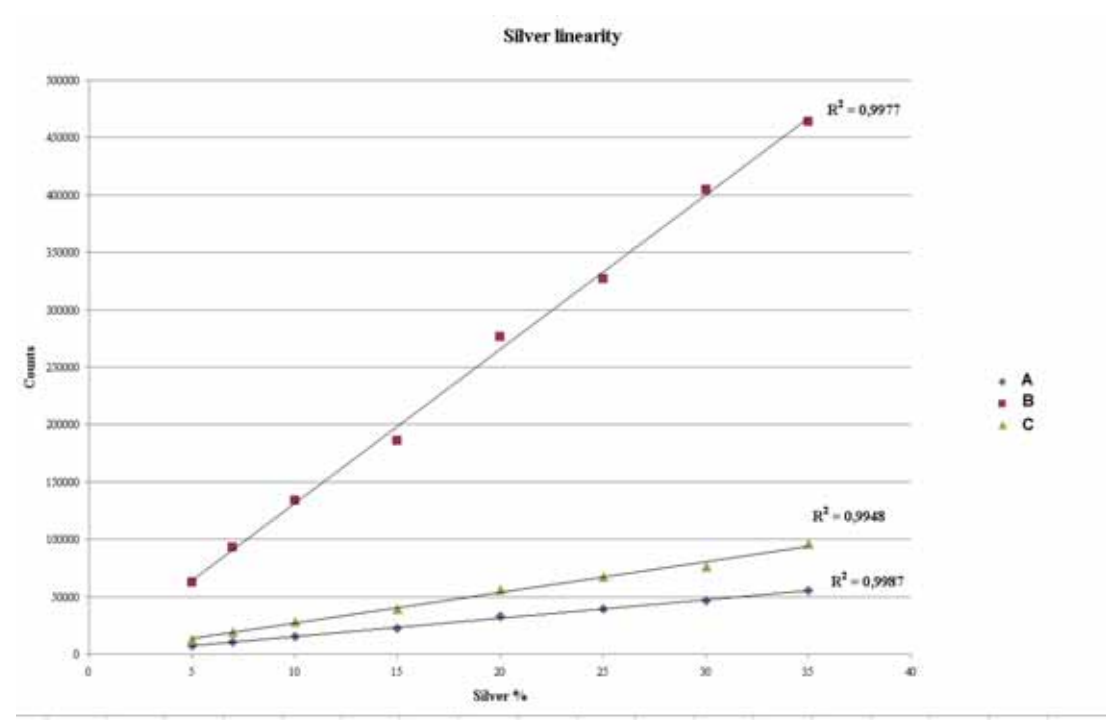

FIG. 4. Linear correlation for Silver concentrations and counts for the three instruments. Instrument B as a SDD detector.

As far as energy resolution is concerned a sample of pure iron was measured under identical conditions with the three different instruments. The energy resolution calculated for the three instruments is reported in Table 2.

TABLE 2. ENERGY RESOLUTION CALCULATED FOR THE THREE INSTRUMENTS
WITH A PURE IRON SAMPLE

Instrument	FWHM Fe (eV)
A	204
B	184
C	291

For a visual comprehension of the differences found in energy resolution, in Figure 5 we report a section of the spectra of the best and worst energy resolution instrument between the Nickel K alpha and the Gold L alpha peak of a white gold alloy sample.
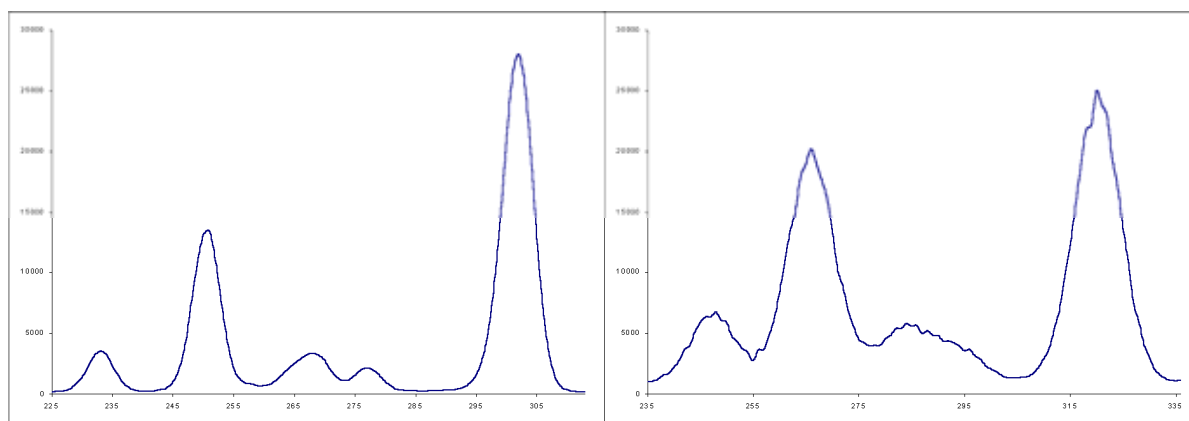
FIG. 5. Spectra comparison for the best and worst energy resolution instrument (instruments B and C) between the Nickel K alpha and the Gold L alpha peaks in a white gold alloy sample.

The main conclusion we can draw is that even with similar costs, commercial bench-top EDXRF systems show very different responses to identical inputs. The one instruments that was using a SDD detector exhibited the best results both in linearity and in energy resolution.

3. Conclusions

EDXRF-analysis is a surface analysis, in the sense that the thickness of the alloy involved in the analysis is of the order of microns to a maximum of tens of microns; from an analytical point of view, this peculiarity can be considered negative, but: (1) gold alloys of moderate to high fineness do not corrode under natural conditions, and consequently the problem of their analysis is not complicated by the presence of superficial corrosion products; (2) the objects to analyse are always very precious from a technical and esthetical and archeometrical point of view; (3) XRF "superficial" analysis are able to distinguish a gold alloy from gilded copper or silver alloys.

EDXRF-analysis is therefore ideal for gold analysis, because bulk and surface analysis are mainly coincident and it is totally non destructive. In many cases when the bulk and the surface are compositionally not the same, EDXRF analysis may point out the fact that is very useful to study the production technology of the pre-colombian goldsmiths and the fake jewels of nowadays production.

REFERENCES

[1]   ALVA, W., SIPAN: descrubrimiento e investigation, Quebecor World Perù S.A., Lima, 2006.
[2]   ALVA, W., DONNAN, C.B., The Royal Tomb of Sipán , Los Angeles Fowler Museum of Cultural history University of California, Berkeley, 1993.
[3]   CESAREO, R., et al., EDXRF-analysis of metals from the Royal Tombs of Sipán, invited paper at SARX 2008 Workshop, Cabo Frio, Brazil 16–20 November 2008.
[4]   AMPTEK Inc., 6 De Angelo Drive, Bedford, MA 01730–2204, USA. http://www.amptek.com.
[5]   BRUNETTI, A., GOLOSIO, B., Software for X-ray fluorescence and scattering tomographic reconstruction, Comput. Phys. Communication **141** (2001) 412–425.
[6]   CESAREO, R., BRUNETTI, A., RIDOLFI, S., Pigment layers and precious metal sheets by energy-dispersive X-ray fluorescence analysis, X-ray Spectrometry **37** (2008) 309.

IMPROVEMENT OF THE XRF QUANTIFICATION AND ENHANCEMENT OF THE COMBINED APPLICATIONS BY EDXRF AND MICRO-PIXE

P. KUMP, M.NEČEMER, Z. RUPNIK P. PELICON
Jožef Stefan Institute,
Ljubljana,
Slovenia

D. PONIKVAR
University of Ljubljana, Faculty of Mathematics & Physics,
Ljubljana,
Slovenia

K. VOGEL-MIKUŠ, M. REGVAR, P. PONGRAC
University of Ljubljana, Biotechnical Faculty,
Ljubljana,
Slovenia

Abstract

The EDXRF and TXRF procedures for experimental set-up, measurement, quantification and all for necessary controls were unified within the computer interface in LABVIEW environment. (Click=XRF). The EDXRF quantification software for intermediate thick samples, utilizing the Emission-Transmission (E-T) technique, was upgraded and determines beside the elemental concentrations also the quantitative information on the residual matrix of the sample. The applications in plant physiology research gave some important results concerning the transport of quite poisonous Cd atoms up to the reproductive organs (seeds) of the hyperaccumulating plant. Beside the EDXRF also the µ-PIXE and EXAFS techniques have been used in this research. The botanical origin of bee honey harvested in Slovenia was determined by a fast and efficient approach utilizing the analyses of mineral content of honey by TXRF and combined by a statistical analysis of a large number of samples collected in years 2006 and 2007.

1. Introduction

The activities in the X ray Fluorescence (XRF) laboratory were devoted to the development of the XRF quantification software and consequently to applications of this analytical technique in the analysis of samples of different origin. The quantification software developed by the IAEA was in the past years upgraded in our laboratory in order to cover the needs of newly introduced XRF systems controlled by a practical computer interface in the LABVIEW environment. The EDXRF systems used in our laboratory apply radioisotope and X ray tube excitation as well as the proton induced X ray emission technique (PIXE). The X ray spectrometers using the standard LN cooled Si(Li) and HPGe detectors and also the SiPIN and Si drift (SDD) electrically cooled detectors were in use. The NIM module electronics composed of the amplifier, ADC, and a suitable, usually computer controlled MCA were used. Lately the integrated electronics systems, designed in our laboratory and also the commercially available digitized signal processors (DSP) were introduced. The computer interface developed in the LABVIEW environment (Click-XRF) enabled the complete adjustments and control of the parameters of the EDXRF system, such as excitation conditions, spectrum acquisition and analysis and quantification. These tasks were integrated and could be reached by simply clicking the mouse on the respective command buttons in the LABVIEW window. The quantification was performed by a single program, which was capable to analyze data obtained by the radioisotope and tube excitation in a standard and

TXRF modes, and to apply different models suitable for analysis of thick, transparent and thin samples of different origin (matrix).

The applications of XRF spectrometry were in the last years mainly oriented into the plant physiology research, especially in study of metal hyperaccumulating plants. These applications have introduced and popularized more quantified approach of research in this field.

In collaboration with PIXE laboratory a very promising research applying micro-PIXE technique have proved to be quite useful. Collaboration with another research group of our Institute resulted in some experiments with synchrotron radiation and EXAFS technique, which yielded important data on transport and accumulation of Cd in seeds of hyperaccumulating plants.

Applications of TXRF spectrometry in the analyses of bee honey with an objective to determine the geographical and botanical origin of bee honey in Slovenia was also intensified during the last years. The advantage of the technique due to simple sample preparation and fast and sufficiently sensitive elemental analysis enabled a low cost analysis of a large number of samples. Only in this way a comprehensive PCA statistical analysis of the obtained data yielded reliable results.

2. Overview of the research performed and the results obtained

2.1.   Software improvements

In Figure 1 a computer interface in LABVIEW environment, which integrates all the commands which are used to carry out the XRF experiment and analysis of spectra, followed by quantification, is presented. The excitation conditions at which the spectrum is measured are defined by System settings and are shown on Figure 2. These data are saved in each of the measured spectra and during quantification a proper calibration file is accordingly selected.
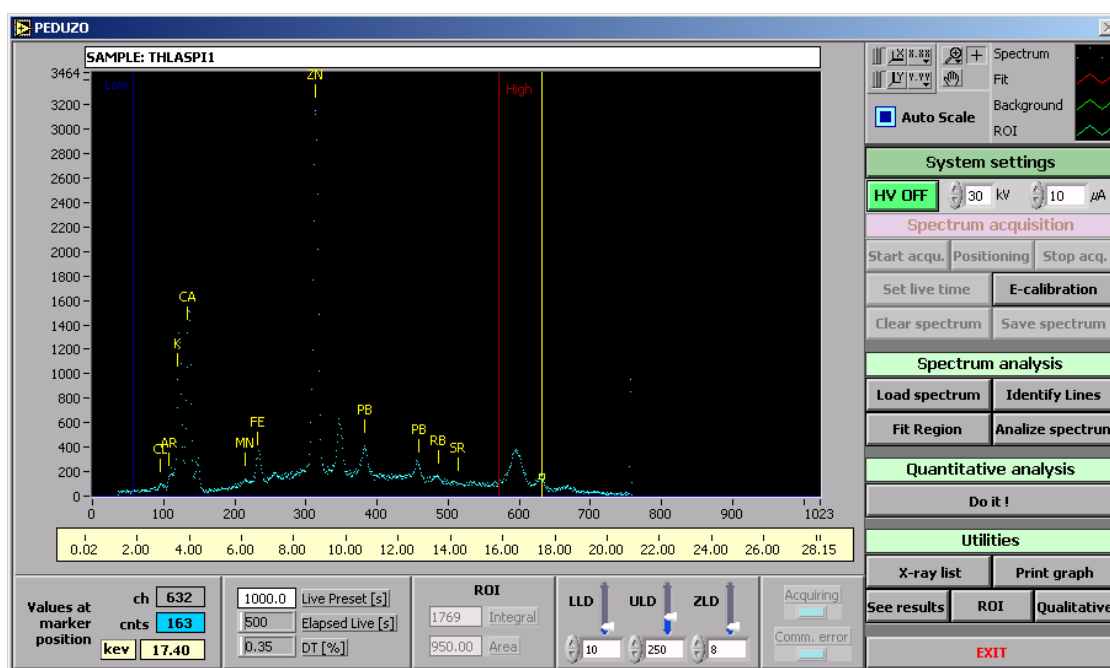

FIG.1. Display showing all commands to perform XRF measurements.
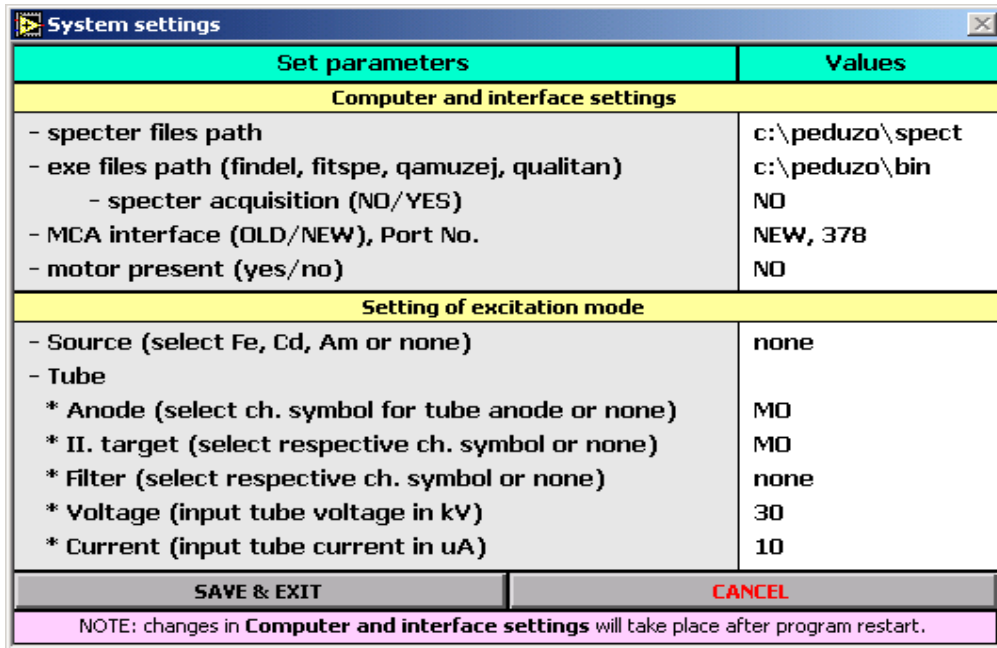
102

FIG. 2. Excitation parameters.

Concerning the quantification software the command **'Do it'**, if pressed, allows us to select quantification models for the intermediate or thick samples (see Fig. 3) and for thin samples (see Fig. 4).
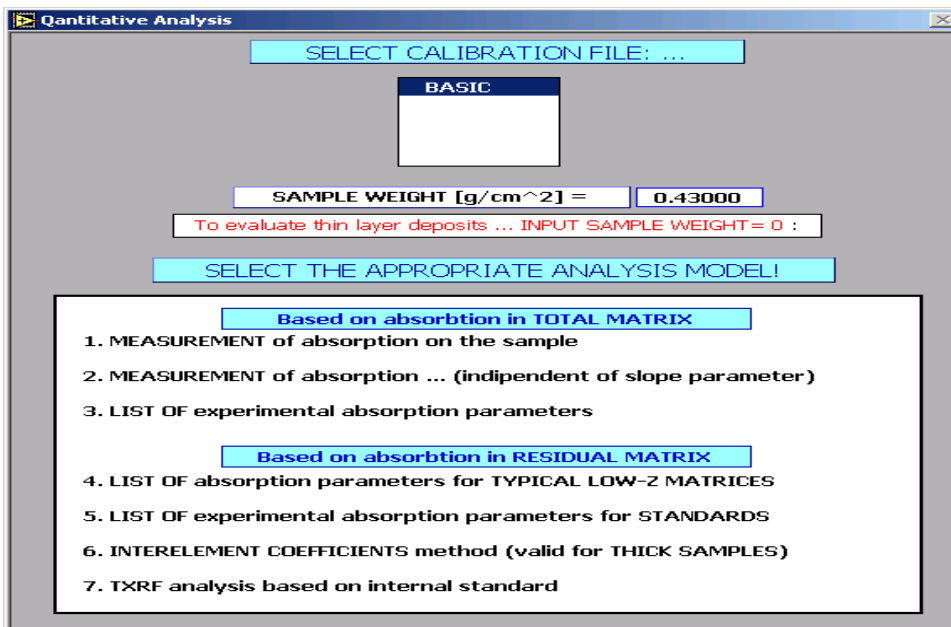

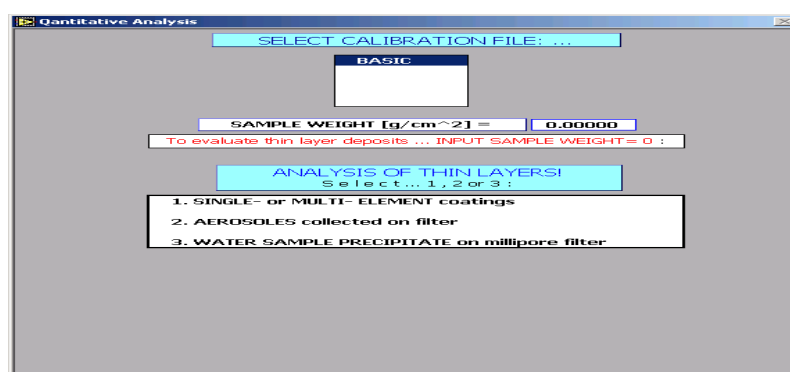*FIG. 3. Quantitative routines included in the software package.*

FIG. 4. Quantification for thin samples.

The quantification of samples with a none zero weight is divided into models based on the absorption measurements in total sample by the Emmission-Transmissiom (E-T) method (models 1 and 2) and into models, which require the knowledge of the residual matrix. The residual matrix is defined as the matrix or the set of elements, which do not respond in the spectrum by measurable intensities, but influence the fluorescent intensities of all the measured elements in the sample by absorption. The measured elements together with the residual matrix form the total matrix of the sample.

Within the framework of this CRP especially the models 1 and 2 were upgraded, though they in principle depend on the well known E-T method of measuring additionally to fluorescent intensities also the absorption in the total matrix of the sample.

The quantification by model 1 is symbolically presented in Figure 5. The E-T method is used to determine the absorption value in the total matrix only at one energy shown also by a cross on Figure 5. The procedure applied reproduces the absorption coefficients in the total matrix by assuming some particular slope (-2.8) of the respective absorption curve in ln-ln presentation. The evaluation of elemental concentrations starts in direction from the heaviest to the lightest element in the sample or from elements with the absorption jump highest in energy towards those with gradually lower energy of jumps in the total absorption curve. The absorption curve for trace elements is assumed as practically smooth, because the jumps are negligible due to low elemental concentrations. In case of elements with higher concentrations the correct absorption jumps are reproduced by iteration utilizing the tabulated values of the respective absorption jumps for 100% pure elements. The iteration procedure is presented symbolically in Figure 5. After all of the measured element concentrations are evaluated and the total absorption curve is reproduced, the absorption of measured elements is subtracted from the total absorption values and the residual matrix and its parameters are in this way also evaluated (see Fig. 5). It is interesting that by this method of quantification only tabulated K or L_α jumps of measured elements are used, and the complete set of absorption coefficients is employed only at the end during the evaluation of the residual matrix. In case that the residual matrix as a function of energy, which is always a smooth curve in the ln σ / ln E graph, does not coincide with the slope of the typical low-Z absorption graphs, the iteration procedure can be repeated with different starting slope in the total absorption curve.
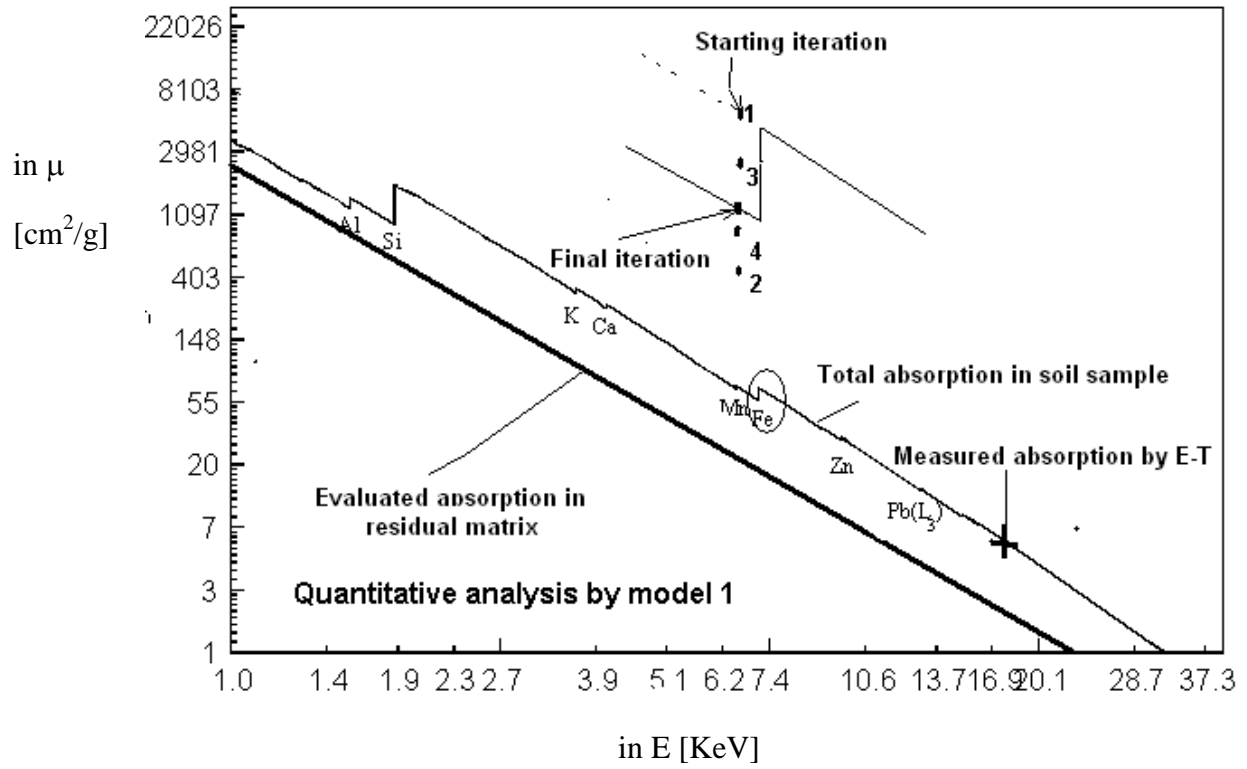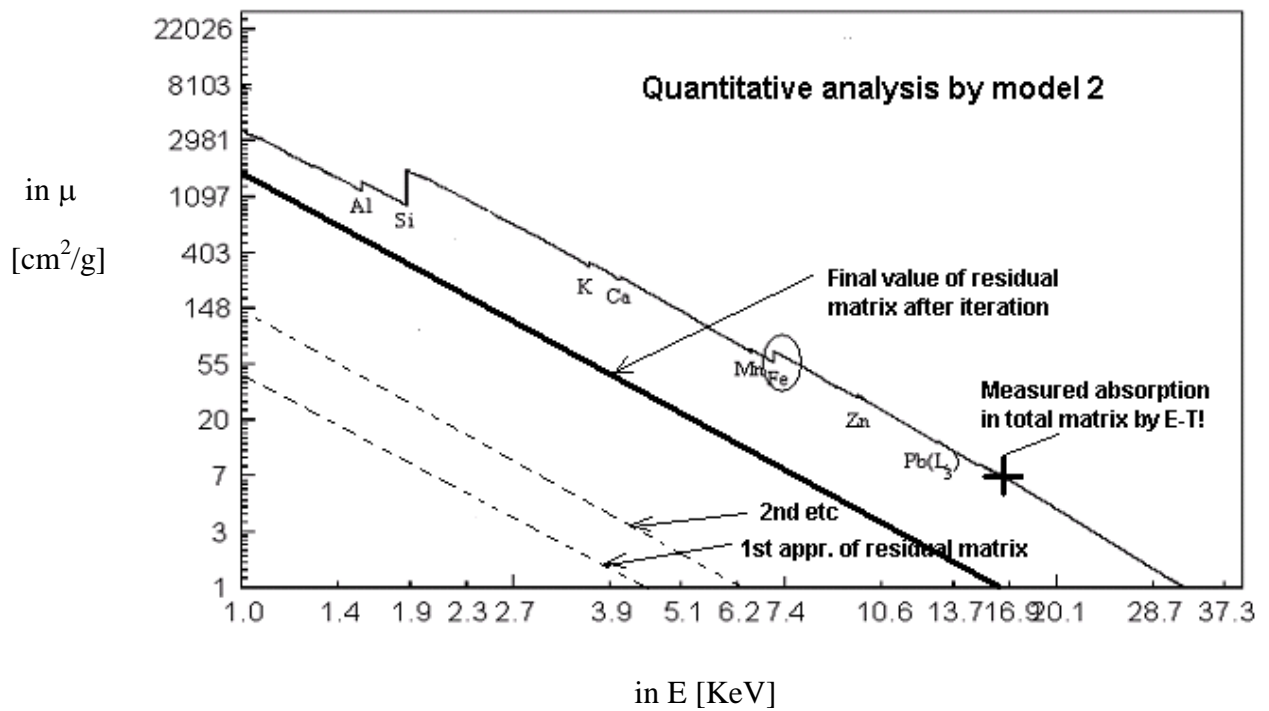
FIG. 5. Quantitative analysis by model 1.

FIG. 6. Quantitative analysis by model 2.

105

The quantification model 2 is symbolically presented in Figure 6. It also employs the E-T method of absorption measurement at a single energy in the analyzed sample, but uses only the measured ratio between the target intensities obtained with and without the sample. In this model the first approximation of the residual matrix is selected as the set of values proportional to the absorption in a typical residual matrix of the analyzed sample. One tenths of the absorption in cellulose is applied in case of the organic sample or one tens of the absorption in oxides or in alumo-silicates is used in case of inorganic samples. From measured intensities then the concentrations are evaluated by iteration process, which corrects for absorption in measured elements and in the adopted residual matrix. At the end of the iteration procedure the elemental concentrations and values of the proper residual absorption are available and the ratio of the E-T intensities can be calculated and compared with the experimental value. The iteration is repeated by using new, usually higher value of the residual absorption until the ratios of E-T intensity values, calculated and experimental become the same within some prescribed accuracy. After each iteration the enhancement corrections are also evaluated. As a result of this quantification process the elemental concentrations as well as the proper absorption in the residual matrix are obtained.

It is necessary to mention that these procedures in model 1 and model 2 utilize the elemental sensitivities and/or geometry constants, which are obtained by running a separate calibration program as well as a program, which evaluates the shape of the excitation radiation. The calibration program employs the intensity measurements on pure elements or stable chemical constants and/or on a standard reference material, which needs to offer the data on elemental concentrations of up to 100% of the matrix.

The mentioned quantification procedures offer usually the concentrations with the uncertainty of 2%–5%. In any case it is very important that the sample is homogeneous and that the fluorescent intensities are properly evaluated from the measured spectrum. The mentioned iteration procedures in the quantification process converge usually very well, except in cases when the E-T measurements or sample weights were not properly determined or the system calibration is not good enough.

The quantification model 7 is used for the evaluation of elemental concentrations in TXRF mode of excitation. The model is based on internal standard. In general the model is used in the analysis of thin samples, but in case of the analysis of powdered samples also the absorption correction can be applied. The quantification program calculates the elemental sensitivities relative to the element of the internal standard. The tabulated fundamental parameters are employed in calculations and the concentration of any element in the sample is proportional to the concentration of the internal standard. The proportionality constant is a product of intensity ratio divided by the elemental sensitivity ratio of element relative to the internal standard.

2.2. Applications in the plant physiology studies

The population of the *T. praecox* plant from a metal polluted site in Žerjav (Slovenia) accumulates exceptionally high metal concentrations of 1.5% Zn and 0.6% Cd without showing toxicity symptoms; a phenomenon known as hyperaccumulation. Hyperaccumulating plants have attracted much interest during the last decade, mainly because of their potential use in phytoremediation.

The X ray spectroscopy techniques including EDXRF, μ-PIXE, and lately also EXAFS have proved to be quite useful in plant biology research [1]. A simple sample preparation and fast multielemental analysis made possible to analyze a large number of soil and plant samples in short time and at rather low cost and acceptable accuracy. In collaboration with the Department of Plant Physiology of the Biotechnical Faculty, University of Ljubljana, an intensive research in studies of hyperaccumulating plants was initiated and still continues.

After applying the EDXRF analyses in bulk samples of plant material the micro-PIXE was applied and proved to be an efficient and powerful technique for qualitative and quantitative element localization studies in the cryo-fixed and freeze-dried leaf cross-sections of metal hyperaccumulating *T. praecox* [2]. According to the element localization patterns, the main Zn detoxification mechanism was Zn sequestration in the symplast of large vacuolated epidermal cells, while mesophyll symplast may be seen as a major site of sequestration and etoxification of Cd and Pb. Relatively high concentrations of Cd found in phloem indicated higher mobility of this element in *T. praecox* tissues compared to Zn and Pb.

Further research of Cd mobility was extended by utilizing the EXAFS absorption spectrometry. These results [3] suggest that binding of Cd to strong ligands is the main detoxification mechanism in *T. praecox* embryos. On the other hand in roots and shoots up to 80% of Cd was bound to weak oxygen ligands provided by the cell walls and organic acids stored in vacuoles. In epidermis only slightly higher percent of oxygen ligands was detected than in mesophyll, pointing out that vacuolar compartmentation is a main detoxification mechanism found in both leaf tissues. In veins almost 60% of total Cd was coordinated with sulfur ligands, indicating that Cd is transported through the plant as a stable metal complex.

The success of phytoremediation may also depend on beneficial associations between plants and soil organisms. The described research [4] is devoted to finding compatible fungal colonizers of hyperaccumulating *T. praecox*, which may therefore be important for applications of these associations in phytoremediation.

2.3. Determining the botanical and geographical origin of bee honey

Utilizing the TXRF analysis in determining the mineral composition of bee honey harvested at different locations in Slovenia proved to be an efficient method for determination of the botanical origin of bee honey, when the obtained data was processed by the PCA and RDA statistical analysis shown in Figure 7. This approach [5] enabled discrimination of the botanical origin of Slovenian nectar honeys such as floral and acacia and of mixed nectar and honeydew types such as lime and chestnut honey, whereas the honeydew honey types such as forest, spruce, and fir honeys cannot be distinguished from each other. The reason is the simultaneous harvesting of different types of honeydew by honeybees, resulting therefore in a mixture of these types of honey. Forest honey is a mixture of different types of honeydew including spruce, fir, and many other types of honeydew. Spruce and fir honeys are also mixtures of several honeydews, but one type of honeydew, for example, spruce, prevails, which is expressed in its sensory characteristics as well. It seems that the above-mentioned analytical approach using only elemental analysis by TXRF is promising for multivariate statistical analysis of other different food products such as nutrients, food supplements, and additives. By such an approach the quality control and determination of the geographical origin, production location, and authenticity could be established.
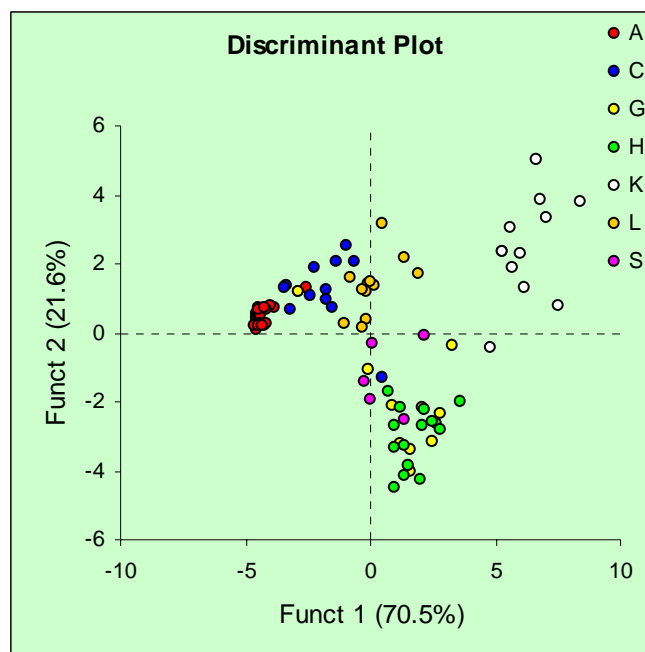
FIG. 7. Results of PCA for identification of origin of bee honey

3. Conclusions

The presented activities in our XRF laboratory will continue also in future. Concerning the EDXRF quantification software it will be further upgraded in order to achieve better accuracy in elemental analyses. The present programs applying the E-T technique need some more upgrading in order to include proper absorption in the residual matrix of the sample, which should be approximated as a combined composition of oxides of all not measured light elements such as Na, Mg, Al, Si, etc. Improvements of the computer interface in LABVIEW environment should include also the data acquisition by the Digital Signal Processors (DSP) of different manufacturers, which are already used in the laboratory. It is also planned to introduce and adapt the presented quantification software also to the WDXRF system.

The applied approach in the analyses of the origin of bee honey will extend also to the establishing of the origin and quality of different food products such as nutrients, food supplements, and additives in combination with statistical analyses. This might reveal and check the authenticity and possible adulteration of these products available on the market.

REFERENCES

[1] NEČEMER, M. et al., Application of X-ray fluorescence analytical techniques in phytoremediation and plant biology studies. Spectrochim. acta, Part B: At. spectrosc.. [Printed.] **11** 63 (2008) 1240–1247. DOI: 10.1016/j.sab.2008.07.006.

[2] VOGEL-MIKUŠ, K. et al., Comparison of essential and non-essential element distribution in leaves of the Cd/Zn hyperaccumulator Thlaspi praecox as revealed by micro-PIXE. Plant cell environ.. [Print ed.] **31** 10 (2008) 1484–1496.

http://dx.doi.org/10.1111/j.1365-3040.2008.01858.x DOI:10.1111/j.1365-3040.2008.01858.x.

[3]   VOGEL-MIKUŠ, K., ARČON, I., KODRE, A., Complexation of Cadmium in Seeds and Vegetative tissues of the Cd Hyperaccumulator *Thlaspi praecox* as Revealed by X ray Absorption Spectrometry, to be published. [XAS analysis of Cd chemical coordination in Cd (hyper)accumulating plants, Experiment report, ESRF, EC 398, 08]

[4]   PONGRAC, P., et al., Roots of Metal Hyperaccumulating Population of Thlaspi Praecox (Brassicaceae) Harbour Arbuscular Mycorrhizal and Other Fungi Under Experimental Conditions. Int. j. phytoremediat. **11** 4 (2009) 348–359. DOI:10.1080/15226510802565527.

[5]   NEČEMER, M. et al., Application of Total Reflection X ray Spectrometry in Combination with Chemometric Methods for Determination of the Botanical Origin of Slovenian Honey*,* J. Agric. Food Chem.*,* Article ASAP, DOI.**:** 10.1021/jf900930b, 2009.04.13.

THE USE OF X RAY ABSORPTION NEAR-EDGE STRUCTURE AND X RAY MAGNETIC CIRCULAR DICHROISM IN DILUTED MAGNETIC SEMICONDUCTORS

NASSER HAMDAN
American University of Sharjah, Sharjah,
United Arab Emirates

NOUAR TABET, HEZAM MAHMOUD
King Fahd University, Petrol & Minerals,
Saudi Arabia

ZAHID HUSSAIN
Lawrence Berkley National Laboratory, CA,
United States of America

Abstract

Preparation and investigation of Fe-doped ZnO system is investigated by different techniques as a case study of the use of combined spectroscopic techniques in material science. Optical spectroscopy, X ray diffraction (XRD), near-edge X ray absorption (XANES) and X ray magnetic circular dichroism (XMCD) have been used in this study. Information about the variation of the crystal structure, optical absorption, energy gab, chemical state and magnetic exchange coupling with Fe doping in ZnO are deduced form the above mentioned techniques to provide a comprehensive understanding of these technologically important diluted magnetic semiconductors. The optical absorption showed an increase of the absorption band intensity, a redshift of the absorption peak and the band edge and in increase in the gab with increasing Fe content. XRD results provided information about structural modification such as reduced anisotropy, reduction of the grain growth and shortening of the c-axis. XANES on the other hand provided useful information about the chemical state of Fe in the structure; information that is not easily found from other techniques. XMCD measurements provided information about the Orbital magnetic moment and the spin magnetic moment and the type of coupling between Fe ions and other species in the material.

1. Introduction

Ferromagnetism and semiconducting properties coexist in magnetic semiconductors such as Eu and Mn- chalcogenides and Cr spinels, but the crystal structure of these materials is very different from that of traditional semiconductors like GaAs, Si, ZnO, and TiO_2, used in industrial applications [1–5]. Magnetic semiconductors based on non-magnetic semiconductors through low level doping with magnetic elements are called diluted magnetic semiconductors (DMS). These materials have emerged as an excellent solution for such structural mismatch.

A tremendous increase in the number of research articles on magnetic nanoparticles impeded in a semiconducting nonmagnetic matrix has been observed during the last few years [4–7]. Because of the complementary properties of both ferromagnetic and semiconducting materials, these systems are of great importance from both theoretical and application point of views. In this introduction, an overview of technological applications of these systems as well as the theoretical significance of understanding these materials will be outlined.

The discovery and utilization of semiconductors that are ferromagnetic at room temperature is necessary for the realization of spintronics. Spintronic is a potentially very important recent development in electronics and magnetic technology. In this technology, electronic devices

rely on manipulating the spins of electrons, in addition to the holes, ions and/or atoms to develop faster, smaller (increased transistor density compared to conventional semiconductors), and less power consumption and dissipation in processing, transmitting and storing information. Spintronics (sometimes called magnetoelectronics) combine both the spin and charge of the electron to obtain devices with new functionality, non-volatility and increased performance. Applications range from on-chip integration of magnetic storage and electronic processing functions over nanometer length scales to quantum computing.

One main class of applications of spintronics is sensors. The first successful application of this kind was the Giant Magneto Resistance (GMR) read head used in hard disks. It was discovered in 1988 and commercialized in 1997 [4]. Nowadays almost all hard disks in the market have GMR heads. These GMR heads are devices of alternating magnetic and nonmagnetic multilayers. The resistance is different if the magnetic layers are ferromagnetic or anti-ferromagnetically coupled that can be achieved by applying an external magnetic field.

The next application that expected to have a large economic impact is the nonvolatile memories that can be accessed even if the computer is turned off, unlike the Si-based semiconductor technology that is used today. These Magnetoresistance random access memories (MRAM) are very close of being commercially available.

The last group of possible application mentioned above is the spin transistor utilizing the concept of spin injector. Spin injectors of spin polarized current from a ferromamagnetic into a semiconductor is necessary to carry out quantum bit (qubit) for operation of quantum computers. This has not been achieved experimentally yet because of large conductivity mismatch between a ferromagnetic metal (Fe) and the semiconductor (In GaAs). Scientists are optimistic to resolve this experimental obstacle through spin injection via the so-called half metallic ferromagnets (HMF).

DMS materials provide an alternative for the conventional magnetic semiconductors especially after the discovery of ferromagnetic properties in some DMS materials above room temperature [1]. Theoretical calculations predict a magnetic transition temperature of most of the group III–V semiconductors doped with 3–5% Mn near 100K. It was demonstrated by Dietl et al. for the first time that GaMnP has a curie temperature above 300 K [8]. Later on, very few non-traditional DMS compounds has proven to have ferromagnetic ordering above 300 K and among them is Co-doped TiO_2 anatase ($Co_xTi_{1-x}O_2$) which was discovered recently and proven to be the most magnetically robust DMS compound with respect to magnetic moment at saturation [9–12].

From theoretical point of view, magnetic coupling in DMS materials occurs through exchange interaction between the magnetic spin and free charge carriers in the semiconductor. Such an interaction can take place via p-d or d-d exchange and can lead to antiferromagnetic or ferromagnetic coupling, depending on the concentration of the magnetic impurity and its local structure. DMS materials are used as spin injectors only if they are ferromagnetic. We have observed significantly different magnetic properties of ($Co_xTi_{1-x}O_2$) prepared by oxygen plasma assisted molecular beam epitaxy (OPA-MBE) and pulsed laser deposition techniques [9]. Furthermore, the magnetic properties of these films were also found to depend on the particle size, concentration of magnetic impurity (x) and on the substrate.

In the field of nano particles and thin films, the properties of the surface and interface will be completely different from those of the bulk material. As the atoms in nano particle system and thin films have different surrounding environments, the magnetic coupling and the electron

interactions in the material will be greatly affected as a result of symmetry breaking. Furthermore, the magnetic ions and semiconducting material in the DMS film will couple differently with different substrate materials. The properties will also depend strongly on the density of magnetic impurity ions and density of charge carriers and vacancies. Therefore, the variation of the magnetic properties that we have observed in our preliminary study [8], could be expected.

The work done for this project was performed at two different laboratories, namely: the surface science laboratory at King Fahd University of Petroleum and Minerals (KFUPM), Dhahran, Saudi Arabia; under the leadership of Professor Noaur Tabet, who is a co-investigator of this project, and at the advanced Light Source (ALS) at Lawrence Berkeley National Laboratory Berkeley CA, in collaboration with Dr. Zahid Hussain, facility deputy for scientific support.

Sample preparation and characterization were performed at KFUPM. The main two characterizations techniques performed on these samples are the X ray diffraction and optical absorption spectroscopy.

X ray absorption Near-Edge Structure (XANES) and X ray Magnetic Circular Dichroism (XMCD) were performed at the advanced Light Source (ALS) Facility at Lawrence Berkeley National Laboratory, a national user facility that generates intense light for scientific and technological research. The ALS is one of the world's brightest sources of ultraviolet and soft X ray beams, and the world's first third-generation synchrotron light source in its energy range. The work was performed at the chemical and material sciences beam line b.l.9.3.2. The beamline is a bend magnet beamline with an energy range 30–1000 eV, provided by a spherical grating (SGM) monochromator with three diffraction gratings (100, 600, 1200 lines/mm) for low, intermediate and high energy ranges respectively. The Resolving power (E/ΔE) is typically 3000 with a maximum of about 8000. The beamline has capability of getting circularly polarized light, for magnetic studies. Although the beamline is equipped with three end stations, the end station that was used in this project is the UHV Advanced Materials Chamber (AMC). The AMC is used to Study the atomic and electronic structure of surfaces; and make use the capability for circularly polarized radiation. The chamber has a precision manipulator, is equipped with Scienta SES 200 electron energy analyzer, sample transfer capability, in situ application of magnetic field, heating up to 2300°C and cooling down to 85 K. The chamber is also equipped with various preparation options such as Sputtering, evaporation, quartz-crystal oscillator, LEED, XPS. It is also equipped with a channeltron, photodiode and a drain current measuring capability for various modes of absorption measurements. This chamber is utilized with various spectroscopic techniques mainly: Photoelectron diffraction, XPS, XANES, and XMCD. Figure 5 and Figure 6 show the schematic diagram of the beamline and the AMC end station respectively.

2. Scientific scope of the CRP

2.1. Overall objectives of the project

The project will help researchers in the region and their collaborators, to improve the characterization of materials by using combined spectroscopic methods, as well as developing integrated instruments and analytical methodology. These techniques are expected to be more widely used in the Middle East region, particularly with the increased interest in using synchrotron facilities. Some of these techniques can also be developed using a conventional laboratory X ray source.

2.2. Specific research objectives:

(1) The study of DMS using a variety of advanced spectroscopic techniques will lead to better understanding of the physical properties of these relatively newly discovered materials of technological importance. The results will show the advantages of adopting a multitechnique approach to study a wide variety of problems in materials science and other fields including monitoring environmental pollution, industrial impact, cultural heritage, human health and agriculture.

(2) To enhance the analytical approaches of the investigators by integrating various software for processing and presentation of the data, through involvement of graduate and undergraduate students at both the participating Institutes in the Middle East.

3. Overview of the research performed

3.1. Sample preparation

A set of Fe doped ZnO thin films were prepared during the first phase of the project, by DC Magnetron sputtering method under special conditions. High purity Zinc Target of radius 5 mm was used with various numbers (0, 2, 4, 6) of Fe wires of 0.25 mm diameter were fixed on the zinc target. Pure oxygen was used instead of argon. The oxygen pressure was maintained at $5X10^{-1}$ Torr. Two Other sets of samples were prepared: with and without heating the glass substrates.

3.2. X ray diffraction

X ray diffraction measurement (XRD) was performed for the samples. The evolution of the crystal structure as Fe content was introduced is shown in Figure 1. The Figure shows an increase in the c-axis anisotropy of the film with increasing Fe content and an increase of the c-axis length. The XRD spectra for the second set of samples while heating the substrate for samples with different Fe content (number of Fe wires) and different substrate temperatures showed a slight variation in the peak position of the 002 line is observed for samples with different iron content. The FWHM increases as the number of Fe wires increases which suggest that the grain size growth is reduced by Fe addition as shown in Figure 2. A slight difference is observed in the peak position of the (002) peak when the substrate temperature was increased [2].
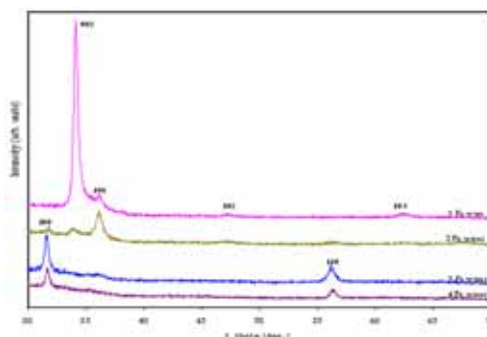

FIG. 1. Evolution of the X ray diffraction patterns of the samples as Fe Content was increased.
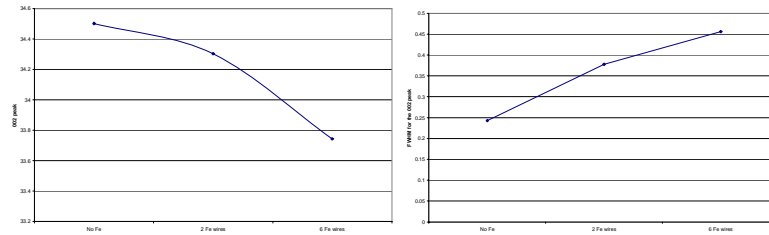
FIG. 2. The peak position and the FWHM of the 002 XRD peak as Fe was increased

3.3. *Optical absorption*

Figure 3 shows the optical transmittance for various samples with energy while Figure 4 shows the optical absorption coefficient as a function of energy. The transmittance spectra show an increase of the absorption band intensity, a redshift of the absorption peak and the band edge with increasing Fe content. These results are consistent with results obtained for Co-doped ZnO [5]. These optical properties suggest that spd exchange interaction and dd transition become dominant with increasing the Fe content, which leads to enhancement of ferromagnetic properties of Fe-doped ZnO films. As in the case of Co-doped Zn-O, Fe substitution for Zn^{2+} drives ferromagnetism in this system without changing the structure [2-4].

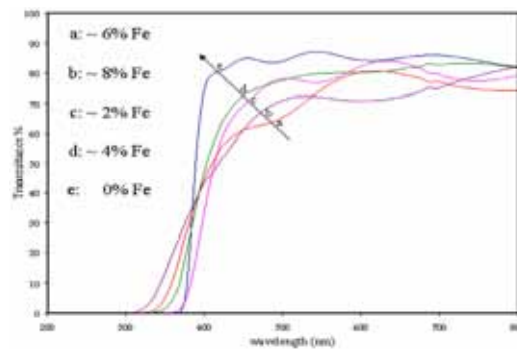*FIG. 3. Optical transmittance spectra of Fe-doped ZnO thin films with different iron concentrations.*
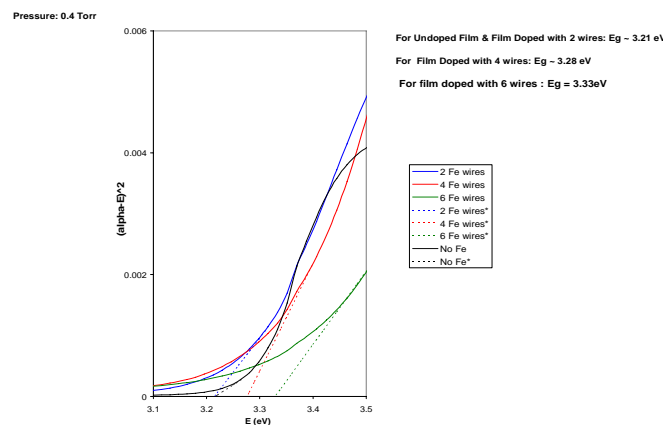

FIG. 4. $(\alpha E)^2$ graph for the determination of optical band gaps of Fe-doped ZnO thin films with different iron concentration.

Optical absorption results are shown in Figure 4. The Figure shows a gab modification with increasing iron content. The gab Eg ~ 3.21 eV for un-doped films and for films doped with

two wires is 3.28 eV, 3.28 eV for films doped with 4 Fe wires and was 3.33 eV for films doped with six Fe wires.

3.4. XANES measurements

The X ray absorption measurements at the Fe $L_{2,3}$-edges , were carried out at beamline 9.3.2 at the Advanced Light Source, Lawrence Berkeley National Laboratory (Figs. 5 and 6). The experiments were performed with a resolution about 0.2 eV. The pressure in the XANES experimental chamber was about 1×10^{-10} Torr. The spectra were recorded by detecting the total electron yield (TEY) from the samples drain current. TEY is a surface-sensitive technique, unlike the X ray fluorescence yield (XFY) which is a bulk-sensitive measurement. Therefore TEY data do not require self-absorption correction. The I_0 signal from a gold grid upstream from the beamline was also recorded for normalization purposes and to monitor the energy calibration from the Cr $L_{2,3}$-edges' absorption signal in I_0 which originates from the Cr on the beamline gratings. The samples were mounted to a molybdenum holder with UHV-compatible double-sided conductive tape. Background subtraction was performed using a linear background fit for the energy region prior to each absorption edge. The monochromator was calibrated by running X ray photoemission spectra (XPS) for Au samples at different photon energies.
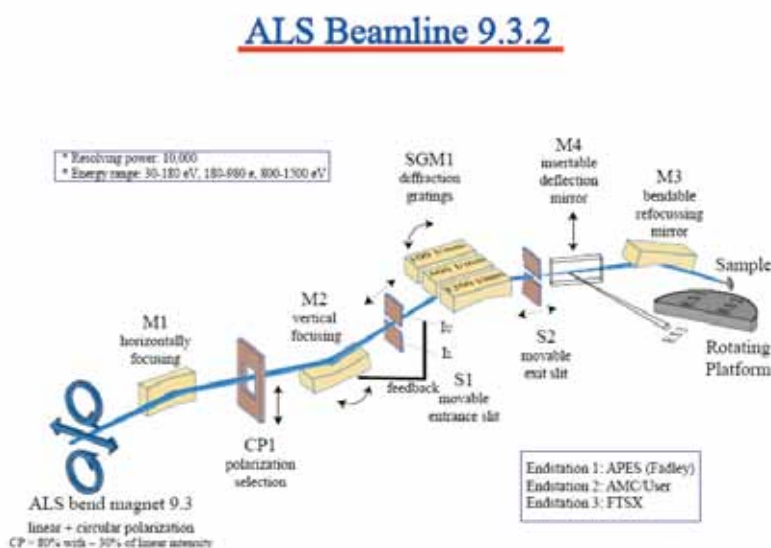

FIG. 5. Schematic diagram of the ALS beamline 9.3.2 showing the main components of the beamline.
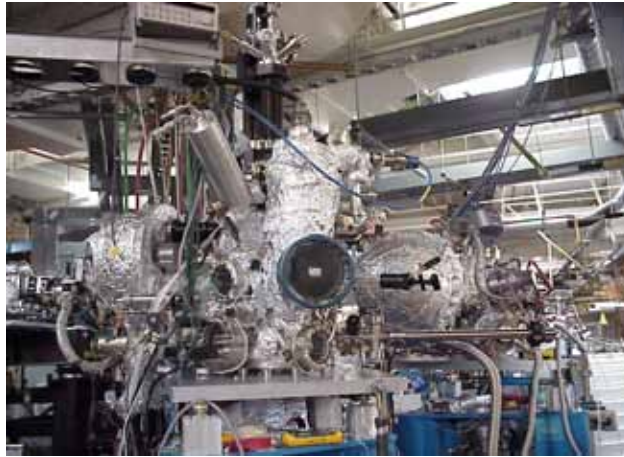
FIG. 6. The Advanced Materials Experimental Chamber at the ALS b.l 9.3.2. The chamber was used for this study.

3.5. XMCD method

XMCD is a technique that is sensitive to magnetic polarization and element specific properties. This technique enables quantitative determination of the element specific spin and orbital magnetic moments and their anisotropy through the sum-rules analysis of experimental data [13]. Such analysis will help in understanding the origin of the observed improvements and may lead to improvements in synthesis and annealing procedures to produce better material with better properties that could be used in technological applications.

X ray absorption spectroscopy (XAS) uses energy dependent absorption of X rays revealing elemental composition of the sample. On the other hand, XMCD utilizes the change of the absorption spectra of circularly polarized X rays when passing through a material in two different directions. Therefore, XMCD combines the sensitivity of the X ray absorption spectra to both the magnetic polarization and the element specific surface sensitivity. XMCD concept was first introduced by Schütz et al. in 1987 [14]. The X ray absorption process become spin dependent by the use of right or left circularly polarized photons which transfer their angular momentum to the excited photoelectron. This will result in $p_{3/2}$ (L_3) and $p_{1/2}$ (L_2) levels have opposite spin-orbit coupling, the spin polarization will be opposite at the two edges. In the absorption process, "spin-up" and "spin-down" are defined relative to the photon helicity or photon spin. (XMCD) technique senses the local anisotropy of charge, spin and angular momentum around an atom that is excited by the absorption of polarized X rays. Orbital magnetic moment m_{orb} and the spin magnetic moment m_{spin} can be obtained from XMCD Experiment. For a review on XMCD, please refer to the article by J. Stohr [15].
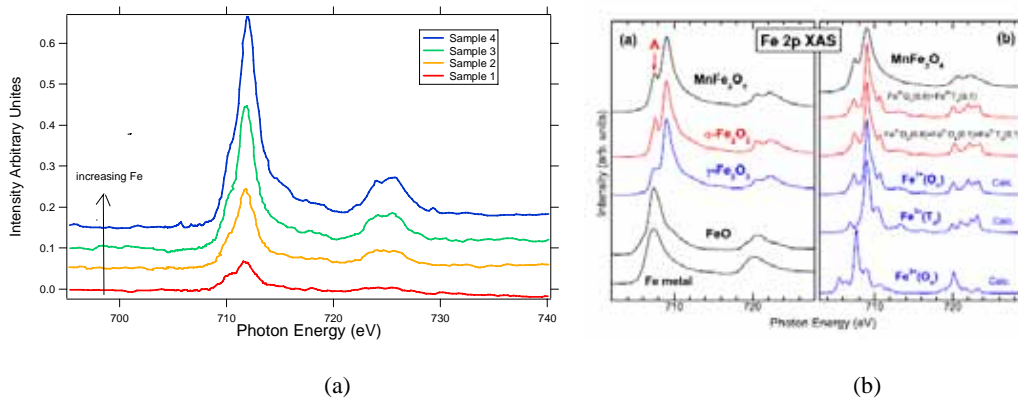
3.6. XANES Results

FIG. 7. (a) XANES spectra at Fe $L_{2,3}$ edges for samples with various Fe content. (b) Fe $L_{2,3}$ edges spectra for various Fe compounds from Ref. [2].

Figure 7(a) shows the XANES spectra for samples with different Fe contents at the Fe L_2 and L_3 edges, while Figure 7(b) represents XANES spectra for $MnFe_2O_4$ and other Fe compounds at the $L_{2,3}$ edges obtained from Ref. [2]. The spectra were obtained with linearly polarized X rays. The Figure indicates a mixed Fe valence state of Fe^{+2} and Fe^{+3}. Unlike XRD results above that indicated that Fe enters the ZnO site as +2 state. The XRD results provide an average and approximate answer to the valance state of Fe through the variation of the lattice parameter c and through the ionic radii of the two valance states of Fe and the ionic radius of Zn^{+2}. On the other hand, XANES results provide an exact value of the proportions of Fe^{+2} and Fe^{+3} states through peak fittings.
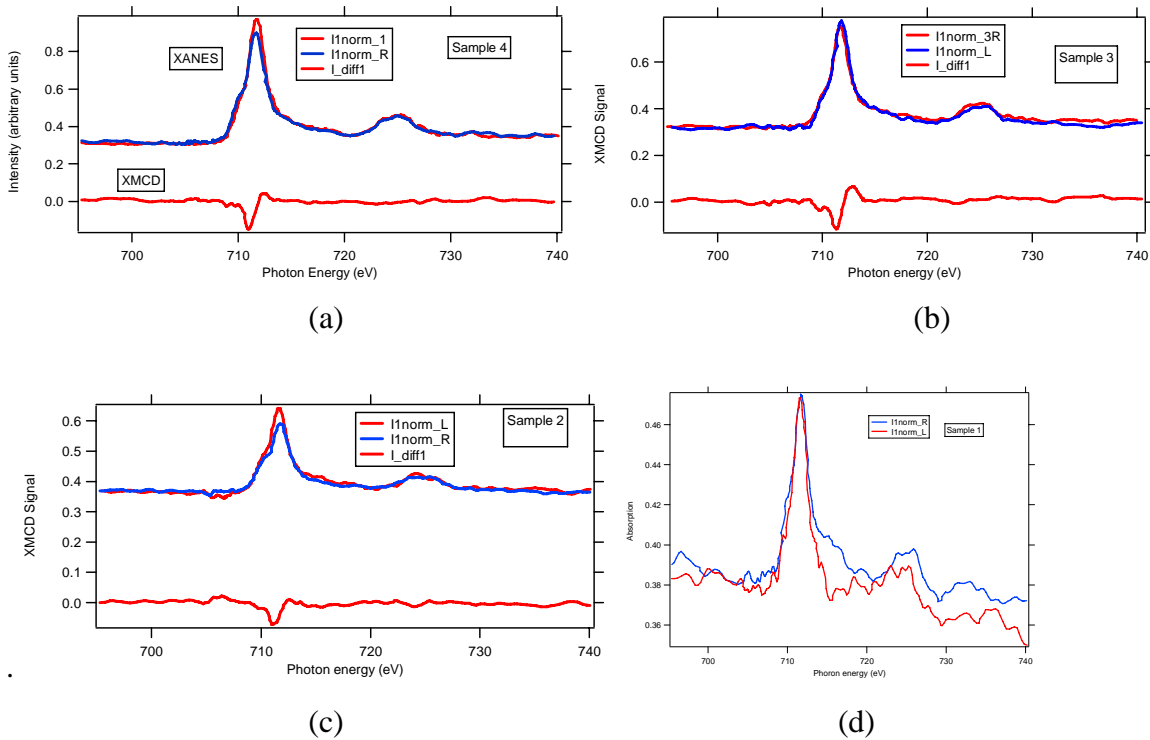

FIG. 8. XANES at the two light polarizations for samples 4, 3, 2 and 1; and XMCD for samples 4, 3, and 2.

Figure 8 (a, b and c) presents the XANES spectra at both the left and right hand polarizations and the XMCD signals for samples with the highest three Fe content. Figure 8(d) shows the XANES spectra for the sample with the lowest Fe content (about 1%) performed at the two light polarizations. The intensity was so weak and noisy and therefore it was not possible to obtain a reliable XMCD signal. Comparing the results of the XMCD for our system with the results in Figure 9 [2, 16] we can conclude that Fe co-exists in both +2 and +3 charge states, which confirms the results obtained by XANES spectra. The XMCD magnetic signal at the L3 edge provides evidence of this result. It can also be inferred that the negative polarity of the XMCD signals indicate an antiferromagnetic exchange pd coupling [17, 18].
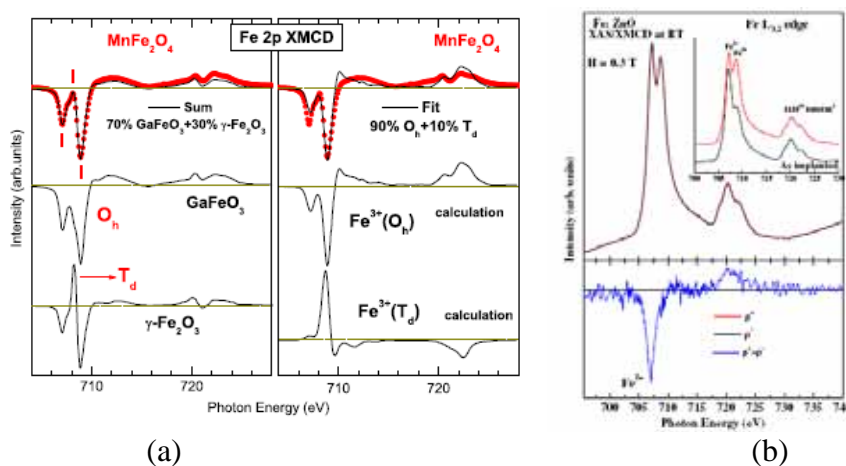

(a)   (b)

FIG. 9. XMCD signal at the $L_{2,3}$ Fe edges for (a) $MnFe_2O_4$ (ref 2) and (b) for FeZnO from Ref. [15].

4. Conclusions

XRD results provided useful information about crystal structure, phase formation, substitution and indicated that the valence state of Fe. On the other hand, optical absorption results provide additional information about band structural variation of the Fe-ZnO with Fe doping. This can be related to the electronic structure and interaction mechanism of Fe electrons with the ZnO matrix. XANES provides information about the chemical state while the XMCD provided information about the type of magnetic coupling and intrinsic magnetic properties of the DMS.

REFERENCES

[1] SHUTTHANANDAN, V., et al., Room-Temperature Ferromagnetism in Ion-Implanted Co-Doped TiO_2（110) Rutile, Applied Physics Letters **84** 22 (2004) 4466–4468.

[2] KANG, et al., Soft X-ray absorption spectroscopy and magnetic circular dichroism study of the valence and spin states in spinel $MnFe_2O_4$, Physical Review **B 77** (2004) 035121.

[3] CHEN, Z.C., et al., Initial study on the structure and optical properties of $Zn_{1-x}Fe_xO$ films, Thin Solid Films **515** (2007) 5462–5465.

[4] PRELLIER, W., FOUCHET, A., MERCEY, B., Oxide-diluted magnetic semiconductors: a review of the experimental status, J. Phys. Condens. Matt. **15** (2003) 1583–1601 (review article).

[5] DIETL, T., Ferromagnetic semiconductors, Semicond. Sci. Technol. **17** (2002) 377-392 (review article).

[6] KAMILLA, S.K., and BASU, S., New semiconductor materials for magnetoelectronics at room temperature, Bull. Mater. Sci. **25** (2002) 541–543.

[7] GOYA, F.G., LEITE, E.R., Ferrimagnetism and spin canting of $Zn^{57} Fe_2O_4$ nanoparticles embedded in ZnO matrix, J. Phys. Condens. Matt. **15** (2003) 641–651.

[8] DIETL, T., MATSKURA, F., CIBERT, J., FERRAND, D., Zener Model Description of Ferromagnetism in Zinc-Blende Magnetic Semiconductors, Science **287** (2000) 1019.

[9] CHAMBERS, S.A., DROUBAY, T., THEVUTHASAN, S., HAMDAN, N.M., ALS Compendium, 2001, Berkeley.

[10] MATSUMOTO, Y., et al., Room-Temperature Ferromagnetism in Transparent Transition Metal-Doped Titanium Dioxide, Science **291** (2001) 854.

[11] CHAMBERS, S. et al. Appli. Phys. Lett. 79 (2001) 3467.

[12] CHAMBERS, S., et al., Epitaxial growth and properties of MBE-grown ferromagnetic Co-doped TiO_2 anatase films on $SrTiO_3(001)$ and $LaAlO_3(001)$, Thin Solid films **418** (2002) 197.

[13] DIAZ, J., et al., Understanding the magnetic anisotropy in Fe-Si amorphous alloys, IEEE Trans. On Magnetics **38** (2002) 2811–2813.

[14] SCHÜTZ, G., et al., Absorption of circularly polarized X-rays in iron, Phys. Rev. Lett. **58** (1987) 737.

[15] STOHR, J., Exploring the microscopic origin of magnetic anisotropies with X-ray magnetic circular dichroism (XMCD) spectroscopy, Journal of Magnetism and Magnetic Materials **200** (1999) 470–497.

[16] KUMAR, et al., Ferromagnetism and metal–semiconducting transition in Fe-doped ZnO thin films, J. Phys. D: Appl. Phys. **41** (2008) 155002.

[17] TAKAOBUSHI, J. et al., Electronic structures of $Fe_{3-x}M_xO_4$ (M=Mn,Zn) spinel oxide thin films investigated by X ray photoemission spectroscopy and X ray magnetic circular dichroism, Physical Review **B 76** (2007) 205108.

[18] KIM, et al., Interface electronic structures of $BaTiO_3@X$ nanoparticles ($X=\gamma-Fe_2O_3$, Fe_3O_4, $\alpha-Fe_2O_3$, and Fe) investigated by XAS and XMCD Physical Review **B 79** (2009) 033402.

MATERIALS CHARACTERIZATION USING CONFOCAL MICRO X RAY FLUORESCENCE ELEMENTAL IMAGING

G. J. HAVRILLA, U. FITTSCHEN, V. MONTOYA, B. PATTERSON
Los Alamos National Laboratory,
Los Alamos, NM,
United States of America

Abstract

Laboratory-based confocal micro X ray fluorescence offers novel characterization capabilities not found in conventional analytical techniques. CMXRF has been used to characterize a range of uranium oxide from 100 to 10 micrometers in diameter, an inertial confinement fusion target composed of a Be doped sphere and compared with radiographic images obtained with micro X ray computed tomography. These two imaging platforms were integrated in the characterization of a surface mount resistor, demonstrating the increased information content of combining the structural information of the MXCT and the elemental information of the CMXRF. Density measurements using the CMXRF have been demonstrated on aerogel samples, identifying a high density skin on cast and machined aerogels. A prototype thermal inkjet picofluidic system has been used to deposit picoliter volumes from 300 to 1 pL of aqueous solutions to create custom reference materials for calibration of MXRF instrumentation.

1. Introduction

Significant progress has been made in furthering the development of confocal micro X ray fluorescence (MXRF) for elemental imaging. This progress has been developed in several areas: 1) initiated integration with micro X ray computed tomography (MXCT), 2) visualization of the confocal data and 3) implementation of a picoliter deposition technology. The integration of CMXRF with MXCT offers a 3D elemental distribution along with a 3D structural visualization. The improved visualization allows easier evaluation of confocal data and subsequently the materials being studied. The biggest advance has been the development of picoliter deposition of samples. This has opened new capabilities of depositing known masses of elements in discrete dimensions. This deposition capability enables calibration of the micro X ray probe beams which can now lead to quantitative measurements which previously were not possible.

2. Overview of the research performed and the results obtained

The ability to provide both elemental information and the spatial distribution of the elements detected in three dimensions is an inherent advantage of confocal MXRF. In addition to the 3D distribution of elements, the confocal probe offers the unique capability of dimensional density measurements. While the density measurement is unique to CMXRF it offers the potential to identify not only structural features not readily identified by the elemental composition but to provide density distributions throughout the material in a non-destructive manner. CMXRF has been applied to a variety of materials for 3D spatially resolved elemental analyses. Materials studied include such diverse samples as uranium oxide particles on a polymer film, paint chips, inertial confinement fusion (ICF) targets and a surface mount resistor. In each of these applications, the ability to discern structural features based on elemental spatial distribution provided unique insight into the material being studied.

In the case of the uranium oxide particles, the CMXRF was able to detect particles ranging in size from over 100 micrometers to less than 10 micrometers. The point of this exercise was to demonstrate the detection capability of the 30×30×60 micrometer confocal probe volume for features smaller than the probe itself. The high density uranium oxide particles were clearly delineated by their elemental signature. Although the smaller particles were detected, the larger probe volume was unable to clearly delineate the actual particle size. However the difference between the uranium oxide particles and the low density polymer support film, offered a unique contrast using the density mapping capability of CMXRF. The X ray scatter provides information on the presence of the polypropylene film even though it cannot be directly detected based on its elemental composition. The 3D image cross section is shown in Figure 1. The orange color is the uranium oxide particles. The gray shows the X ray scatter, in particular the polypropylene film which was used as a substrate for the particles.
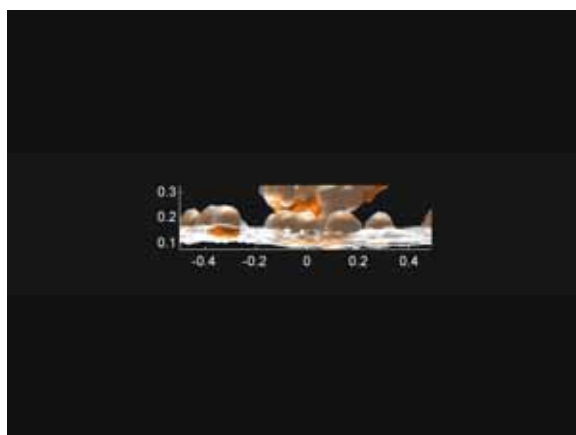
FIG. 1. 3D CMXRF image of uranium oxide particles on polypropylene film.

The ICF target and the surface mount resistor offered opportunities to initiate and demonstrate the integration of MXCT structural imaging with the 3D elemental imaging of CMXRF. The ICF target consisted of a 2.47 mm diameter sphere with a 147 micrometer Be coating [1]. The Be coating has 2 doping elements, copper on the inner portion and argon through the entire 147 micrometer thickness.

Figure 2A shows a reconstructed cross section of the Be capsule obtained with an Xradia MXCT instrument. The contrast in density between the copper doping and the Be substrate are clearly delineated. However the MXCT image is based purely on absorption of the X ray s and provides no elemental information. Figure 2B however, is a composite plot of a cross section of the MXCT line profile through the edge of the capsule, shown by the dotted line and the solid lines are elemental line profiles obtained from the CMXRF. There is a clear correlation of the outer Ar doped Be portion and the inner Cu doped Be portion. The iron appears to be present throughout the entire Be shell while the Ni appears to be only a contaminant in the Cu doped region. Although the density difference of the Cu doping enables the MXCT to distinguish the two doped portions of the Be capsule, the CMXRF provides a clear elemental signal of the Cu doping region compared to the Ar doped region.

The Ar profile would be detected if the sample was in a vacuum environment since we were able to detect the Ar with the conventional MXRF instrument. While the CMXRF does not have the micrometer level resolution of the MXCT, the elemental profiles track the MXCT structural cross section quite well.
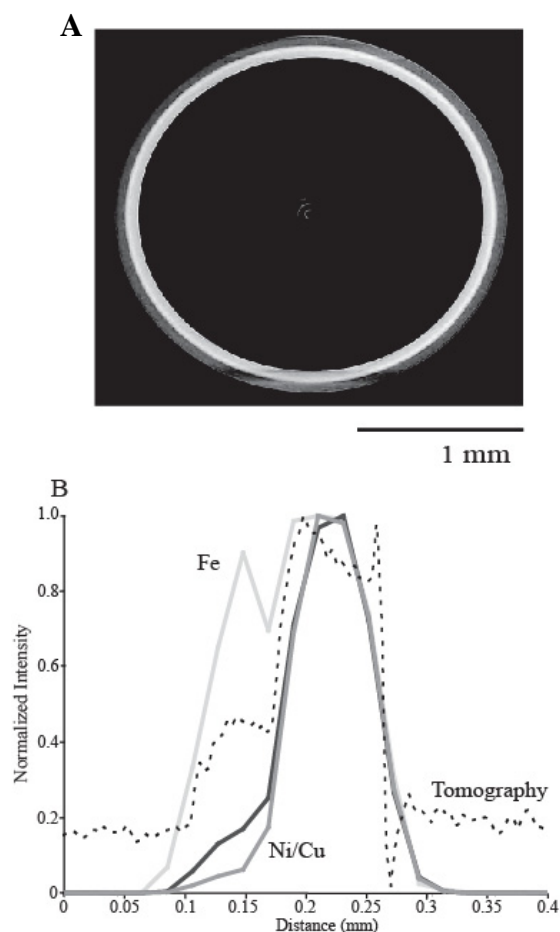
FIG. 2. A) MXCT reconstruction of ICF cross section. B) Line profiles from MXCT (dashed) and CMXRF elemental profiles (solid).

The integration of structural and elemental features in three dimensions offers unparalleled information and knowledge about a material. The structural features are obtained from the MXCT while the elemental is given by the CMXRF. The ability to integrate data from these two different datasets offers new opportunities to study materials. One feature of integrating the two datasets is the ability to correlate elemental composition with structural features not readily identified in the CMXRF images. The secondary feature is to use the MXCT to provide a guide in bounding the elemental images. In using MatLab for visualizing the elemental distributions, the selected isovalues are currently not calibrated spatially and typically exceed the actual dimensions of the material.

The MXCT with its higher spatial resolution and fixed spatial parameters offers one approach in providing spatial bounds for the CMXRF elemental images. Figure 3 (top) shows a picture of a surface mount resistor along with a simple X,Y map of the elements present. The readily recognized features are the numbers which are presumably TiO_2, the nickel plating for soldering, the manganese again presumably a paint pigment and aluminum from the ceramic Al_2O_3 package. This is contrasted with the CMXRF 3D elemental image shown in Figure 4. This shows the Ni, and the Ti, however this time the Al cannot be detected due to the air environment. The ability to detect X ray scatter is demonstrated by the gray which is the Al_2O_3 ceramic. The new feature shown here is the lead at the center of the resistor. While lead was detected in the X,Y map, it was not clear where the lead correlated in the white light picture of Figure 3 (top).
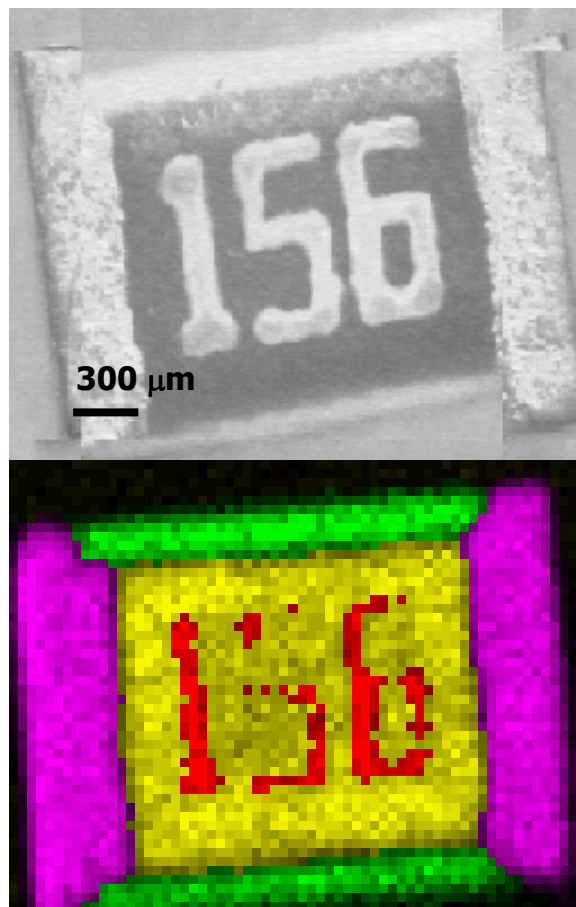

FIG. 3. Picture of surface mount resistor (top) with 2D X,Y elemental map overlay (bottom) showing Ni (magenta), Ti (red), Mn (yellow) and Al (green).

124

This became clear when we overlay the CMXRF image of just the Ni and Pb maps with the structural image of the MXCT reconstruction shown in Figure 5. The MXCT provides a spatial guide for the appropriate selection of the lead isovalues and we see almost a complete match of the CMXRF elemental image with the MXCT structural image. The encouraging aspect of the overlaid images is the excellent correlation of the CMXRF image with the MXCT image. The small cut-out which looks like the numeral '7' matches quite well. We are continuing to develop this integration of the CMXRF with the MXCT images in order to achieve a more realistic elemental image with validated isovalues in visualizing this 3D data. The density measurement capability of CMXRF provides a unique insight into materials which cannot be obtained with other technology [2].

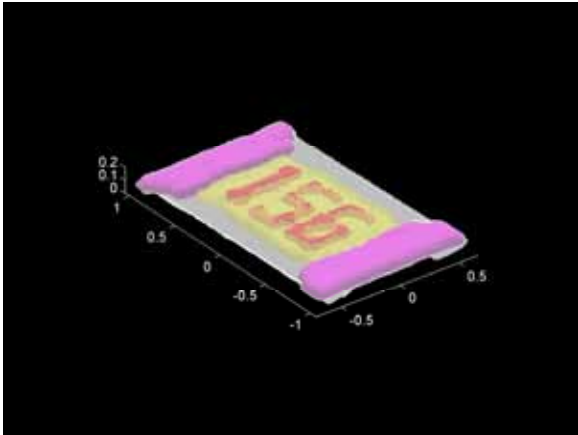
FIG. 4. CMXRF 3D image of surface mount resistor. Elements shown are Ni (magenta) Ti (red), Pb (yellow) and X ray scatter is gray.
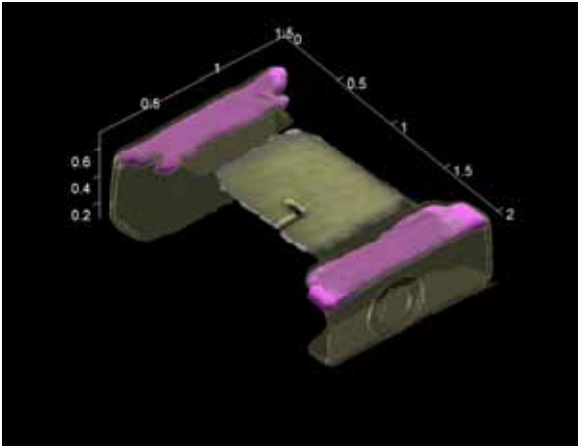

FIG. 5. Overlay of MXCT structural image (gray) with CMXRF elemental images of Ni (magenta) and Pb (yellow).

In Figure 6A the X ray scatter from an aerogel is shown. Since the aerogel is primarily silica, there is no elemental signal present. The silicon X rays are absorbed by the air environment. However, we have discovered the X ray scatter is proportional to the density of the aerogel. This is shown in Figure 6B, which is a plot of the bulk density of five different aerogels, measured several times. The linear relationship between the X ray scatter and the bulk density provides a novel method for density measurements. This is achieved because the confocal volume is probing a volume in space within the material. The confocal volume can detect either the elemental signal or the X ray scatter. The Bremsstrahlung scatter is directly proportional to the density of the material as demonstrated by the linear relationship shown in Figure 6B. This relationship has been quite useful in determining the presence of a skin in the aerogels. The skin is due to void shrinkage as the aerogel dries and had been assumed to be uniform over the bulk of the material. A line scan from the surface through the aerogel sample to the opposite surface is shown in Figure 6C (black).
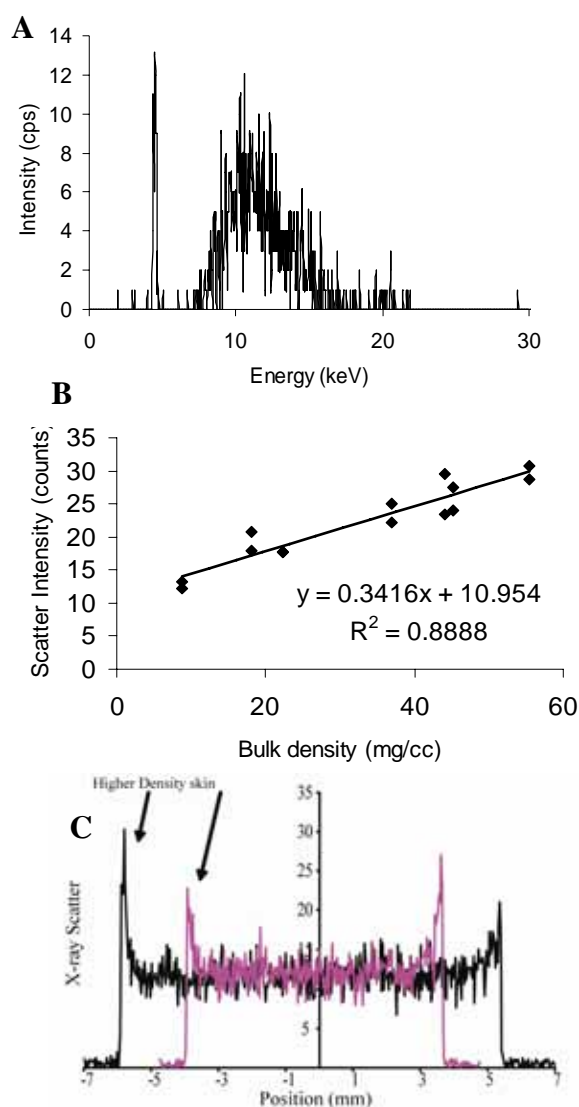

FIG. 6 A) X ray scatter spectrum from aerogel. B) Plot of X ray scatter and bulk density for measured aerogels. C) Line profiles of 37 mg/cm^3 aerogel before (black and after machining (violet). Arrows indicate high density skin.

126

These line profiles clearly illustrate the skin formation on the aerogel part. The black trace is the from a 37 mg/cm3 bulk density specimen. The violet plot is the same aerogel sample with approximately 2 mm removed from the radius of the sample. Hence the material is 4 mm in diameter smaller. The trace of the machined material again shows a skin at the surface of the aerogel. This is due to the collapse of the voids near the surface. The thickness of the skin is approximately 200 micrometers. This clears shows that the shrinkage only occurs near the surface. This is a significant problem because the density is not uniform throughout the sample. This measurement is only possible with CMXRF measuring the X ray scatter which has an intensity relationship with the density of the material.

The ability to quantify elements in 3D remains elusive primarily due to the need for a robust model to correct for absorption effects in the measurements as well as a need for 3D references. Even a good 2D reference material that is known to be homogeneous at the micrometer scale would be useful. Unfortunately there are few reference materials which can be used to calibrate micro X ray fluorescence instruments. The ability to deposit known masses in known dimensions at given spatial positions would alleviate the primary problem for calibrating the CMXRF instrumentation. This problem is solved with a prototype instrument based on thermal inkjet technology. The instrument is called a Thermal Inkjet Picofluidic System (TIPS) manufactured by Hewlett Packard. Previous work using dismantled inkjet print cartridges, although successful, did not sufficient control of the print parameters [3]. Since the TIPS device enables such control there are several key parameters which have been studied to reproducibly deposit aqueous solutions for quantitative XRF analyses. One of the issues has been evaporation control. Although the nozzles on the TIPS are quite small, there is still an appreciable and measureable amount of evaporation which occurs. This evaporation results in concentration of the analytes within the chamber prior to deposition. This means that without any compensation or mitigation the first number of droplets deposited is much higher in concentration than the actual solution. The evaporation can be controlled in two ways: 1) humidity control of the deposition chamber or 2) the quite time between deposits can be varied. Although humidity control can be easily achieved, not all deposition systems have an environmental chamber to raise the humidity to at least 60% to minimize any evaporation effects. On the other hand, optimizing the quite time can achieve the same results. The quite time control is done in conjunction with a purge deposition to clear the holding chamber of the TIPS nozzle prior to initiating the deposition. With a quite time of around 180 ms, the intensities of droplets with chamber humidities from around 20% to 90% show no discernable difference in elemental intensity. With the evaporation issue under control, the deposition of various picoliter volumes and concentration of elements provides linear calibrations for a number of elements over several orders of magnitude. The mass deposited ranges from a few picograms to over 300 picograms. The volumes deposited range from 1 pL to 250 pL. By combining different concentrations, different deposition volumes as well as using arrays of droplets, mass depositions exceeding 100 ng can be achieved. The array depositions are useful for large area excitation beams such as conventional EDXRF and WDXRF which typically have excitation areas ranging from several mm to several cm in diameter. This has been demonstrated with TXRF [4], where an array of around 8000 droplets exhibited an increase in linearity compared with typical VPD measurements.

The droplet dimensions vary from around 10 micrometers to over 50 micrometers on polypropylene. The substrate surface affects the size of the dried residue droplet, however, in most cases the dried droplet residue is usually less than 80 micrometers depending on the mass, volume and substrate. The thickness ranges from around 200 nm to almost 3 micrometers. These thicknesses are still within the thin film regime which allows

quantification without too much interelement absorption effects. One of the key features of these picoliter depositions is the uniformity of the deposit. While there are still some issues to understand in achieving complete homogeneity, these initial studies indicate quite acceptable homogeneity at the micrometer level. This is shown in Figure 7, which is an Auger electron map of the Ni distribution of a 25 fg droplet on Si. The homogeneity of the Ni distribution is quite good across the nominally 5 micrometer deposit. Hence, this demonstrates the feasibility of creating any desired elemental micro-reference material of known mass which can be used to calibrate not only XRF instrumentation but other micro-analytical techniques as well.
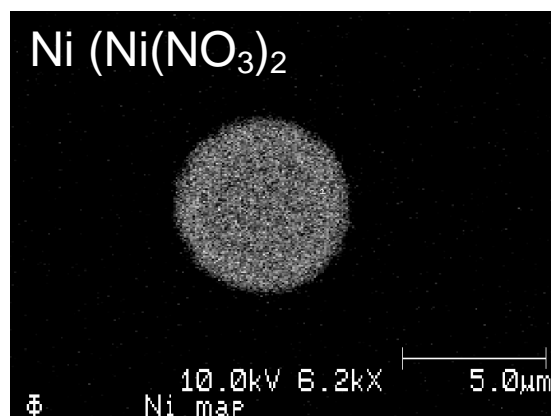

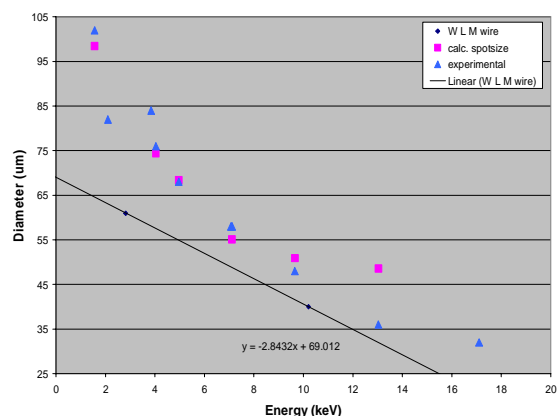*FIG. 7. Auger electron map of Ni distribution of 25 fg Ni deposit.*

FIG. 8. X ray beam size energy dependence calibration using TIPS elemental deposits.

A final demonstration of the useful calibration nature of these picoliter depositions is shown in Figure 8. This figure shows the measured energy beam width in a commercial MXRF instrument by doing line scans through known size elemental deposits. Since the instrument uses a monolithic polycapillary, the X ray beam width changes with energy and hence the element detected. The blue triangles are the experimentally measured beam widths, while the magenta squares are calculated from NIST SRM thin film elemental intensities. The straight line fit through the two blue diamonds is the typical beam calibration using a tungsten wire and the L and M lines. This shows the utility of having elemental deposits of known mass and size in calibrating the X ray energy dependence. The measured beam size ranges from nominally 30 micrometers at 17 keV (Mo) to almost 100 micrometers at around 1.5 keV (Al). Such beam size calibrations are critical in being able to accurately quantify different elements within a multielement deposit. This sort of calibration can be extended to CMXRF as shown in Figure 9.
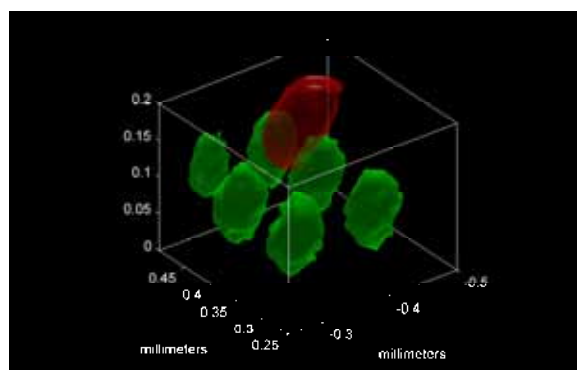

FIG. 9. CMXRF 3D elemental image of 100 pg Ni (green) deposits and iron (red) dust particle.

A small array of 100 pg nickel deposits (green) was imaged in 3D to illustrate the confocal beam size. In addition, the red figure in the image is the iron signal from a dust particle which landed on the deposit. The droplets and the dust particle are about 5 times smaller than the nominally 30×30×60 micrometer confocal volume. Thus the Ni droplet image shows the confocal beam shape. The ultimate utility of this deposition capability is to enable the creation of 3D reference materials. Such 3D reference materials of known thickness, mass and dimensions will enable refinement of confocal modelling for accurate quantification of elements at depth.

3. Conclusions

Confocal micro X ray fluorescence offers unique capabilities for three dimensional elemental imaging not found in conventional analytical techniques. There is enhanced information content when confocal MXRF and micro X ray computed tomography are integrated, with MXCT offering the potential to provide a calibration for bounding the elemental visualization dimensions. CMXRF also provides new capability of density measurements based on X ray scatter detected via the confocal volume. This is a new non-destructive approach to not only comparing density within a specimen but identifying structural features which cannot be detected using MXCT. The ultimate goal of quantifying elemental species at depth is one step closer with the TIPS prototype instrument for depositing and creating custom reference materials. There is significant potential for creation of 3D reference materials which can aid in modelling confocal MXRF measurements and ultimately quantification of elements at depth within samples.

Acknowledgements

REFERENCES

[1]   PATTERSON, B.M., et al., Nondestructive Investigations of a Copper and Argon-Doped Sputtered Beryllium Capsule Using X-Rays In Three Dimensions, Fusion Science and Technology **55** (2009) 417–423.

[2]   PATTERSON, B.M., et al., Staying on Target, Nuclear Weapons Journal in Press, 2009.

[3]   FITTSCHEN, U.E.A., et al., Characteristics of picoliter droplet dried residues as standards for direct analysis techniques, Anal. Chem. **80** (2008) 1967–1977.

[4]   SPARKS, C., FITTSCHEN, U.E.A., HAVRILLA, G.J., Automated Picoliter Solution Deposition for TXRF Analysis of Semiconductor Samples, Denver X ray Conference, Denver, CO, August 4–8, 2009, Book of Abstracts pg 106.

RELATED RESEARCH ARTICLES RESULTING FROM THE CRP

ARGENTINA

[1]   VÁZQUEZ, C., et al., Pigment characterization by scanning electron microscopy and X ray diffraction techniques: archaeological site El Trebol, Nahuel Huapi, Rio Negro, Argentina, Report IAEA/AL/181, 29–34, Vienna (2007).

[2]   DARCHUK, L., et al., Composition of pigments on human bones found in excavations in Argentina studied with micro-Raman spectrometry and scanning electron microscopy. e-PRESERVATIONScience **6** (2009) 112–117.

[3]   VAZQUEZ C., MAIER M.S., PARERA S.D., YACOBACCIO H., SOLA P., Combining TXRF, FT-IR and GC-MS information for identification of inorganic and organic components in black pigments of rock art from Alero Hornillos 2 (Jujuy, Argentina), Anal Bioanal Chem **391** (2008) 1381–1387.

[4]   VAZQUEZ C., Total reflection X ray fluorescence and archaeometry: Application in the Argentinean cultural heritage. Spectrochimica Acta Part B **63** (2008) 1415–1419.

AUSTRALIA

[1] SIEGELE, R., IONESCU, M., COHEN, D., doiba Manual, ANSTO External Report No ANSTO/E765, 1–115, April 2008.

[2] COHEN, D.D., STELCER, E., SIEGELE, R., IONESCU, M., Silicon detector dead layer thickness estimates using proton bremsstrahlung from low energy atomic number targets. X ray Spectrometry **37** (2008) 125–128.

[3] COHEN, D.D., STELCER, E., SIEGELE, R., IONESCU, M., PRIOR, M., Experimental bremsstrahlung yields for MeV proton bombardment of beryllium and carbon, Nuclear Instr. and Methods B **266** (2008) 1149–1153.

AUSTRIA

Reviewed publications

[1] MEIRER, F., et al., Feasibility study of SR-TXRF-XANES analysis for iron contaminations on a silicon wafer surface. Surf. Interface Anal. **40** (2008) 1571–1576

[2] FITTSCHENA. U.E.A., et al., Characterization of atmospheric aerosols using Synchroton radiation total reflection X ray fluorescence and FeK-edge total reflection X ray fluorescence-X ray absorption near-edge structure. Spectrochimica Acta Part B **63** (2008) 1489–1495

[3] MEIRER, F., et al., Parameter study of self-absorption effects in Total Reflection X ray Fluorescence-X ray Absorption Near Edge Structure analysis of arsenic. Spectrochimica Acta Part B **63** (2008) 1496–1502.

[4] MEIRER, F., PEPPONI, G., STRELI, C., WOBRAUSCHEK, P., ZÖGER, N., Grazing exit versus grazing incidence geometry for X ray absorption near edge structure analysis of arsenic traces. Journal of Applied Physics **105** (2009) 074906; 074906-1 – 074906-7.

Reports

[5]   MEIRER, F., et al., Characterization of iron-contaminations on silicon wafer surface. Bericht für Hasylab Annual Report; (2008) 2 S.

[6]   MEIRER, F., et al., Parameter study of self-absorption effects in TXRF-Xanes analysis of arsenic. Bericht für Hasylab Annual Report (2008) 2 S.

[7]   MEIRER, F., et al., A new Grazing-Exit-XRF setup at HASYLAB beamline L. Bericht für Hasylab Annual Report (2008) 2 S.

[8]   ZÖGER, N., et al., Elemental Imaging in Osteoarthritis; Bericht für HASYLAB Annual Report; (2007) 2 S.

[9]   ZÖGER, N., et al., Micro XANES in Pb-rich Zones of Human Bone. Bericht für HASYLAB Annual Report (2005; 2006).

[10]   ZÖGER, N., et al., Elemental Imaging in Human Articular Bone with Duplicated Tidemarks"; Bericht für ANKA Annual Report (2006) 2 S.

Conference contributions

[11]   MEIRER, F., et al., Parameter study of self-absorption effects in TXRF-XANES measurements"; Vortrag: TXRF Conference, Trento (Italy); 06/2007.

[12]   MEIRER, F., et al., Self-absorption effects in TXRF-XANES measurements - a parameter study; Poster: ICXOM 2007, Kyoto (Japan); 09/2007.

[13]   MEIRER, F., PEPPONI, G., STRELI, C., P. WOBRAUSCHEK, P., ZÖGER, N., A new Grazing-Exit-XRF setup at HASYLAB beamline L; Vortrag: EXRS Conference, Croatia; 16–20 June 2008.

[14]   MEIRER, F., PEPPONI, G., STRELI, C., P. WOBRAUSCHEK, P., ZÖGER, N., Grazing-Exit-XRF experiments at HASYLAB beamline L; Vortrag: Denver X ray Conference, Denver Colorado; 4–8 August.2008.

[15]   MEIRER, F., et al. Determination of the Oxidation State of Iron-Contaminations on Silicon Wafer Surfaces with K-Edge TXRF Xanes; Poster: Denver X ray Conference, Colorado Springs (USA) 08/2007.

[16]   MEIRER, F., et al., K-edge TXRF XANES measurements of Fe contaminations on Si wafer surfaces for determination of their oxidation state; Poster: 57. Jahrestagung der Österr. Physikalischen Gesellschaft (ÖPG), Krems (Österreich) 09/2007.

[17]   STRELI, C., et al., Synchrotron radiation induced Total Reflection X ray Fluorescence Analysis; Vortrag: CSI XXXV 2007, Xiamen (China) 09/2007.

[18]   STRELI, C., et al., Synchrotron radiation induced Total Reflection X ray Fluorescence Analysis-absorption spectroscopy (SRTXRF-XAS); Vortrag: EXRS Conference, Croatia; 16–20 June 2008.

[19]   STRELI, C., et al., Synchrotron Radiation induced TXRF absorption spectroscopy"; Vortrag: SARX Conference, Rio de Janeiro, Brasilien (invited); 17–21 November 2008.

[20]   STRELI, C., et al., Synchrotron radiation induced TXRF for XANES application at HASYLAB, Beamline L; Vortrag: ICXOM 2007, Kyoto (Japan) (invited); 09/2007.

[21]   ZÖGER, N., et al., Speciation of Pb in the tidemark of human articular bone - a feasibility study; Poster: ICXOM 2007, Kyoto (Japan); 09/2007.

[22]   ZÖGER, N., et al., μ-XRF and μ.XANES at calcification fronts on human articular cartilage; Poster: 56. Jahrestagung der Österr. Physikalischen Gesellschaft (ÖPG), Graz; 21 September 2006.

[23] ZÖGER, N., et al., Confocal Synchrotron radiation induced μ-XRF of osteoarthritic bone samples; Poster: CSI XXXV 2007, Xiamen (China); 09/2007.

[24] ZÖGER, N., et al., Elemental Distribution on Ostehoarthritic joints by confocal micro-XRF; Vortrag: ICXOM 2007, Kyoto (Japan); 09/2007.

[25] ZÖGER, N., Elemental imaging in osteoarthritic bones by confocal synchrotron Micro-XRF; Poster: 57. Jahrestagung der Österr. Physikalischen Gesellschaft (ÖPG), Krems (Österreich); 09/2007.

[26] ZÖGER, N., et al., Elemental Imaging in Osteoarthritic Joint Bones; Poster: Denver X ray Conference, Colorado Springs (USA); 08/2007.

[27] ZÖGER, N., et al., μ-XRF and μ-XANES at calcification fronts of human articular cartilage; Poster: EXRS Conference, Paris (France); 19–23 June 2006.

[28] ZÖGER, N., et al., Lead in human cartilage: imaging and speciation by micro-XRF and Micro-XANES; Poster: 55th Denver X ray Conference, Denver (USA); 07–11 August 2006.

BELGIUM (K. Janssens)

Publications in international journals with peer review (2007–2009)

[1] LIND, O.C., et al., Characterization of U/Pu particles originating from the nuclear weapon accidents at Palomares, Spain, 1966 and Thule, Greenland, 1968. Sci. Tot. Environ. **376** (2007) 294–305.

[2] DENECKE, M.A., et al., Microanalysis (micro-XRF, micro-XANES and micro-XRD) of a tertiary sediment using micro-focused synchrotron radiator; Microscopy and Microanalysis **13** (2007) 165–172.

[3] BRENKER, F.E., et al., Carbonates from the lower part of transition zone or even the lower mantle; Earth and Planetary Science Letters **260** (2007) 1–9.

[4] TERZANO, R., et al., Assessing the Origin and Fate of Cr, Ni, Cu, Zn, Pb, and V in Industrial Polluted Soil by Combined Microspectroscopic Techniques and Bulk Extraction Methods, Environmental Science & Technology (2007).

[5] BUGANI, S., CAMAITI, M., MORSELLI, L., VAN DE CASTEELE, E., JANSSENS, K., Investigation on porosity changes of Lecce stone due to conservation treatments by means of X ray nano- and improved micro-computed tomography: preliminary results; X ray Spectrometry **36** (2007) 316–320.

[6] DENECKE, M.A., et al., μ-X ray fluorescence and μ-X ray diffraction investigations of sediment from the Ruprechtov nuclear waste disposal natural analog site; Spectrochimica Acta B **63** (2008) 484–492.

[7] TERZANO, R., et al., Zinc Distribution and Speciation within Rocket Plants (Eruca vesicaria L. Cavalieri) Grown on a Polluted Soil Amended with Compost as Determined by XRF Microtomography and Micro XANES; Journal of Agricultural and Food Chemistry **56** (2008) 3222–3231.

[8] VAN DER SNICKT, G., DE NOLF, W., VEKEMANS, B., JANSSENS, K., μ-XRF/μ-RS vs. SR μ-XRD for pigment identification in illuminated manuscript; Applied Physics A **92** (2008) 59–68.

[9] DIK, J., et al., Visualization of a Lost Painting by Vincent van Gogh Using Synchrotron Radiation Based X ray Fluorescence Elemental Mapping; Analytical Chemistry **80** (2008) 6436–6442.

[10] JAROSZEWICZ, J., DE NOLF, W., JANSSENS, K., MICHALSKI, A., FALKENBERG, G., Advantages of combined µ-XRF and µ-XRD for phase characterization of Ti-B-C ceramics compared with conventional X-ray diffraction; Analytical and bioanalytical chemistry **391** (2008) 1129–1133.

[11] WAGNER, B., et al., Complementary analysis of historical glass by scanning electron microscopy with energy dispersive X ray spectroscopy and laser ablation inductively coupled plasma mass spectrometry; Microchemist Acta **162** (2008) 415–424.

[12] AIBÉO, C.L., et al., Micro-Raman analysis for the identification of pigments from 19th and 20th century paintings; Journal of Raman spectroscopy **39** (2008) 1091–1098.

[13] VAN DER SNICKT, G., et al., Characterization of a degraded cadmium yellow (CdS) pigment in an oil painting by means of synchrotron radiation based X ray techniques; Analytical chemistry **81** (2009) 2600–2610.

[14] LIND, O.C., et al., Solid state speciation and potential bioavailability of depleted uranium particles from Kosovo and Kuwait; Journal of environmental radioactivity **100** (2009) 301–307.

Reports 2007–2009

[15] DE NOLF, W., JANSSENS, K., ROUCHON, V., FALKENBERG, G., Study of the degradation on historical documents induced by iron gall ink by means of scanning µ-XRF/µ-XRD; HASYLAB Jahresbericht 2006 / Schneider J. [edit.], e.a., Hamburg, 2007.

[16] ALFELD, M., et al., Depth profiling of multilayered systems by means of confocal µ-XRF in the laboratory and at HASYLAB BL L: a comparison; HASYLAB Jahresbericht 2006 / Schneider J. [edit.], e.a., Hamburg, 2007.

[17] JAROSZEWICZ, J., et al., Combined use of µ-XRF and µ-XRD for characterization of radioactive particles released during the Chernobyl accident; HASYLAB Jahresbericht 2006 / Schneider J. [edit.], e.a., Hamburg, 2007. http://www-hasylab.desy.de/science/annual_reports/2006_report/main.htm.

[18] JAROSZEWICZ, J., DE NOLF, W., JANSSENS, K., MICHALSKI, A., FALKENBERG, G., Combined use of µ-XRF and µ-XRD to determine the heterogeneity, the chemical and phase composition of Ti–B–C ceramics prepared by the Pulse Plasma Sintering (PPS) method; HASYLAB Jahresbericht 2006 / Schneider J. [edit.], e.a., Hamburg, 2007.

[19] TERZANO, R., et al., µ-XANES Speciation of Zn in Rhizospheric soil and in Edible Plants Grown on a Polluted Soil Amended with Compost; HASYLAB Jahresbericht 2006 / Schneider J. [edit.], e.a., Hamburg, 2007.

[20] TERZANO, R., et al., Determination of Zn Distribution inside Edible Plants Grown on a Polluted Soil Amended with Compost by XRF Microtomography; HASYLAB Jahresbericht 2006 / Schneider J. [edit.], e.a., Hamburg, 2007.

[21] TERZANO, R., et al., Identification of the Geochemical Forms of Cr, Zn, Ni, Pb, V, and Cu in an Industrial Polluted Soil by Combined µ-XRF/µ-XRD and µ-XANES; HASYLAB Jahresbericht 2006 / Schneider J. [edit.], e.a., Hamburg, 2007.

[22] DENECKE, M.A., et al., Confocal µ-XRF and µ-XAFS studies of fractured granite following a radiotracer migration experiment; HASYLAB Jahresbericht 2006 / Schneider, J. [edit.], Hamburg, 2007.

[23] DE NOLF, W., Vekemans, B., Janssens, K., van der Snickt, G., Falkenberg, G., Pigment identification by scanning µ-XRF/µ-XRD; HASYLAB Jahresbericht 2006 / Schneider, J. [edit.], Hamburg, 2007.

[24] DE NOLF, W., Jaroszewicz, J., Janssens, K., Falkenberg, G., -2θ-resolution obtainable during - XRPD experiments at Beamline L.; HASYLAB Jahresbericht 2007 / Schneider, J. [edit.], Hamburg, (2008) 1655-1656.

[25] TERZANO, R., et al., Assessing the origin and fate of Cr, Ni, Cu, Zn, Pb, and V in an industrial polluted soil by combined micro-spectroscopic techniques and bulk extraction methods; HASYLAB Jahresbericht 2007 / Schneider, J. [edit.], Hamburg, 2008.

[26] LIND, O.C., et al., Characterization of Yenisey River U-particles using a combination of μ-XRF, μ-XRD and U-LIII μ-XANES; HASYLAB Jahresbericht 2007 / Schneider, J. [edit.], Hamburg, (2008) 1279–1280.

[27] DE NOLF, W., et al., Combined micro-XRF/XRPD tomography on historical and modern paint multilayer samples at Beamline L; HASYLAB Jahresbericht 2007 / Schneider, J. [edit.], Hamburg, (2008) 1633–1634.

[28] DIK, J., et al., High-E scanning m-XRF experiment on test paintings. HASYLAB Jahresbericht 2007 / Schneider, J. [edit.], Hamburg, (2008) 1589–1590.

[29] TERZANO, R., et al., Identification of the geochemical forms of CR, Zn, Ni, Pb, V, and Cu in an industrial polluted soil by combined μ-XRF/μ-XRD and μ-XANES; HASYLAB Jahresbericht 2006 / Schneider, J. [edit.], Hamburg, 2008.

[30] TERZANO, R., et al., Quantitative Fe determination inside tomato roots by confocal μ-XRF; HASYLAB Jahresbericht 2007 / Schneider, J., Hamburg, (2008) 1513–1514.

[31] LIND, O.C., et al., Reexamination of U and Pu in particles from Thule and Palomares by μ-XRD; HASYLAB Jahresbericht 2007 / Schneider, J. [edit.], Hamburg, (2008) 1297–1298.

BELGIUM (Rene Van Grieken)

[1] WOROBIEC, A. et al., Study of the winter and summer changes of the air composition in the church of Szalowa, Poland, related to conservation, Microchimica Acta **156** (2007) 253–261.

[2] SPOLNIK, Z., et al., Influence of different types of heating systems on particulate air pollutant deposition: The case of churches situated in a cold climate; Journal of Cultural Heritage **8** (2007) 7–12.

[3] WOROBIEC, A., et al., Characterisation of Amazon Basin aerosols at the individual aerosol particle level by X ray microanalytical techniques; Atmospheric Environment **41** (2007) 9217–9230.

[4] AVIGO JR, D., et al., Particulate matter analysis at elementary schools in Curitiba, Brazil; Analytical and Bioanalytical Chemistry **391** (2008) 1459–1468.

[5] KONTOZOVA-DEUTSCH, V., et al., Application of EPMA and XRF for the investigation of particulate pollutants in the field of cultural heritage; Microchimica Acta **161** (2008) 465–469.

[6] GODOI, R.H.M., et al., Inhalable particulate matter from lime industries: chemical composition and deposition in human respiratory tract; Atmospheric Environment **42** (2008) 7027–7033.

[7] OSAN, J., et al., Comparison of sediment pollution in the rivers of the Hungarian Upper Tisza Region using non-destructive analytical techniques; Spectrochimica Acta B **62** (2007) 123–136.

[8] STRANGER, M., POTGIETER-VERMAAK, S.S., VAN GRIEKEN, R., Comparative overview of indoor air quality in Antwerp, Belgium; Environment International **33** (2007) 789–797.

[9]   WOROBIEC, A., et al., Characterisation of concentrates of heavy mineral sands by micro-Raman spectroscopy and CC SEM/EDX with HCA; Applied Geochemistry **22** (2007) 2078–2085.

[10]   WOROBIEC, A., et al., Comprehensive microanalytical study of welding aerosols with X ray and Raman based methods; X ray Spectrometry **36** (2007) 328–335

[11]   GODOI, R.H.M., POTGIETER-VERMAAK, S., GODOI, A.F.L., STRANGER, M., VAN GRIEKEN, R., Assessment of aerosol particles within the Rubens' House Museum in Antwerp, Belgium; X ray Spectrometry **37** (2008) 298–303.

[12]   SAMEK, L., et al., Impact of electric overhead radiant heating on the indoor environment of historic churches; Journal of Cultural Heritage **8** (2007) 361–369.

[13]   HOREMANS, B., WOROBIEC, A., BUCZYNSKA, A., VAN MEEL, K., VAN GRIEKEN, R., Airborne particulate matter and BTEX in office environments; Journal of Environmental Monitoring **10** (2008) 867–876.

[14]   KONTOZOVA-DEUTSCH, V., et al., Investigation of gaseous and particulate air pollutants at the Basilica Saint-Urbain in Troyes, related to the preservation of the medieval stainded glas windows; Microchimica Acta **162** (2008) 425–432.

[15]   STRANGER, M., POTGIETER-VERMAAK, S.S., VAN GRIEKEN, R., Characterisation of indoor air quality in primary schools in Antwerp, Belgium; Indoor Air **18** (2008) 454–463.

[16]   VOROBIEC, A., et al., A seasonal study of atmospheric conditions influenced by the intensive tourist flow in the Royal Museum of Wawel Castle in Cracow, Poland; Microchemical Journal **90** (2008) 99–106.

[17]   STEFANIAK, E.A., et al., Recognition of uranium oxides in soil particulate matter by means of µ-Raman spectrometry; Journal of Nuclear Materials **381** (2008) 278–283.

[18]   VOROBIEC, A., et al., Historical changes in air pollution in the tri-border region of Poland, Czech Republic and Germany; Environment Protection Engineering **34** (2008) 81–90.

[19]   DE MAEYER-WOROBIEC, A., DEKOV, V.M., LAANE, R.W.P.M., VAN GRIEKEN, R., EPXMA survey of shelf sediments (Southern Bight, North Sea): A glance beyond the XRD-invisible; Microchemical Journal **91** (2009) 21–31.

[20]   DE HARTOG, J.J. et al., Associations between PM2.5 and heart rate variability are modified by particle composition and beta-blocker use in patients with coronary heart disease; Environmental Health Perspectives **117** (2009) 105–111.

[21]   NOWAK, D., et al., Morphology and the chemical make-up of the inorganic components of black corals; Materials Science and Engineering **C 29** (2009) 1029–1038.

[22]   STRANGER, M., POTGIETER-VERMAAK, S.S., VAN GRIEKEN, R., Particulate matter and gaseous pollutants in residences in Antwerp, Belgium; Science of the Total Environment **407** (2009) 1182–1192.

[23]   STEFANIAK, E.A., et al., Combined SEM/EDX and micro-Raman spectroscopy analysis of uranium minerals from a former uranium mine; Journal of Hazardous Materials **168** (2009) 416–423.

[24]   DARCHUK, L., et al., Composition of pigments found in excavations and on human bones (in Argentina) with micro-Raman spectrometry and scanning electron microscopy; e-Preservation Science **6** (2009) 112–117.

[25]   KIPS, R., et al., Determination of fluorine in uranium oxyfluoride particles as an indicator of particle age, Spectrochimica Acta B **64** (2009) 199–207.

[26] RAVINDRA, K., STRANGER, M., VAN GRIEKEN, R., Chemical characterization and multivariate analysis of atmospheric PM2.5 particles; Journal of Atmospheric Chemistry **59** (2008) 199–218.

[27] DAMLA, N., et al., Characterization of "gas concrete" materials used in buildings of Turkey; Journal of Hazardous Materials **168** (2009) 681–687.

CROATIA

[1] JAKŠIĆ, M., et al., New capabilities of the Zagreb ion microbeam system; Nucl. Instrum. Methods B **260** (2007) 114–119.

GERMANY

Refereed Journals

[1] SCHAUMANN,W., et al., Preparation and characterization of polymer layer systems for validation of 3D Micro X ray fluorescence spectroscopy, Spectrochimica Acta Part B **64** (2009) 334–340.

[2] SOKARAS, D., et al., Quantitative analysis in confocal micro-PIXE — general concept and layered Materials, J. Anal. At. Spectrom. **24** (2009) 611–621.

[3] WOLFF, T., et al., Performance of a polycapillary halflens as focussing and collecting optic – a comparison", J. Anal. At. Spectrom. **24** (2009) 669–675.

[4] REINHARDT, F., et al., Evaluation of high-resolution X ray absorption and emission spectroscopy for the chemical speciation of binary titanium compounds, Analytical Chemistry (2009). DOI: 10.1021/ac8018069.

[5] REICHE, I., et al., Development of a nondestructive method for underglaze painted tiles — demonstrated by the analysis of Persian objects from the nineteenth century, Anal Bioanal Chem. (2008). DOI 10.1007/s00216-008-2497-7

[6] ZITNIK, M., et al., 3D imaging of aerosol particles with scanning proton microprobe in a confocal arrangement", Applied Physics Letters **93** (2008) 094104.

[7] KANNGIESSER, B., MANTOUVALOU, I., MALZER, W., WOLFF, T., HAHN, O., "In-Situ Analysis of Corrosion Layers of Historical Glass Objects by 3D Micro X ray Fluorescence Analysis", J. Anal. At. Spectrom. **23** 6 (2008) 814–819.

[8] BJEOUMIKHOV, A., et al., Capillary µFocus X ray lenses with Parabolic and Elliptic Profile", Nucl. Instr. and Meth. A **587** 2–3 (2008) 458–463.

[9] MANTOUVALOU, A.. et al., Reconstruction of Thickness and Composition of Stratified Materials by means of 3D Micro X ray Fluorescence Spectroscopy", Anal. Chem. **80** (2008) 819–826. DOI: 10.1021/ac701774d.

[10] KANNGIESSER, B., et al., 3D Micro-PIXE at Atmospheric Pressure: A New Tool for the Investigation of Art and Archaeological Objects, Nucl. Instr. and Meth. B **264** 2 (2007) 383–388, DOI:10.1016/j.nimb.2007.09.019.

[11] KANNGIESSER, B., MALZER, W., PAGELS, M., LÜHL, L., WESELOH, G., 3D Micro-XRF under cryogenic conditions - a pilot experiment for spatially resolved trace analysis in biological specimens; Anal Bioanal Chem. **389** 4 (2007) 1171–1176.

[12] KARYDAS, A.-G., et al., 3D Micro-PIXE – a new technique for depth resolved elemental analysis, J. Anal. At. Spectrom. **22** (2007) 1260–1265.

[13] HAHN, O., et al., Non-destructive investigation of the scroll material: "A composition concerning Divine providence" 4Q413. ", Dead Sea Discoveries **14** 3 (2007).

[14] MÜLLER, M., BECKHOFF, B., ULM, G., KANNGIESSER, B., Absolute determination of cross sections for resonant Raman scattering on silicon, Phys. Rev. A **74** (2006) 012702.

[15] PAGÈS-CAMAGNA, S., et al., New insights into the colour origin of archaeological Egyptian Blue and Green by XAFS at the Cu K-edge", X ray Spectrom. **35** (2006) 141–145.

[16] KANNGIESSER, B., MALZER, W., FUENTES RODRIGUEZ, A., REICHE, I., 3D micro-XRF Investigations of Paint Layers with a tabletop set-up", Spectrochimica Acta B **60** (2005) 41–47.

[17] MALZER, W., KANNGIESSER, B., "A model for the confocal volume of 3D micro X ray fluorescence spectrometer", Spectrochimica Acta B **60** 9–10 (2005) 1334–1341.

[18] HAHN, O., KANNGIESSER, B., MALZER, W., "Non-destructive investigation of writing materials in historical manuscripts- X ray fluorescence analysis of iron gall inks, pencils, and coloured pencils", Studies in Conservation **50** (2005) 23–32.

Book Publications:

[19] BECKHOFF, B. KANNGIESSER, B., LANGHOFF, N., WEDELL, R., WOLFF, H., (eds.), "Handbook of Practical X ray Fluorescence Analysis", Springer-Verlag ISBN 3-540-28603-9, (2006).

[20] KANNGIEßER B., HASCHKE, M., chapter "Micro X ray Fluorescence Spectroscopy" in "Handbook of Practical X ray Fluorescence Analysis", Springer-Verlag ISBN 3-540-28603-9, (2006).

GREECE

Refereed journals:

[1] SOKARAS, D., KARYDAS, A.G., Secondary fluorescence enhancement in Confocal X ray Microscopy Analysis, Anal. Chem., 2009, accepted.

[2] SOKARAS, D., et al., Quantitative Analysis in Confocal micro-PIXE - General concept and layered MATERIALS, J. Anal. At. Spectrom., 2009, DOI: 10.1039/B817100A.

[3] WOLFF, T., et al., Performance of a polycapillary halflens as focusing and collecting optic—a comparison", J. Anal. At. Spectrom., 2009, DOI: 10.1039/B817828C

[4] ZITNIK, M., et al., Three-dimensional imaging of aerosol particles with scanning proton microprobe in a confocal arrangement, Appl. Phys. Lett. **93** (2008) art. no. 094104

[5] BECKHOFF, B., et al., Reference-free X ray fluorescence analysis of an ancient Chinese ceramic, X ray Spectrom. **37** (2008) 462–465.

[6] ZACHARIAS, N., et al., Solid-state luminescence for the optical examination of archaeological glass beads, Optical Materials **30** 7 (2008) 1127–1133.

[7] ZACHARIAS, N., et al., Thermally and optically stimulated luminescence of an archaeological glass collection from Thebes, Greece, Journal of Non-Crystalline Solids **354** 2–9 (2008) 761–767.

[8] KARYDAS, A.G., Application of a portable XRF spectrometer in the analysis of museum metal collections", Annali di Chimica **97** 7 (2007) 419–432.

[9] KANNGIEßER, B., et al., 3D Micro-PIXE at Atmospheric Pressure: A New Tool for the Investigation of Art and Archaeological Objects, Nucl. Instr. and Meth. In Phys. Res. B **264** (2007) 383–388.

[10] KARYDAS, A-G., et al., 3D Micro-PIXE – a new technique for depth resolved elemental analysis, J. Anal. At. Spectrom. **22** (2007) 1260–1265.

Books, conference proceedings:

[11] TARATORI, P., KARYDAS, A.G., MOSCHONA-KATSAROU, D., Non-destructive XRF analysis of the Mycenenan armour of Dendron, Proceedings of the 5th Symposium of the Hellenic Society for Archaeometry, Athens. Greece. 8–10 October 2008.

[12] KARYDAS, A.-G., ZARKADAS, C., A portable X ray Fluorescence spectrometer in support of the archaeological research and conservation science for the area of Thessaly, Proceedings of the workshop Archaeological research at Thessaly and Mainland, Volos, 16.3 – 19.3.2006, Vol. I: Thessaly (2009) 713–722.

[13] NIKOLAOU, E., PAPATHANASIOU, A., ASDERAKI-TZOUMERIOTI, E., KARYDAS, Al., TSATSOULI, K., Funerary bronze urn from ancient Demetrias, Proceedings of the workshop Archaeological research at Thessaly and Mainland, Volos, 16.3 – 19.3.2006, Vol. I: Thessaly p699–712, 2009.

[14] ZARARSIZ, A., et al., Characterization of Neolithic wall-painting pigments (ÇATALHÖYÜK 7000–8000 B.C.) by means of a hand-held XRF spectrometer, International Workshop - SMW08, IN SITU MONITORING OF MONUMENTAL SURFACES, Florence, 27–29 October 2008, Conference Proceedings Edited by: Piero Tiano, Carla Pardini, 2008.

[15] DRAKAKI, E., et al., Laser cleaning experimental investigations on ancient coins, 15th International School on Quantum Electronics: Laser Physics and Applications (Proceedings Volume), Proceedings of SPIE Volume: 7027 Editor(s): T. Dreischuh; E. Taskova; E. Borisova; A. Serafetinides, 2008.

[16] M. GIANNOULAKI, M., et al., A systematic approach for the damage assessment of museum metals collections based on statistics and portable techniques: the case study of ancient Messene, Greece, PARCHAIA, Case Studies on Research Planning, Characterisation, Conservation and Management of Archaeological Sites Edited by Nicolò Marchetti and Ingolf Thuesen, BAR International Series **1877** (2008) 121–129.

[17] KARYDAS, A.G., ANGLOS, D., HARITH, M.A., Mobile Spectrometers for Diagnostic Micro-Analysis of Ancient Metal Objects. In Metals and Museums in the Mediterranean: Protecting, Preserving and Interpreting, ed. V.Argyropoulos, (2008) 141–177.

[18] KARYDAS, A.G., BRECOULAKI, H., BOURGEOIS, B., JOCKEY, Ph., In-situ XRF Analysis of raw pigments and traces of polychromy on Hellenistic sculpture at the Archaeological museum of Delos" The Study of Marbles and Other Stones in Antiquity, Proceedings of the 7th ASMOSIA Conference in Thassos, Greece, Y. Maniatis (ed), BCH **51** (2008).

[19] SOKARAS, D., et al., The new external ion-beam station at the Demokritos Tandem 5.5 MV accelerator: A unique analytical tool in the fields of cultural heritage and environmental science, Proceedings of 17th Symposium of Hellenic Nuclear Physics Society, University of Ioannina, Ioannina, Edit. by A. Pakou, T.J. Kosmas, N.G. Nicolis, 30–31 May, 2008.

[20] KANTARELOU, V., SOKARAS, D., ZARKADAS, Ch., KARYDAS, G.A., Development of a portable micro-XRF spectrometer and its applications for the characterization of ancient and historical metal alloys, Proceedings of 17th Symposium of Hellenic Nuclear Physics Society, University of Ioannina, Ioannina, Edit. by A. Pakou, T.J. Kosmas, N.G. Nicolis, 30–31 May, 2008.

[21]   ARGYROPOULOS, V., et al., Developing Innovative Portable Diagnostic Techniques and Approaches for the Analysis of Metal Artefacts from Museum Collections, Proceedings of the 7th European Conference "SAUVEUR", Safeguarded Cultural Heritage, Understanding &Viability for the Enlarged Europe, EC (2007) 79–89.

[22]   DEGRIGNY, C., et al., Innovative protection systems for large collection of metal artefacts conserved in the Mediterranean Basin – PROMET, Proceedings of the 7th European Conference "SAUVEUR", Safeguarded Cultural Heritage, Understanding &Viability for the Enlarged Europe, EC (2007) 879–881.

[23]   ARGYROPOULOS, V., et al., A conservation strategy for documenting the corrosion of outdoor bronze monuments in Greece, Proceedings of the 7th European Conference "SAUVEUR", Safeguarded Cultural Heritage, Understanding &Viability for the Enlarged Europe, EC (2007) 887–889.

[24]   KANTARELOU, V., et al., A novel approach on the combined in-situ application of LIBS and μ-XRF spectrometers for the characterization of copper alloy corrosion products, METAL-07, Vol. 2, Innovative investigation of metal artifacts, (2007) 35–41.

[25]   DEGRIGNY, C., et al., Methodology for the in-situ analyses of historic steel armours with portable milli and micro-XRF spectrometers, METAL-07, Vol. 2, Innovative investigation of metal artifacts, (2007) 26–34.

[26]   GIANNOULAKI, M., et al., A conservation survey of museum metals collections: A case study of Ancient Messene Museum, METAL-07, Vol. 1, When Archaeometry and conservation meet, (2007) 67–72.

[27]   KANTARELOU, V., et al., Micro-XRF Analysis of High Tin Bronze Mirrors at the museum of Ancient Messene in Greece", Proceedings of the International Conference on Conservation Strategies for Saving Indoor Metallic Collections (CSSIM), Cairo, 25 February to 1 March 2007, Edited by V. Argyropoulos, A. Hein and M.A. Harith, (2007) 93–99.

ITALY

[1] CESAREO, R., et al., Portable systems for EDXRF-analysis of works of art; in Portable X ray Fluorescence Spectrometry; Ed. P.J. Potts and M. West, RSC Publ. , Cambridge, UK, (2008) 206–243.

[2] CESAREO, R., et al.: Energy dispersive X ray fluorescence analysis of a pre-columbian funerary mask from the Museum of Sican; XRS 09-0030 accepted for publication.

[3] CESAREO, R., Rizzutto, M.A., Brunetti, A., Metal location and thickness in a multilayer sheet by measuring K- and L-ratios; submitted to NIM B, May 2009.

[4] CESAREO, R., et al.: Pre-columbian alloys from the royal tombs of Sipan analyzed with a portable EDXRF equipment; presented at IRRMA 7, Prague 2008; to be published in Intern. J. of Radiation and Isotopes, 2009.

SLOVENIA

[1] PONGRAC, P., et al., Changes in elemental uptake and arbuscular mycorrhizal colonisation during the life cycle of Thlaspi praecox Wulfen. Chemosphere (Oxford). [Print ed.] **69** 10 (2007) 1602–1609.

[2] ČRTALIČ, H., et al., Dinamika privzema elementov in glivne kolonizacije pri ranem mošnjaku. Collectanea studentium physiologiae plantarum, **2** 3 (2007) 11–14.

[3] VOGEL-MIKUŠ, K., et al., Localisation and quantification of elements within seeds of Cd/Zn hyperaccumulator Thlaspi praecox by micro-PIXE. Environ. pollut. (1987). [Print ed.] **147** (2007) 50–59.

[4] VOGEL-MIKUŠ, K., et al., Comparison of essential and non-essential element distribution in leaves of the Cd/Zn hyperaccumulator Thlaspi praecox as revealed by micro-PIXE. Plant cell environ. [Print ed.] **31** 10 (2008) 1484–1496.

[5] NEČEMER, M., et al., Application of X ray fluorescence analytical techniques in phytoremediation and plant biology studies. Spectrochim. acta, Part B: At. spectrosc. [Print ed.] **11** 63 (2008) 1240–1247.

[6] PONGRAC, P., et al., Roots of Metal Hyperaccumulating Population of Thlaspi Praecox (Brassicaceae) Harbour Arbuscular Mycorrhizal and Other Fungi Under Experimental Conditions. Int. j. phytoremediat., letn. **11** 4 (2009) 348–3597.

[7] NEČEMER, M., et al., Application of total reflection X ray spectrometry in combination with chemometric methods for determination of the botanical origin of Slovenian honey. J. agric. food chem. **57** 10 (2009) 4409–4414.

UNITED STATES OF AMERICA

[1] PATTERSONB.M., DEFRIEND OBREY, K.A., HAVRILLA, G.J., NIKROO, A., HUANG, H., Nondestructive Investigations of a Copper and Argon-Doped Sputtered Beryllium Capsule Using X-Rays In Three Dimensions, Fusion Science and Technology **55** (2009) 417–423.

[2] PATTERSON, B.M., et al., Staying on Target, Nuclear Weapons Journal in Press, 2009.

[3] FITTSCHEN, U.E.A., et al., Characteristics of picoliter droplet dried residues as standards for direct analysis techniques, Anal. Chem. **80** (2008) 1967–1977.

[4] SPARKS, C., FITTSCHEN, U.E.A., HAVRILLA, G.J., Automated Picoliter Solution Deposition for TXRF Analysis of Semiconductor Samples, Denver X ray Conference, Denver, CO, August 4–8, 2009, Book of Abstracts pg 106.

ARGENTINA   C. VAZQUEZ   Comisión Nacional de Energía Atómica (CNEA); Gerencia Quimica
Av. Gral. Paz 1499
San Martin
1650 BUENOS AIRES
ARGENTINA
Tel: 0054 11 6772 7963
Fax: 0054 11 67727886
Email: vazquez@cnea.gov.ar

AUSTRALIA   D. D. COHEN   Australian Nuclear Science and Technology Organisation (ANSTO); Institute for Environmental Research, Private Mail Bag 1
MENAI, NSW 2234
AUSTRALIA
Tel: 0061 2 97173042
Fax: 0061 2 97173257
Email: dcz@ansto.gov.au

AUSTRIA   C. STRELI   Atominstitut TU Wien (ATI); Strahlenphysik
Stadionallee 2
1020 WIEN
AUSTRIA
Email: streli@ati.ac.at

BELGIUM   K. JANSSENS   University Antwerpen; Dept.t of Chemistry
Universiteitsplein 1
2610 ANTWERPEN
BELGIUM
Tel: 0032 3 8202373
Fax: 0032 3 8202376
Email: koen.janssen@ua.ac.be

BEGLIUM   R. VAN GRIEKEN   Universiteit Antwerpen, Dept. of Chemistry
Universiteitsplein 1
2610 Antwerp-Wilrijk
Tel: +32-3-265-2362
Fax: +32-3-265-2376
Email: rene.vangrieken@ua.ac.be

CROATIA   V. DESNICA   Academy of Fine Arts; Department for Conservation and Restoration; Laboratory for Science and Technology in Art
Ilica 85
10000 ZAGREB
CROATIA
Tel: 00385 1 4824-385
Fax: 00385 1 4680239
Email: vdesnica@irb.hr

CUBA	G. MESA	Centro de Estudios Aplicados al Desarrollo Nuclear (CEADEN) Calle 30, 502, esq. 1ra. y 3ra. Avenida, Playa Apartado Postal 6122 LA HABANA 10300 CUBA Tel: 00 537 2093905 Fax: 00 537 2021518 Email: guille@ceaden.edu.cu
GREECE	A.-G. KARYDAS	National Center of Scientific Research "Demokritos"; Institute of Nuclear Physics Agia Paraskevi P.O. Box 60228 15310 ATHENS GREECE Tel: 0030 210 6503523 Fax: 0030 210 6511215 Email: karydas@inp.demokritos.gr
ITALY	S. RIDOLFI	ARS Mensurae Via Aretusi 29 00188 ROMA ITALY Tel: 0039 06 3320431 Fax: 0039 17 82266895 Email: stefano@arsmensurae.it
SLOVENIA	P. KUMP	Jozef Stefan Institute; Department of Low and Medium Energy Physics Jamova 39 P.O.Box 3000 1001 LJUBLJANA SLOVENIA Tel: 00386 61 1773687 Fax: 00386 61 219385 Email: peter.kump@ijs.si
UNITED ARAB EMIRATES	H. NASSER	The American University of Sharjah; Physics Department P.O. Box 26666 SHARJAH UNITED ARAB EMIRATES Tel: 00971 6 5152509 Fax: 00971 6 5585066 Email: nhamdan@aus.edu
UNITED STATES OF AMERICA	G. HAVRILLA	University of California, Los Alamos; Los Alamos National Laboratory (LANL) P.O. Box 1663 MS K484 LOS ALAMOS, NM 87545 UNITED STATES OF AMERICA Tel.: +505-667-9627 Email: havrilla@lanl.gov

IAEA
International Atomic Energy Agency

Where to order IAEA publications

In the following countries IAEA publications may be purchased from the sources listed below, or from major local booksellers. Payment may be made in local currency or with UNESCO coupons.

AUSTRALIA
DA Information Services, 648 Whitehorse Road, MITCHAM 3132
Telephone: +61 3 9210 7777 • Fax: +61 3 9210 7788
Email: service@dadirect.com.au • Web site: http://www.dadirect.com.au

BELGIUM
Jean de Lannoy, avenue du Roi 202, B-1190 Brussels
Telephone: +32 2 538 43 08 • Fax: +32 2 538 08 41
Email: jean.de.lannoy@infoboard.be • Web site: http://www.jean-de-lannoy.be

CANADA
Bernan Associates, 4501 Forbes Blvd, Suite 200, Lanham, MD 20706-4346, USA
Telephone: 1-800-865-3457 • Fax: 1-800-865-3450
Email: customercare@bernan.com • Web site: http://www.bernan.com

Renouf Publishing Company Ltd., 1-5369 Canotek Rd., Ottawa, Ontario, K1J 9J3
Telephone: +613 745 2665 • Fax: +613 745 7660
Email: order.dept@renoufbooks.com • Web site: http://www.renoufbooks.com

CHINA
IAEA Publications in Chinese: China Nuclear Energy Industry Corporation, Translation Section, P.O. Box 2103, Beijing

CZECH REPUBLIC
Suweco CZ, S.R.O., Klecakova 347, 180 21 Praha 9
Telephone: +420 26603 5364 • Fax: +420 28482 1646
Email: nakup@suweco.cz • Web site: http://www.suweco.cz

FINLAND
Akateeminen Kirjakauppa, PO BOX 128 (Keskuskatu 1), FIN-00101 Helsinki
Telephone: +358 9 121 41 • Fax: +358 9 121 4450
Email: akatilaus@akateeminen.com • Web site: http://www.akateeminen.com

FRANCE
Form-Edit, 5, rue Janssen, P.O. Box 25, F-75921 Paris Cedex 19
Telephone: +33 1 42 01 49 49 • Fax: +33 1 42 01 90 90
Email: formedit@formedit.fr • Web site: http://www. formedit.fr

Lavoisier SAS, 145 rue de Provigny, 94236 Cachan Cedex
Telephone: + 33 1 47 40 67 02 • Fax +33 1 47 40 67 02
Email: romuald.verrier@lavoisier.fr • Web site: http://www.lavoisier.fr

GERMANY
UNO-Verlag, Vertriebs- und Verlags GmbH, Am Hofgarten 10, D-53113 Bonn
Telephone: + 49 228 94 90 20 • Fax: +49 228 94 90 20 or +49 228 94 90 222
Email: bestellung@uno-verlag.de • Web site: http://www.uno-verlag.de

HUNGARY
Librotrade Ltd., Book Import, P.O. Box 126, H-1656 Budapest
Telephone: +36 1 257 7777 • Fax: +36 1 257 7472 • Email: books@librotrade.hu

INDIA
Allied Publishers Group, 1st Floor, Dubash House, 15, J. N. Heredia Marg, Ballard Estate, Mumbai 400 001,
Telephone: +91 22 22617926/27 • Fax: +91 22 22617928
Email: alliedpl@vsnl.com • Web site: http://www.alliedpublishers.com

Bookwell, 2/72, Nirankari Colony, Delhi 110009
Telephone: +91 11 23268786, +91 11 23257264 • Fax: +91 11 23281315
Email: bookwell@vsnl.net

ITALY
Libreria Scientifica Dott. Lucio di Biasio "AEIOU", Via Coronelli 6, I-20146 Milan
Telephone: +39 02 48 95 45 52 or 48 95 45 62 • Fax: +39 02 48 95 45 48
Email: info@libreriaaeiou.eu • Website: www.libreriaaeiou.eu

JAPAN
Maruzen Company, Ltd., 13-6 Nihonbashi, 3 chome, Chuo-ku, Tokyo 103-0027
Telephone: +81 3 3275 8582 • Fax: +81 3 3275 9072
Email: journal@maruzen.co.jp • Web site: http://www.maruzen.co.jp

REPUBLIC OF KOREA
KINS Inc., Information Business Dept. Samho Bldg. 2nd Floor, 275-1 Yang Jae-dong SeoCho-G, Seoul 137-130
Telephone: +02 589 1740 • Fax: +02 589 1746 • Web site: http://www.kins.re.kr

NETHERLANDS
De Lindeboom Internationale Publicaties B.V., M.A. de Ruyterstraat 20A, NL-7482 BZ Haaksbergen
Telephone: +31 (0) 53 5740004 • Fax: +31 (0) 53 5729296
Email: books@delindeboom.com • Web site: http://www.delindeboom.com

Martinus Nijhoff International, Koraalrood 50, P.O. Box 1853, 2700 CZ Zoetermeer
Telephone: +31 793 684 400 • Fax: +31 793 615 698
Email: info@nijhoff.nl • Web site: http://www.nijhoff.nl

Swets and Zeitlinger b.v., P.O. Box 830, 2160 SZ Lisse
Telephone: +31 252 435 111 • Fax: +31 252 415 888
Email: infoho@swets.nl • Web site: http://www.swets.nl

NEW ZEALAND
DA Information Services, 648 Whitehorse Road, MITCHAM 3132, Australia
Telephone: +61 3 9210 7777 • Fax: +61 3 9210 7788
Email: service@dadirect.com.au • Web site: http://www.dadirect.com.au

SLOVENIA
Cankarjeva Zalozba d.d., Kopitarjeva 2, SI-1512 Ljubljana
Telephone: +386 1 432 31 44 • Fax: +386 1 230 14 35
Email: import.books@cankarjeva-z.si • Web site: http://www.cankarjeva-z.si/uvoz

SPAIN
Díaz de Santos, S.A., c/ Juan Bravo, 3A, E-28006 Madrid
Telephone: +34 91 781 94 80 • Fax: +34 91 575 55 63
Email: compras@diazdesantos.es, carmela@diazdesantos.es, barcelona@diazdesantos.es, julio@diazdesantos.es
Web site: http://www.diazdesantos.es

UNITED KINGDOM
The Stationery Office Ltd, International Sales Agency, PO Box 29, Norwich, NR3 1 GN
Telephone (orders): +44 870 600 5552 • (enquiries): +44 207 873 8372 • Fax: +44 207 873 8203
Email (orders): book.orders@tso.co.uk • (enquiries): book.enquiries@tso.co.uk • Web site: http://www.tso.co.uk

On-line orders
DELTA Int. Book Wholesalers Ltd., 39 Alexandra Road, Addlestone, Surrey, KT15 2PQ
Email: info@profbooks.com • Web site: http://www.profbooks.com

Books on the Environment
Earthprint Ltd., P.O. Box 119, Stevenage SG1 4TP
Telephone: +44 1438748111 • Fax: +44 1438748844
Email: orders@earthprint.com • Web site: http://www.earthprint.com

UNITED NATIONS
Dept. I004, Room DC2-0853, First Avenue at 46th Street, New York, N.Y. 10017, USA
(UN) Telephone: +800 253-9646 or +212 963-8302 • Fax: +212 963-3489
Email: publications@un.org • Web site: http://www.un.org

UNITED STATES OF AMERICA
Bernan Associates, 4501 Forbes Blvd., Suite 200, Lanham, MD 20706-4346
Telephone: 1-800-865-3457 • Fax: 1-800-865-3450
Email: customercare@bernan.com · Web site: http://www.bernan.com

Renouf Publishing Company Ltd., 812 Proctor Ave., Ogdensburg, NY, 13669
Telephone: +888 551 7470 (toll-free) • Fax: +888 568 8546 (toll-free)
Email: order.dept@renoufbooks.com • Web site: http://www.renoufbooks.com

Orders and requests for information may also be addressed directly to:

Marketing and Sales Unit, International Atomic Energy Agency
Vienna International Centre, PO Box 100, 1400 Vienna, Austria
Telephone: +43 1 2600 22529 (or 22530) • Fax: +43 1 2600 29302
Email: sales.publications@iaea.org • Web site: http://www.iaea.org/books